



The
University
Of
Sheffield.

Characterisation of silica aerogels for vibro-acoustic applications

By:

Hasina Begum

A thesis submitted in partial fulfilment of the requirements for the degree of
Doctor of Philosophy

The University of Sheffield
Faculty of Engineering
Department of Mechanical Engineering

31 December 2021

Dedicated to my late father, who never saw the woman I became.

And to my mother, who made me the woman that I am.

Abstract

This article-based thesis comprises of a collection of four journal papers, three of which are published and one of which is currently accepted for publication in the Journal of Acoustical Society of America pending revisions. Each article constitutes a chapter written and formatted in manuscript form. The overall aim of these papers is to understand the acoustical properties of silica aerogels used for vibro-acoustic applications. There has been a lack of knowledge on the relationship between the acoustical and non-acoustical properties of aerogels which usually come in highly porous, granular (e.g., millimetre-size particles) and powder (e.g., micron-size particles) aerogels. For this purpose, silica aerogels have been provided in the powder and powder-embedded fibreglass mat form by our industry partner – Armacell. Alongside this, aerogels have also been synthesised in monolithic and granular form in the laboratory. These materials have been carefully characterised acoustically and non-acoustically to provide new insights into the relations between their chemical, microstructural and acoustical characteristics.

This thesis uses an extensive materials characterisation process to support the experimental and analytical modelling procedure used to allow us to predict the in-situ performance of these materials in industry after carefully understanding the physical morphology such as pore size and porosity which underpins their acoustic phenomena. Advanced theoretical models have been

used to explain the observed acoustical behaviour and has linked this to the material microstructure. It has been found that most of the current work only focuses on absorption, transmission loss, layer thickness and morphology like pore and particle size. The work carried out in this thesis focuses on mathematical models that use fundamental acoustical quantities such as frequency-dependent bulk modulus, complex dynamic density, and complex dynamic compressibility. These properties have been linked to the intrinsic material parameters and parameters of the air filling the porous structure of aerogels.

In the case of powder aerogels, it has been found that the dynamic loss factor is a key parameter required to predict the measured acoustic absorption coefficient. It has also been found that the sound absorption depends non-linearly on the sound pressure excitation. In the case of powder silica aerogels embedded into fiberglass mats it has been found that the classical model for the visco-thermal and inertia effects in the pores can predict unrealistic pore size and porosity value to achieve good fit with the data. In the case of granular silica aerogels, it has been found that the rarefied gas flow and heat transfer in the inner-particle transport macropores, inter-scale (voids to/from inner-grain pores) pressure diffusion, and inter-scale (transport- to/from meso pores) mass diffusion can be a dominant phenomenon.

This research suggests that a refined model is required to predict the acoustical properties of aerogels to take into account their complex hierarchical pore structure and properties of air in sub-micron pores.

Acknowledgements

First and foremost, I would like to praise and thank God for granting me countless blessings and giving me the opportunity to complete this PhD thesis. God is truly the Greatest and none of this would have been possible without Him.

I would like to sincerely thank my supervisors, Professor Kirill Horoshenkov and Dr. Anton Krynkin for their plethora of knowledge, technical guidance, and invaluable time, throughout the entirety of my research. Their support and encouragement truly drove this PhD to progress to the full potential that it did. Kirill, you went above and beyond, you cared so much, and you always helped me to excel in everything that I did. This undeniably allowed me to thoroughly enjoy my work right until the very end and I am immensely grateful to have shared my PhD experience with you – a father figure that I never had in one of the most crucial moments of my life.

There are several other people whom I would like to extend my thanks to and without whom this project would not have exceeded to the final product that it is now. I would like to thank Dr. Paolo Bonfiglio for all his technical support and time in designing the acoustic impedance tube and allowing me to visit Materiacustica in Ferrara to receive first-hand training and become a competent acoustician on this setup. I am extremely grateful to Dr. Wim Malfait, Dr. Shanyu Zhao, and Dr. Matthias Koebel for allowing me to visit Empa, Swiss Federal

Laboratories for Materials Science and Technology in Switzerland as a visiting researcher. I am grateful to have had the opportunity to work with you and to have had your full support in producing my own silica aerogel materials for acoustic testing. This made the second half of my PhD a very memorable experience and one that I will cherish forever.

A very special person I would also like to thank here is Dr. Rodolfo Venegas. Rodolfo, you really shaped my PhD towards the end, I feel very grateful to have had your input in my work, particularly with merging the understanding of hierarchical porous materials and appreciating mathematical modelling in acoustics. I feel honoured to have collaborated with you and obtained your expert advice.

Further thanks are extended to the technicians: Mr. Mathew Hall and Dr. Christopher Hill. Mathew, thank you so much for your quick response with anything and everything I needed in the lab. Chris, thank you for always being at hand to help and prepare samples for use in the scanning electron microscope. My research was highly dependent on this equipment, and I thank you for always giving me your time.

This PhD would certainly not have been possible without the joint funding from the EPSRC, the CDT in Polymers, Soft Matter, and Colloids and my industrial sponsors – Armacell. Special thanks here must go to my industrial supervisor's Dr. Mark Swift and Mr. Pavel Holub for providing all their assistance in this work.

Finally, I want to thank my beloved mother. Thank you for being the best supporter in my work from day 1. Although you did not always understand my work, you always gave me your time and you always listened to everything I had to say and for that I am truly grateful to have had you throughout this whole process.

Publications

Journal Publications

- J1 Z. Mazrouei-Sebdani, H. Begum, S. Schoenwald, K.V. Horoshenkov, W.J. Malfait, "A review on silica aerogel-based materials for acoustic applications," *J. Non-Cryst. Sol.*, 562, 120770, 2021.
<https://doi.org/10.1016/j.jnoncrysol.2021.120770>.
- J2 H. Begum, K.V. Horoshenkov, "Acoustical Properties of Fiberglass Blankets Impregnated with Silica Aerogel," *Appl. Sci.*, 11, 4593, 2021.
<https://doi.org/10.3390/app11104593>
- J3 H. Begum, K.V. Horoshenkov, M. Conte, W.J. Malfait, S. Zhao, M.M. Koebel, P. Bonfiglio, R. Venegas, "The acoustical properties of tetraethyl orthosilicate based granular silica aerogels," *J. Acoust. Soc. Am.*, 149(6), 4149–4158, 2021. <https://doi.org/10.1121/10.0005200>.
- J4 H. Begum, Y. Xue, J.S. Bolton, K.V. Horoshenkov, "The acoustical properties of air-saturated aerogel powders" , *J. Acoust. Soc. Am.*, 151(3), 1502–1515, 2022.
<https://doi/10.1121/10.0009635>

Conference publications

C1 K.V. Horoshenkov, H. Begum, "Are aerogels an emerging noise control solution or is it just beefed up fiber glass?" , J. Acoust. Soc. Am., 144, 1755, 2018. <https://doi.org/10.1121/1.5067773>

C2 H. Begum, K.V. Horoshenkov, M. Conte, W.J. Malfait, S. Zhao, M. M. Koebel, P. Bonfiglio, R. Venegas, "Acoustical properties of granular silica aerogels" , *Forum Acusticum 2020 (FA2020)*, Lyon, France, 7th–11th December 2020.
<https://doi.org/10.48465/fa.2020.0543>

C3 H. Begum, K.V. Horoshenkov, M. Conte, W.J. Malfait, S. Zhao, M. M. Koebel, P. Bonfiglio, R. Venegas, "Acoustical properties of TEOS based granular silica aerogels" , *SAPEM 2020+1 (Symposium on the Acoustics of Poro-Elastic Materials)*, West Lafayette (Indiana), USA, 29th March–2nd April 2021.
https://sapem2021.matelys.com/proceedings/07-04_Begum_etal.pdf

C4 H. Begum, K.V. Horoshenkov, M. Conte, W.J. Malfait, S. Zhao, M. M. Koebel, P. Bonfiglio, R. Venegas, "Acoustical properties of TEOS based granular silica aerogels" , *Aerogel Industry-Academia Forum*, Dübendorf, Switzerland, 13th–15th July 2021.
https://www.empa.ch/documents/16797158/16797311/Hasina+Begum-Abstract_Aerogel+Industry-Academia+Forum.pdf/21d746db-25a8-4d4b-bbef-f34b1b5eae89

Declaration

I, the author, Hasina Begum confirm that the Thesis is my own work. I am aware of the University' s Guidance on the Use of Unfair Means (www.sheffield.ac.uk/ssid/unfair-means). This work has not been previously been presented for an award at this, or any other, University.

Table of Contents

Abstract.....	v
Acknowledgements	ix
Publications	xiii
Journal publications.....	xiii
Conference presentations & publications	xiv
Declaration.....	xvi
List of Tables	xxii
List of Figures.....	xxv
Nomenclature	xxxvi
Greek Symbols.....	xxxvi
Roman Symbols.....	xxxix
Script Symbols	xli
Acronyms.....	xlii
Chapter 1	45
1.1 Background.....	45
1.2 Aims and Objectives.....	47
1.3 Thesis outline	49
References.....	53
Chapter 2: Literature Review	55
2.1 Abstract.....	55
2.2 Silica aerogel	57
2.3 Synthesis.....	58
2.3.1 Gelation	58

2.3.2 Aging	60
2.3.3 Hydrophobization/surface modification.....	60
2.3.4 Drying.....	61
2.4 Silica aerogel properties.....	63
2.4.1 Microstructure	64
2.4.2 Thermal conductivity	65
2.4.3 Mechanical properties.....	65
2.5 Aerogel applications.....	68
2.6 Sound absorption and insulation	71
2.6.1 An introduction to sound absorption/insulation.....	71
2.6.2 Types of acoustic measurements	75
2.6.3 Sound absorption measurement.....	76
2.6.4 Sound insulation measurement.....	79
2.7 Acoustic properties of silica aerogel and aerogel composites	82
2.7.1 Sound velocity and impedance in silica aerogels.....	82
2.7.2 Sound absorption/insulation in pure/hybrid silica aerogels	84
2.7.3 Sound absorption/insulation of silica aerogel-polymer composites	98
2.7.4 Sound absorption/insulation of aerogel-textile compounds.....	100
2.7.5 Sound absorption/insulation of aerogel renders	114
2.7.6 Sound absorption/insulation of aerogel glazing systems.....	117
2.8 Aerogel-based products versus conventional acoustic materials.....	120
2.9 Summary, open questions, road to market.....	124
References.....	129
Chapter 3: The acoustical properties of air-saturated aerogel powders.....	156
3.1 Abstract.....	156

3.2 Introduction.....	158
3.3 Materials and Methods.....	163
3.3.1 Materials Characterisation	163
3.4 Modelling of aerogel granule stacks	169
3.4.1 Acoustical theories for predicting sound absorption	172
3.4.2 Bulk modulus and equivalent density predictions with the JCA model	175
3.4.3 Bulk modulus and equivalent density predictions with the 3- parameter model	178
3.4.4 Effective density and bulk modulus as inputs in the Biot poro-elastic model.....	179
3.5 Results & Discussion – Characterisation of acoustical-related bulk properties.....	181
3.5.1 Fitting the measured sound absorption coefficient spectra.....	181
3.6 Conclusions.....	198
References.....	201
Appendix A.....	207
Chapter 4: Acoustical properties of fiberglass blankets impregnated with silica aerogel	213
4.1 Abstract.....	213
4.2 Introduction.....	215
4.3 Materials and Methods.....	220
4.3.1 Materials preparation	220
4.3.2 Materials Characterisation	221
4.4 Modelling of the acoustical properties of fibrous and granular media	223

4.5 Results & Discussion	226
4.5.1 Microstructural analysis	226
4.5.2 Acoustical properties	230
4.6 Conclusions.....	238
References.....	240
Chapter 5: The acoustical properties of tetraethyl orthosilicate based granular silica aerogels.....	247
5.1 Abstract.....	247
5.2 Introduction.....	249
5.3 Materials and Methods.....	252
5.3.1 Aerogel synthesis	252
5.3.2 Characterisation.....	257
5.4 Modelling of the acoustical properties of aerogels	261
5.5 Results	269
5.5.1 Density, nitrogen sorption analysis and microstructure	269
5.5.2 Acoustical properties	275
5.6 Discussion.....	281
5.7 Conclusions.....	284
References.....	287
Chapter 6: Conclusion & future work.....	296
6.1 Conclusions.....	296
6.2 Future work.....	300

List of Tables

2.1	Selected silica aerogel applications.	68
2.2	Silica and silica-polymer related aerogels acoustic application related papers.	109
2.3	Comparison of conventional and aerogel-based acoustic insulation materials.	122
3.1	Bulk properties characterised by fitting the JCA-Biot-TMM/ACM with the measurements and used to predict sound absorption coefficient spectra.	185
3.2	Bulk properties used for the 3P-Biot-TMM/ACM to predict sound absorption coefficient spectra.	185

3.3	The coefficients in the equation for the dynamic loss factor for two aerogels.	191
4.1	Values of the non-acoustical parameters inverted from fitting the model to the measured complex reflection coefficient data for the five types of fibreglass blankets.	235
5.1	Materials and quantities used to prepare polyethoxydisiloxane (PEDS).	253
5.2	The preparation of three standard equivalents at weight percentages of silica (expressed as SiO ₂) for samples with TEOS concentration of 30, 60 and 90%.	255
5.3	Materials and quantities used to age aerogels.	256

- 5.4 Properties of density, pore structures, surface area, adsorption 274
(ads) and desorption (des) coefficients of silica aerogels for PEDS
E30, PEDS E60, and PEDS E90.
- 5.5 The results of the inversion of the three materials studied in this 279
work.

List of Figures

- 2.1 Schematic design of silica aerogels synthesis. The surface modification (typically hydrophobization) is optional. The drying step can be carried out at ambient pressure or using supercritical CO₂ or ethanol drying. 63
- 2.2 2.2 Silica aerogel microstructure and mechanical properties. (A) TEM image, (B) SEM image, (C) E-modulus as a function of density, (D) Stress-strain curves during uniaxial compression: ρ_x represents density (g/cm³) and x corresponds to the volume concentration of polyethoxydisiloxane in the initial colloidal suspension. 67
- 2.3 2.3 (A-C) The three main types of porous absorbing materials and (D) Resonance absorbers of type Helmholtz. 73
- 2.4 Impedance tubes (A) Standing wave method and (B) Transfer function method. 77

2.5	Sound absorption coefficient for different heights of an aerogel particle layer.	86
2.6	Sound absorption coefficient of different insulation materials at a thickness of 20 mm.	86
2.7	Sound absorption coefficient of silica aerogels and silica aerogel blankets with different thickness, compared to fibreglass sound absorbers.	88
2.8	Sound absorption coefficient of silica aerogel, compared to a melamine foam (thickness 50 mm).	91
2.9	Sound absorption coefficient of polyimide-silica aerogels.	92
2.10	Transmission loss for (A) aerogel granules and (B) GSA-AG composites (granular size: 1.7 mm) via the proposed	93

“Inferential Method” using a two-microphone impedance tube.

- 2.11 (A) Transmission loss of 1-4 mm silica aerogel granule layers for different thicknesses and (B) Comparison between aerogels and rock wool panel in 30 mm thickness. 94
- 2.12 (A) SEM image with no aerogel content, (B) SEM image with 2% aerogel content, (C) Sound absorption coefficient, and (D) Transmission loss, for coating grade PU and its composites with 1-4% aerogel. 100
- 2.13 Sound absorption coefficient of the 5 mm thickened PET nonwoven-silica aerogel blankets prepared by dipping a PET nonwoven in a TEOS based sol. 103
- 2.14 SEM images of (A) control PET, (B) PET nonwoven-silica aerogel blankets (MeOH:TEOS molar ratio: 110), and (C) PET nonwoven-silica aerogel blankets (MeOH:TEOS molar ratio: 28). 105

2.15	SEM images of an aerogel-nonwoven bonded compound.	107
2.16	Sound absorption coefficient of the aerogel-nonwoven bonded compounds (A) with different aerogel contents and (B) the different number of layers for the sample with 2% of aerogel (0.067 g/m ³ , 6.6 mm).	108
2.17	Mixing and applying of an aeogel-based plaster. (A) original components, (B) mixing phase, (C) final composition, and (D) in situ application on the wall.	115
2.18	Sound transmission loss for a glazing system (glass-aerogel-glass of 4-6-4 mm).	119
2.19	Sound reduction index (R) for the conventional window and the glazing prototype with aerogel in the interspace.	120

3.1	SEM images of Type 1 and 2 aerogels taken at different magnifications (1000 x (a) and (e), 5000 x (b) and (f), 80,000 x (c) and (g) and 200,000 (d) and (h)).	167
3.2	Photographs of the powder samples used in the impedance tube experiments.	168
3.3	2-microphone impedance tube setup to measure the surface impedance of a porous layer.	168
3.4	Normal incidence sound absorption coefficients, α' s, measured at different in-tube sound pressure levels in standing wave tube experiments for (a) Enova IC3100 and (b) JIOS AeroVa D20. The SPL shown in the legend corresponds to the incident, broadband sound pressure levels measured with the two microphones.	171
3.5	(a) Normal incidence absorption coefficients, α' s, of Enova IC3100 (Type 1) at different incident sound pressure levels by experimental measurement (blue-solid lines), the JCA-	186

Biot(poro-elastic)-TMM/ACM model prediction (orange-dashed lines), the 3P-Biot(poro-elastic)-TMM/ACM model prediction (green-dotted lines), (b) Cumulative squared error between JCA-Biot(poro-elastic)-TMM/ACM model prediction and experimental measurement, and (c) Cumulative squared error between 3P-Biot(poro-elastic)-TMM/ACM model prediction and experimental measurement.

- 3.6 (a) Normal incidence absorption coefficients, α' s, of JIOS AeroVa D20 (Type 2) at different incident sound pressure levels by experimental measurement (blue-solid lines), the JCA-Biot(poro-elastic)-TMM/ACM model prediction (orange-dashed lines) and the 3P-Biot(poro-elastic)-TMM/ACM model prediction (green-dotted lines), (b) Cumulative squared error between JCA-Biot(poro-elastic)-TMM/ACM model prediction and experimental measurement, and (c) Cumulative squared error between 3P-Biot(poro-elastic)-TMM/ACM model prediction and experimental measurement. 188

3.7	The dependence of the coefficient a on the sound pressure level.	192
3.8	The dependence of the coefficient b on the sound pressure level.	192
3.9	The spectra for the normalised drag force acting on a particle of Type 1 and Type 2 aerogel in the case of 112 dB broadband sound pressure level incident on the surface of the aerogel specimen in the impedance tube.	195
3.10	The spectra for the displacement of the air molecules in the sound wave incident on the surface of Type 1 and Type 2 aerogel specimen in the impedance tube.	196
4.1	10 mm diameter of fiberglass blanket samples cut for fitting into the impedance tube.	222

4.2	2-microphone impedance tube setup to measure the surface impedance of a porous layer.	223
4.3	SEM images taken at different magnifications (3000x (a), 800x (b) and 200x (c)) showing the fibreglass blanket without any aerogel.	228
4.4	SEM images taken at different magnifications (3000x (a), 800x (b) and 200x (c)) showing the fibreglass blanket structure with an aerogel filling ratio of 25%.	228
4.5	SEM images taken at different magnifications (3000x (a), 800x (b) and 200x (c)) showing the fibreglass blanket structure with an aerogel filling ratio of 50%.	229
4.6	SEM images taken at different magnifications (3000x (a), 800x (b) and 200x (c)) showing the fibreglass blanket structure with an aerogel filling ratio of 75%.	229

4.7	SEM images taken at different magnifications (3000x (a), 800x (b) and 200x (c)) showing the fibreglass blanket structure with an aerogel filling ratio of 100%.	230
4.8	SEM images taken at different magnifications (3000x (a), 800x (b) and 200x (c)) showing the fibreglass blanket structure with an aerogel filling ratio of 100%.	231
4.9	Examples of the measured (marker) and predicted (solid lines) complex reflection coefficient data for fibreglass blanket without any aerogel (top), 50% aerogel impregnated aerogel (middle) and 100% aerogel impregnated blanket (bottom).	233
5.1	Structure of monolithic silica aerogel as a) a photographic image, b) drawing and c) TEM image.	257
5.2	Vertically standing 10 mm impedance tube.	260

5.3	Photographs of the 50 mm x 50 mm container with granular silica aerogel 2-3 mm sieved mix (left) and 40 mm ³ of it in the 10 mm diameter, 50 mm deep impedance tube sample holder (right).	270
5.4	SEM images of micrometric grains of the 2-3 mm fraction of a) PEDS E30, b) PEDS E60, c) PEDS E90.	270
5.5	Analysis of the size of 50 individual pores using ImageJ software applied to SEM images of a) PEDS E30, b) PEDS E60, c) PEDS E90.	271
5.6	BET isotherm linear plots of a) PEDS E30, b) PEDS E60, c) PEDS E90.	273
5.7	Schematic for 3 generic types of pores, i) ink bottle, ii) straight with both ends open and iii) straight with only one end open.	273

5.8	The measured absorption coefficient spectra for a nominal 50 mm hard-backed layer of the four materials studied in this work.	277
5.9	Model validation. The measured (circles) and predicted (lines) reflection coefficient for a hard-backed layer of loosely packed glass beads.	278
5.10	Examples of the measured and predicted reflection coefficient for hard-backed layers of aerogel granulate. A) PEDS E30, b) PEDS E60, c) PEDS E90.	281
5.11	Acoustically determined porosity for PEDS E30, PEDS E60 and PEDS E90.	282

Nomenclature

Greek symbols

α	Acoustic absorption coefficient
k_c	Wavenumber
ω	Angular frequency
R	Reflection coefficient
ν	Poisson' s ratio
δ	Viscous boundary layer thickness/depth
η	Dynamic viscosity
ρ	Density
ρ_0	Ambient density
ρ_b	Bulk density
ρ_s	Skeletal density
ρ_e	Effective density
ρ_p	Viscosity effects in the pores, well approximated with that of the voids

K_f	Bulk modulus
k_p	Dynamic viscous permeability
η	Dynamic viscosity in air
γ	Specific heat ratio
σ	Airflow resistivity
σ_s	Standard deviation of the pore size
ϕ	Porosity
α_∞	Tortuosity
Λ	Viscous characteristic length
Λ'	Thermal characteristic length
k'_0	Static thermal permeability
σ_s	Standard deviation of the pore size
η_m	Mechanical loss factor
u	Acoustic velocity
u_0	Acoustic velocity amplitude
$\tilde{\rho}$	Complex dynamic density

\tilde{C}	Complex dynamic compressibility
C_p	Effective compressibility
ϕ_p	Voids porosity
ϕ_t	Inner particle macropore radius and their associated porosity (transport pore)
ϕ_n	Apparent porosity of the smallest pores
C_{mn}	Compressibility of the effective fluid in the macro- and mesopores
C_m	Effective compressibility of the fluid that saturates the macropores
C_n	Compressibility of the fluid that saturates the mesopores
F_{pmn}	Pressure diffusion process
F_{mn}	Mass diffusion process

Roman symbols

I_a	Absorbed sound intensity
I_i	Incident sound intensity
R	Sound reduction index
f_H	Higher frequency
A	Cross sectional area
V	Volume
L	Length
K_f	Bulk modulus
B^2	Prandtl number
f_c	Critical frequency
c/c_0	Sound velocity in air
h/d	Thickness
E/E_1	Young' s modulus
$ F $	Normalised drag force amplitude
F_g	Particle gravity force

g	Gravity acceleration
s_b/\bar{s}	Median pore size
j	Imaginary number
D_k	Knudsen number
r	Radius
dV	Pore volume
d_n	Pore width
V_p	Pore volume
D_p	Pore size of the mesopores
S_{BET}	Specific surface area
r_p	Effective particle radius
r_t	Inner particle macropore radius
D_e	Effective diffusion coefficient
H_e	Effective linearised sorption equilibrium constant
Z_s	Normalised surface impedance
Z_c	Normalised characteristic impedance

Script symbols

°C Degrees Celsius

$\sqrt{\bar{x}^2}$ Root mean square

wt. % Weight per weight, this represents the weight of the solute/
weight of the solvent.

Acronyms

SEM	Scanning electron microscope
TEM	Transmission electron microscope
BET	Brunauer–Emmet–Telle
BJH	Barrett–Joyner–Halenda
TEOS	Tetraethyl orthosilicate
TMOS	Tetramethyl orthosilicate
MTMS	Methyltrimethoxysilane
VTMS	Vinyltrimethoxysilane
HMDSO	Hexamethyldisiloxane
HMDS	Hexamethyldisilazan
TMCS	Tetramethylchlorosilane
PEDS	Polyethoxydisiloxane
PDMS	Polydimethylsiloxane
PVB	Polyvinylbutyrale
VAE	Vinylacetate/ethene

GSA-SDS	Gelatine silica aerogel-sodium dodecyl sulfate
UPVC	Unplasticized polyvinyl chloride
r-PET	Recycled polyethylene terephthalate
PET	Polyethylene terephthalate
PU	Polyurethane
PE	Polyethylene
HCl	Hydrochloric acid
HNO ₃	Nitric acid
CO ₂	Carbon dioxide
SiO ₂	Silicon dioxide
NH ₄ OH	Ammonium hydroxide
MeOH	Methanol
EtOH	Ethanol
SA	Silica aerogel
SCD	Super critical drying
APD	Ambient pressure drying

FD	Freeze drying
IUPAC	International Union of Pure and Applied Chemistry
TLM	Transmission loss method
ACM	Arbitrary coefficient method
TMM	Transfer matrix method
DMA	Dynamic mechanical analysis
NFD	Near-field damping
JCA	Johnson-Champoux-Allard
JCAL	Johnson-Champoux-Allard-Lafarge
3P	3-parameter

Chapter 1: Introduction

1.1 Background

There is a global need to reduce the energy consumption in Europe whereby 40% comes from the building sector [1]. Thermal insulation products often require good sound absorption and insulation properties to control noise. Noise control engineering is incredibly important to the quality of life in one's psychological and physical well-being and some applications are heavily regulated by standards and legislation [2]. Mitigating noise emissions and transmission combined with thermal insulation creates a holistic and sustainable design for the industry building and outdoor environments.

The acoustic flow is controlled by sound absorptive materials that are highly resistive in nature. The effectiveness of a sound absorber is measured by the sound absorption coefficient, which is the ratio of sound energy absorbed by the material surface to the sound energy incident upon the surface. Porous materials are the most common class of acoustic absorbers used in noise control applications because they are lightweight, energy efficient alternatives to the heavy sound barriers [3] and resonant absorbers. Most common types of absorbers are non-wovens, mineral wool, foams, fibreglass, and granular

materials. The acoustical properties of these materials have been studied extensively [4,5]. A relatively new product on the acoustic absorption market is silica aerogels. Aerogels combine an outstanding thermal insulation with high acoustic absorption.

These materials have gained popularity also due to their highly porous nature which allows sound waves to undergo multiple interactions in the complex pore structure making them effective acoustic absorbers [6]. Such properties include high porosity of ~95%, high thermal conductivity of $\sim 0.015 \text{ W m}^{-1} \text{ K}^{-1}$, low bulk density of $\sim 0.120 \text{ g/cm}^3$ and high surface area of 700–900 m^2/g [7].

Silica aerogels are already commercially available, e.g., from Aspen Aerogels and Cabot Corporation. These are produced in many different forms, e.g., powder/granulates, aerogel impregnated blankets, coatings and as hybrid spray-foam systems [8]. Although the thermal properties of silica aerogels are relatively well understood, the acoustical properties of these materials have not been studied extensively. It has been common to measure the acoustical properties of a layer of aerogel, but not interpret these results with a valid theoretical model [8]. My PhD research aims to address this gap in knowledge. It focuses on a careful characterisation of the experimental acoustic performance of aerogels that is explained with advanced analytical models.

1.2 Aims and Objectives

The main aim of this PhD project was to understand the measured acoustic performance of silica aerogels. Recently Armacell decided to invest in the development of new composite noise control solutions which combine traditional porous media such as foams and mineral wool with aerogels. The vibro-acoustic performance of these solutions is largely unknown, but there is strong evidence that these solutions could be superior to the traditional noise control products.

Due to a conflict of interest, it was difficult to fully characterise every material provided for by Armacell. It was therefore decided to use a selection of their commercially available products (i.e., aerogel blankets and powders) and produce my own silica aerogels in the form of granules to carry out this research project. This allowed me to physically change the properties of aerogels in a systematic way. I was able to modify pore morphology, grain size and density and compare to those that were widely available, commercially, and understand the acoustical properties therein.

This thesis project focussed on understanding the acoustical properties of composite aerogel materials, as this is one of the most attractive and commercially viable ways of using such materials in industry. Fiberglass is well known for its outstanding sound insulation properties. Moreover, aerogels have

also shown to have good thermal and acoustic performance. Yet, how the two behave together and at what composition provides maximum acoustical benefit is still largely unknown. It was decided to introduce different volume fractions of aerogel powder into fibreglass blankets. This was difficult to recreate in a methodical manner and was therefore decided, by Armacell, that they could provide controlled, mechanically injected percentage volume fractions of aerogel powder into fibreglass to understand which composition provides the best acoustically pleasing material.

It was interesting to see the acoustical performance of granular aerogels and those in their composite form with fibreglass. It is known that many commercially available aerogels are used in small, loose powder form (in the order of 20–40 μm). Industries prefer to manufacture in this way, due to ease in time and cost. Micron-sized aerogels behaved much differently to granular aerogels (in the millimetre size). They showed lightly damped, resonance behaviour at low frequency and it was because of this interest, that such materials of a physically different size were investigated further.

From this, the objectives of the PhD study were:

- (i) to carry out a full microstructural and acoustical characterisation of silica aerogel blankets manufactured by Armacell;
- (i) synthesise new silica aerogel materials;

- (ii) apply a valid mathematical model to predict the acoustical properties of aerogels;
- (iii) to support the material production and quality control teams at Armacell to meet the industry standards for vibro-acoustic and thermal insulation performance of their products.

Silica aerogels were provided for by sponsor company, Armacell, in the form of pure silica aerogel powder (of the micron grain size) and powder impregnated into fiberglass mats. A two-step, acid-base sol-gel process was used to produce millimetric grain-sized aerogels of different sol silica concentration and density followed by an ambient pressure drying (APD) process instead of the typical supercritical drying (SCD) process with a CO₂ solvent exchange. This work was completed in collaboration with Empa (Switzerland). The materials were measured for their sound absorption properties using a special impedance tube. The results validated using a range of mathematical models from references [9–12].

1.3 Thesis outline

The thesis comprises of a collection of four journal papers, four of which are published. Each article constitutes a chapter written and formatted as when it was submitted for publication. Chapter 2 is a review paper published in the

Journal of Non-Crystalline Solids [8]. It makes a careful analysis of the existing data and the models used to predict the acoustical properties of silica aerogel-based products used for sound absorption and/or insulation. The work identifies the clear need for more methodical evaluations on the acoustic properties of pure silica aerogels and aerogel-composites and validation using more advanced analytical models and paves the way for more research which are reported in Chapters 3-5.

Chapter 3 is the paper published in the Journal of Acoustical Society of America. This paper studies the acoustical properties of air-saturated aerogel powders of micrometric grain sizes. There has been little or no systematic research into the non-linearity of the acoustical properties of these types of aerogel powders. Also, it is not clear which physical processes control the acoustic absorption and/or attenuation in very light, loose powders.

Chapter 4 is the paper published in the Special Issue of the Journal of Applied Science [1]. It explains, with the help of a model, the observed acoustical properties of fibreglass blankets impregnated with different concentrations of silica aerogel powders. Although it has been known that fibrous blankets offer high acoustic absorption and thermal insulation performance, it has been largely unclear how the incorporation of aerogel powder affects the overall acoustic absorption performance. There has been a lack of studies that explain the measured absorption properties of these materials with a valid

mathematical model [10]. Chapter 4 contributes to this knowledge gap through a mathematical simulation which predicts the complex acoustic reflection coefficient of aerogel blankets with different filling ratios measured in a careful experiment.

It was found that for powder silica aerogels embedded into fiberglass mats, the model was not able to fully capture the physical behaviour of the blanket layer. When the blankets had a filling ratio of 0 to 50% aerogel powder, the inverted porosity values matched the measured porosity values within 3%. When the filling ratio reached 100%, the inverted porosity value was significantly less at 50.5% to that of the measured porosity value at 93.6%. This shows that the model only accounted for the classical visco-thermal and inertia effects in the pores. It was then recommended to refine this, as an unrealistic pore size and porosity value was always required to achieve good fit in the data.

Chapter 5 is the paper published in the Journal of the Acoustical Society of America [6]. This work found that while visco-thermal and inertia effects are important in classical granular materials such as glass beads, the rarefied gas flow and heat transfer in the inner-particle transport macropores, inter-scale (voids to/from inner-grain pores) pressure diffusion, and inter-scale (transport-to/from meso pores) mass diffusion needs to be accounted for to predict the acoustical properties of granular aerogels. It was important to understand that such effects were controlled by the presence of transport and mesopores in

silica aerogels and perhaps only a proportion of the mesopore length in the direct vicinity of the transport pores or grain surface influence the acoustical properties.

Chapter 6 is a summary of the key research findings from each of the four chapters. It also contains the recommendations and provides recommendations for future work and justification for the need for more research in this area of material science and acoustic engineering.

This PhD work has also resulted in several reports and talks given to our industry partner, Armacell, or presented at various conferences and workshops. These documents have not been published openly, but they report useful data from other experiments carried out to determine chemical and microstructural properties of aerogels. It is a part of the supplementary material that can be found on the Google Drive [13]. This repository also contains an extensive set of analytical data on the chemistry and physics of silica aerogels studied in this work.

References

1. H. Begum, K.V. Horoshenkov, "Acoustical Properties of Fiberglass Blankets Impregnated with Silica Aerogel," *Appl. Sci.*, 11, p. 4593, 2021.
<https://doi.org/10.3390/app11104593>
2. D.A. Bies, C.H. Hansen, "Engineering Noise Control: Theory and practice," (4th ed.). CRC Press. 2009.
<https://doi.org/10.1201/9781315273464>
3. J.V. Buskirk, P. Middleton, "Rieter Automotive: Lightweight Noise Protection' , *Tech. Text.*, 42, p. 45. 1999.
4. K.V. Horoshenkov, "A review of acoustical methods for porous material characterisation," *Int. J. Acoust. Vib.*, 22, pp. 92–103, 2017.
5. J.-F. Allard and N. Atalla, *Propagation of Sound in Porous Media: Modeling Sound Absorbing Materials* (2nd ed. Wiley, Chichester, 2009), pp. 327.
6. H. Begum, K.V. Horoshenkov, M. Conte, W.J. Malfait, S. Zhao, M.M. Koebel, P. Bonfiglio, R. Venegas, "The acoustical properties of tetraethyl orthosilicate based granular silica aerogels," *J. Acoust. Soc. Am.*, 149, pp. 4149–4158, 2021. <https://doi.org/10.1121/10.0005200>
7. B. Fubini, "Surface Chemistry and Quartz Hazard," *Ann. Occup. Hyg.*, 42(8), pp. 521–530, 1998.
[https://doi.org/10.1016/S0003-4878\(98\)00066-0](https://doi.org/10.1016/S0003-4878(98)00066-0)

-
8. Z. Mazrouei-Sebdani, H. Begum, S. Schoenwald, K.V. Horoshenkov, W.J. Malfait, "A review on silica aerogel-based materials for acoustic applications," *J. Non-Cryst. Sol.*, 562, p. 120770, 2021.
<https://doi.org/10.1016/j.jnoncrysol.2021.120770>
 9. R. Venegas, C. Boutin, O. Umnova, "Acoustics of multiscale sorptive porous materials," *Phys. Fluids*, 29(8), p. 082006, 2017.
<https://doi.org/10.1063/1.4999053>
 10. K.V. Horoshenkov, A. Hurrell and J.-P. Groby, "A three-parameter analytical model for the acoustical properties of porous media," *J. Acoust. Soc. Am.*, 145(4), 2512–2517 (2019),
<https://doi.org/10.1121/1.5098778> and
<https://doi.org/10.1121/10.0000560> (Erratum).
 11. D.L. Johnson, J. Koplik, and R. Dashen, "Theory of dynamic permeability and tortuosity in fluid-saturated porous media," *J. Fluid Mech.* 176, 379–402 (1987), <https://doi.org/10.1017/S0022112087000727>
 12. Y. Champoux and J.-F. Allard, "Dynamic tortuosity and bulk modulus in air-saturated porous media," *J. Appl. Phys.* 70(4), 1975–1979 (1991),
<https://doi.org/10.1063/1.349482>
 13. [Online] Available:
<https://drive.google.com/drive/folders/1epZ2liKfw5BaCpxAMN4OVgu9mAOxG5Qu?usp=sharing> Accessed on 09 December 2021

Chapter 2: Literature review

A review on silica aerogel-based materials for acoustic applications

This chapter is published as:

Z. Mazrouei-Sebdani, H. Begum, S. Schoenwald, K.V. Horoshenkov, W.J. Malfait, "A review on silica aerogel-based materials for acoustic applications," *J. Non-Cryst. Sol.*, 562, p. 120770, 2021.

<https://doi.org/10.1016/j.jnoncrysol.2021.120770>

Co-authorship statement:

The principal author of the paper is Z. Mazrouei-Sebdani. The contribution of H. Begum is Section 2.6, 2.7 and review and editing of the paper.

2.1 Abstract

Silica aerogels are popular in terms of production volume and real-world applications. Although the current market growth rate is driven exclusively by thermal insulation, aerogels may also be attractive for acoustic applications with the potential in aiding sound absorption/insulation. This paper is a summary of

the acoustics related studies of silica aerogel-based products. It introduces silica aerogels, some acoustic characterisation methods, and reviews systematically the available data on sound absorption/insulation of silica aerogels, polymer-silica aerogel composites, nonwoven-silica aerogel blankets, and aerogel renders/glazing. The work identifies areas where further research is required, including experimental and theoretical work on the physics of sound absorption in mesoporous materials, and more systematic and standardised evaluations of the acoustic properties of aerogel and aerogel-composites. Aside from this call to action, the opportunities, and barriers for the commercialisation of silica aerogel products for acoustic applications are presented.

Keywords: Silica aerogel; composite-aerogels; acoustic application; insulation properties

2.2 Silica aerogel

Aerogels are predominantly mesoporous, open-cell solids with large internal porosity and hence low density [1-3]. The microstructure, more than the specifications of the material that makes up the tortuous network of nanoparticles or fibres, is primarily responsible for aerogel's exceptional material properties, such as high surface area, high mesoporosity, and ultra-low thermal conductivity. Aerogels are typically derived from wet gels, themselves prepared by sol-gel processes, and are dried using supercritical fluids, most often CO₂, freeze-drying, or evaporative drying [3]. A wide variety of materials, including polymers, biopolymers, and metal oxides can be turned into aerogels, but silica aerogels are by far the most common, particularly in terms of production volume [4]. The most widely adopted commercial application of silica aerogel capitalises on the ultra-low thermal conductivity, which is reduced to half of that of standing air because the mesopores are smaller than the mean free path length of the air molecules. Silica aerogel thermal superinsulation constitutes a rapidly globally growing market. Other potential applications of aerogels include acoustic insulation, catalysts and catalyst supports, gas filters and gas storage materials, conducting and dielectric materials, but these have not yet made a significant impact in the market [5,6].

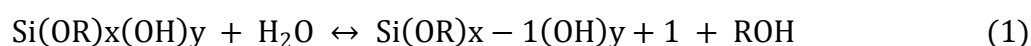
2.3 Synthesis

2.3.1 Gelation

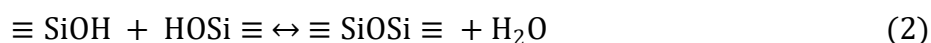
A silica gel is produced by a sol-gel process where a silica sol, i.e., a stable colloidal suspension of silica nanoparticles, is destabilised, typically through the addition of a gelation catalyst to change pH and thereby surface charge. The gels can be classified according to the pore fluid, e.g. hydrogel (water), organogel (organic solvent), alcogel (alcohol), and aerogel (air) [7,8]. During the sol-gel transition, the primary particles are formed and then they aggregate into the secondary particles (clusters), and finally interconnect in a pearl necklace morphology [9], as shown in Figure 2.1. Industrially relevant silica precursors include waterglass, ion-exchanged waterglass, and silicon alkoxides [10-13]. Waterglass is a sodium silicate solution with a Na/Si molar ratio above 1.5. It can be gelled by the addition of an acid (partial neutralisation). It is arguably the most inexpensive silica precursor. The sodium ions in waterglass can have a strong, negative effect on microstructure and properties. Therefore, ion-exchanged waterglass, a silicic acid solution obtained, e.g., by passing waterglass solution through an ion-exchange resin, is another common precursor. Ion-exchanged waterglass can be gelled by the addition of a base (partial neutralization), and it is more flexible in its use compared to non-ion-exchanged waterglass, but the ion-exchange step adds a considerable cost. The gelation solvent for both regular and ion-exchanged waterglass is typically

water, which may necessitate additional solvent exchanges during subsequent processing, although ethanol can be added as a co-solvent [14,15], and single-step exchanges have been developed [11,16-19].

Silicon alkoxides, particularly tetraethyl orthosilicate (TEOS) and tetramethyl orthosilicate (TMOS) have transformed the aerogel field. Alkoxide based silica sols are produced through hydrolysis (Eq. 1) and water/alcohol condensation (Eqs. 2 and 3, respectively) reactions of the form:



where x and y the initial number of alkoxy ($x=4,3,2,1$) and silanol groups ($y=0,1,2,3$); and R =methyl/ethyl.



These reactions run simultaneously and are catalysed by the addition of an acid or base. Aside from monomeric TEOS, oligomeric ethyl silicates with higher SiO_2 contents are also available. Alkoxide-based aerogels are often produced through a two-step acid-base synthesis procedure where a stable, acidic silica sol is produced from TEOS or TMOS, followed by base-catalysed gelation [3,20,21]. Inherently hydrophobic silica aerogels derived from methyltri(m)ethoxysilane can have exceptional thermal and mechanical properties [3,22-25], but are not the topic of this review paper, because they

are not yet commercially available in large quantities and should be considered as $\text{SiO}_{1.5}(\text{CH}_3)$ rather than SiO_2 aerogels.

2.3.2 Aging

The gel prepared in the first step is aged in its mother solution, or less commonly in freshly prepared silica. This aging process strengthens the gel by reinforcing the inter-particle necks and prevents excessive shrinkage during the drying step [26,27] (Figure 2.1).

2.3.3 Hydrophobization/surface modification

Because of the extreme susceptibility of hydrophilic silica aerogels to be damaged by liquid water and water vapour, the vast majority of commercially available silica aerogels have been hydrophobized prior to drying [28,29]. By far the most common strategy is silylation of the silica gel's surfaces with trimethylsilyl groups by soaking gels in a solution of trimethylchlorosilane, hexamethyldisilazane, or hexamethyldisiloxane. Hydrophobization can be a time- and cost-intensive process and there is extensive scientific and patent literature on increasing the effectiveness of the hydrophobization step [11,17,30,31]. Aside from the increased long-term stability, hydrophobization

also enables ambient pressure drying as a potentially more cost-effective drying technique (see Section 2.3.4).

2.3.4 Drying

Drying is the final, and arguably most critical step in aerogel production. The small pore size results in very large capillary stress due to surface tension at the solid-solvent-gas interface during evaporative, ambient pressure drying (APD). This capillary stress leads to pore collapse and densification unless special precautions are taken [32]. The first solution eliminates capillary stress by circumventing the pore fluids boiling curve, either through supercritical fluid drying (SCD) at pressures and temperatures above the supercritical point or by freeze-drying (FD) at temperatures and pressures below the triple point. Ice crystal growth during FD increases macroporosity at the expense of mesoporosity, reduces surface area, and is not particularly relevant for silica aerogel production. Supercritical drying directly from the organic solvent (typically an alcohol), which was developed by Kistler for the first-ever produced aerogels nearly a century ago [1], has some inherent limitations in terms of safety because of the solvent flammability and the high temperature/pressure required to surpass approach the critical point, e.g. 243°C and 63 bar for ethanol [33-35], but the efficiency of the process can be increased by confining the

samples in moulds to limit the need for excess alcohol through a Rapid Supercritical Extraction process (RSCE) [36-39].

An alternative drying scheme, based on CO₂ with its critical point at 31°C and 73 bar, as the supercritical fluid eliminates the problems of flammability and high process temperature, is now a routine procedure in academic research as well as in industrial production, particularly for silica aerogel blankets [27,35,40]. Supercritical drying does not require a prior hydrophobization step, but such a treatment is carried out nonetheless for most commercial products to improve service life stability. Even with CO₂ instead of alcohol as the processing fluid, SCD still requires high-pressure autoclaves and, therefore, it is a batch-type process by definition. However, SCD remains an industrially established production method, particularly for silica aerogel blankets and polymer aerogels. The discovery of silylation of the silica surfaces effectively prevents silanol condensation (see eq. 2) and irreversible pore collapse during evaporative drying [41] opened up the possibility for ambient pressure drying. Ambient pressure drying has now become a routine process in industrial silica aerogel production, particularly for silica aerogel granulate and powder. During ambient pressure drying, capillary forces and contaminant gel shrinkage do occur, but the gels can spring-back to recover most of the original volume if the samples have the required mechanical stability, e.g., through aging [42].

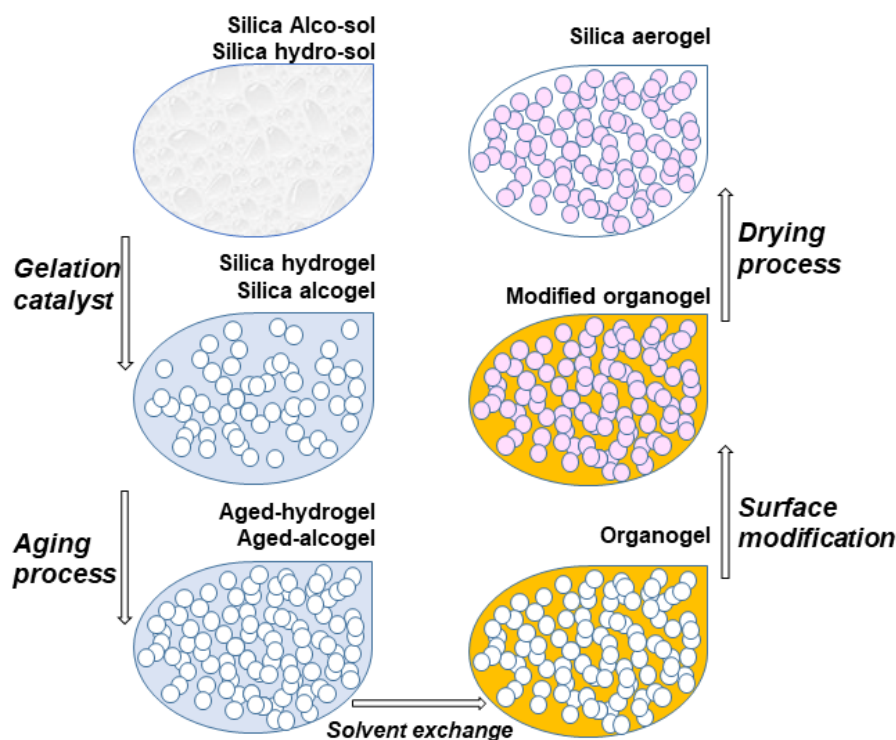


Figure 2.1 Schematic design of silica aerogels synthesis. The surface modification (typically hydrophobization) is optional. The drying step can be carried out at ambient pressure or using supercritical CO₂ or ethanol drying.

2.4 Silica aerogel properties

Silica aerogel is available commercially in particulate form (granulate and powder) and as fibre-reinforced blankets, but large monolithic pieces of aerogel are not available in significant quantities. Despite the variety of silica precursors, hydrophobization agents, and drying technologies (see Section 2.3), most high-quality, industrially produced silica aerogels have surprisingly uniform

properties when recalculated to the aerogel phase itself, i.e., excluding fibre reinforcement or inter-granular macroporosity: envelope or bulk densities of $\sim 0.120 \text{ g/cm}^3$ corresponding to porosities of $\sim 95\%$, high mesopore volumes, surface areas of $700\text{--}900 \text{ m}^2/\text{g}$, and thermal conductivities around 15 mW/mK .

2.4.1 Microstructure

Silica aerogels have fractal structures according to small-angle X-ray and neutron scattering data, and thus have a similar appearance when observed at different length scales. Primary silica nanoparticles ($\sim 5 \text{ nm}$ diameter) link up to form a pearl-necklace type skeleton that can be visualised by the higher magnification offered by TEM (Figure 2.2(A)). At lower magnification (SEM), secondary particles ($\sim 20 \text{ nm}$ in diameter), i.e., porous aggregates of primary particles, enclose the aerogel mesopores (Figure 2.2(B)). Nitrogen sorption analysis confirms the high mesopore volume, even though extracting pore size distributions from the isotherms is hampered by the aerogel deformation during the sorption analysis [43].

2.4.2 Thermal conductivity

Silica aerogels are thermal superinsulators with thermal conductivities as low as half that of standing air (less than 15 mW/mK for aerogel versus 26 mW/mK for air) and this is by far their most important unique selling point [2]. Aerogels owe their low thermal conductivity to the small pore sizes (<50 nm) compared to the mean free path length of the gas molecules (~70 nm for air at ambient pressure and temperature), which limits gas-phase conduction through the Knudsen effect. In addition, solid conduction through the silica skeleton is limited by the highly tortuous network structure of nanopores [44].

2.4.3 Mechanical properties

The highly porous and tortuous, pearl necklace structure of silica aerogels is highly effective at reducing thermal conductivity, but it inevitably limits mechanical strength. Therefore, it is a major barrier against the more widespread adoption of aerogels. The mechanical properties of neat silica aerogels display a complex dependence on the bulk or envelope density (Figure 2.2(C) and 2.2(D)) [16]. At envelope densities below ~0.090 g/cm³, silica aerogels are not brittle but deform plastically and irreversibly upon compression and their Young' s modulus (E) is very low. At higher densities, e.g., above ~0.150 g/cm³, silica aerogels are brittle, albeit their Young' s

modulus is much higher. At the intermediate densities typical for most commercial silica aerogels, around 0.120 g/cm^3 , silica aerogels behave elastically and recover most of the original volume after decompression. However, they are still relatively brittle with a rather low compressive strength. As for most aerogel materials, Young's modulus displays a power-law behaviour on envelope density, with $E \sim \rho^{3.6}$ (Figure 2.2(C)) [16].

Reinforcement of silica aerogels has been a very active field of research and seminal studies by Leventis, Meador and co-workers who have shown impressive improvements in mechanical strength albeit at the cost of higher densities and thermal conductivities and reduced translucency [45-48]. More recent studies have shown that reinforced aerogels can maintain their low thermal conductivity and achieve modest improvements in mechanical strength [49,50]. None of these stronger silica aerogels are currently available in industrial quantities, but commercialisation is ramping up through start-up companies, e.g., Aerogel Technologies (USA) and TIEM Factory (Japan). The aerogel industry overcomes the mechanical drawbacks in two main ways: i) through the production of particulate silica aerogel (powder or granulate) as a semi-finished product that is incorporated into a matrix to impart mechanical strength; and ii) through the incorporation of silica aerogel into a fine fibre blanket that improves handling and mechanical stability, e.g., by impregnating non-wovens with a silica sol or silica aerogel slurry.

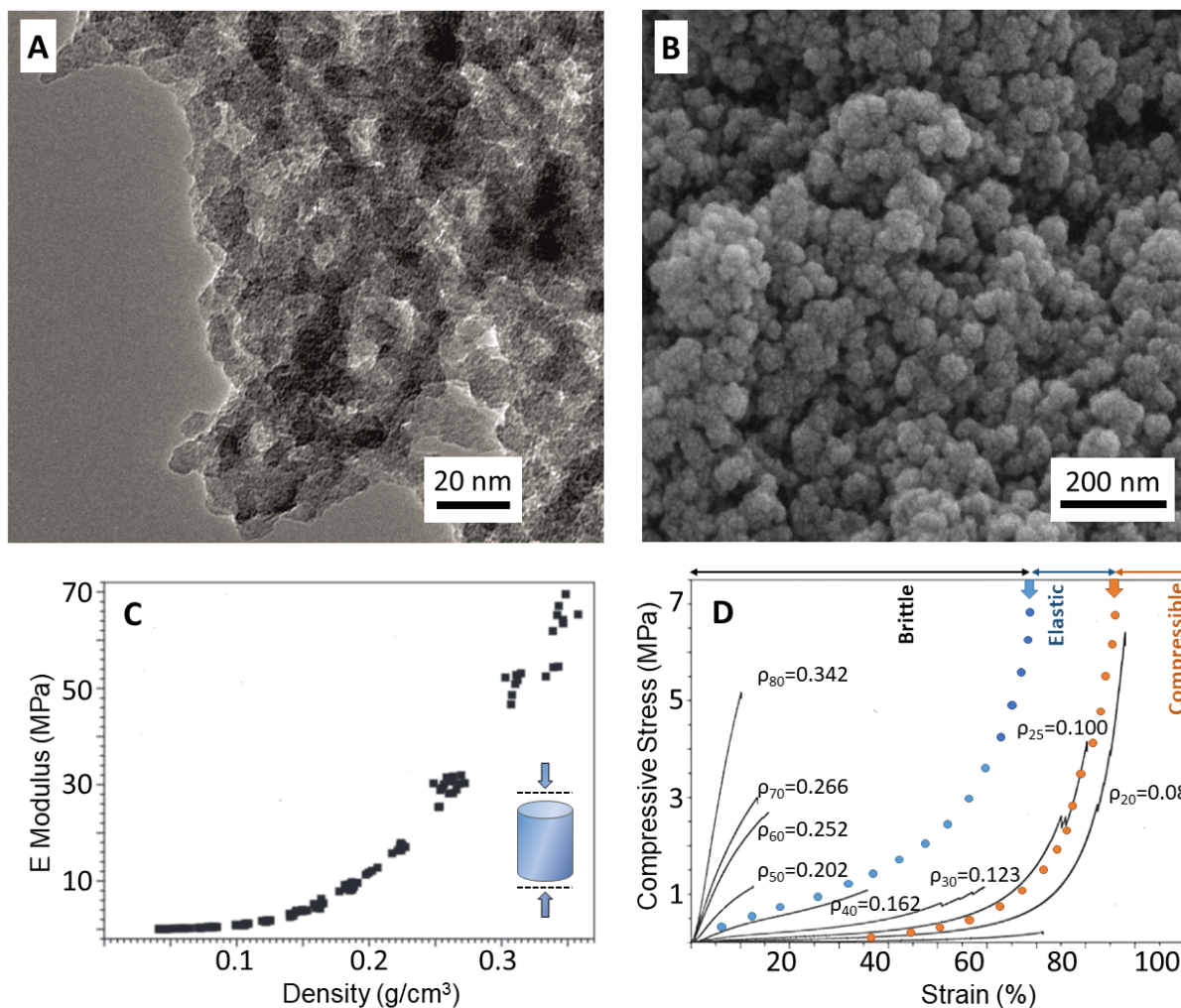


Figure 2.2 Silica aerogel microstructure and mechanical properties. (A) TEM image [31], (B) SEM image [51], (C) E-modulus as a function of density, (D) Stress-strain curves during uniaxial compression: ρ_x represents density (g/cm^3) and x corresponds to the volume concentration of polyethoxydisiloxane in the initial colloidal suspension [16]. Revised/reproduced with permission from references [16,31,51].

2.5 Aerogel Applications

Thermal insulation is by far the dominant application of aerogels that has been successfully transferred to the marketplace [44,52]. The main markets are pipeline insulation (oil-and-gas), aerospace, industrial insulation, and building insulation. The production ramp-up by Aspen Aerogel (blankets) [53,54] and Cabot (granulate) in early 2000 has been followed by strong market growth and the entry of new, mostly Asian producers in the last 5 years. Aside from thermal conductivities, a wide variety of other applications that take advantage of the other exceptional properties have been proposed (Table 2.1), but until now, none of these have made a significant impact on the market.

Table 2.1. Selected silica aerogel applications.

Application	Examples	Technology readiness
Thermal insulation	Low heat transfer materials especially for constructions, [52-59], other applications like pipes, appliances, transportation, machinery, space vehicles [55,60-64], and	Large-scale industrial production [52-54,56]

	firefighter and thermal protective clothing [65,66]	
Acoustics	Acoustic matching layers for ultrasonic transducers with low sound velocity and impedance [55,63,67-74] Sound absorption/insulation especially for Construction [60,62,63,75-91] Footfall sound insulation [92,93]	Pilot production [79,86,87]
Filtration, separation, and sorption	Liquid/gas filters and absorbers for paints, varnishes, functional liquids [18,94]	Academic research
Electrical application	Dielectrics, microwave electronics, electrically conductors, electrodes [55,60,88] High voltage insulator, sensor material, impedance adjustment, Cerenkov detectors [63] thermoelectric and piezoelectric materials [92]	Academic research

Optics	Silica glass, mirror backings, laser glass, light source, solar windows, anti-reflective layer for solar cells [55,61]	Niche applications
	Cherenkov Counters [55,92]	
Space application	Space dust particles absorber [55,74,92]	Niche applications
	Thermal insulators [55,74]	[95]
Kinetic energy absorbing	Tank baffles, star dust impact, shock absorption [63]	Academic research
Fillers	Fillers for paints, elastomers, thermoplastics, and thermosets [8,63,82,96-99]	Academic research
Carriers	Carrier materials for fungi/herbs/pesticides and drugs [63,92,100]	Academic research
Catalysis	Biocatalysts, automobile gas pollutant reducers [92,101]	Academic research

2.6 Sound absorption and insulation

2.6.1 An introduction to sound absorption/insulation

Noise is defined as any perceived sound that is objectionable to a human being [85]. This harmful noise must be controlled to have an acoustically pleasing and safe environment [102]. There are several methods to control the noise's adverse effect either by sound insulation or sound absorption according to the end-use requirements [85]. When a sound wave impinges on a material, it is partially reflected, transmitted, and absorbed.

Sound absorbing materials usually are low density porous materials, with a moderate airflow resistance which can absorb most of the sound energy and prevent sound reflections by allowing sound to penetrate their open cavities or channels [85]. Porous absorbing materials can be classified as cellular, fibrous, or granular materials, e.g., foams, nonwovens, or porous concrete, respectively. Depending on the solid skeleton, and the size and geometry of the pores, the air molecules within the pores/channels of the porous material are forced to vibrate and lose some of their original energy through conversion into heat due to thermal/viscous losses at the walls of the interior pores. In fibrous materials, much of the sound energy can also be absorbed by viscous friction and inertia effects around the individual fibres. Sound absorbing materials are often used in conjunction with barriers to improve their sound insulation effectiveness [4].

Porous media dominate noise control applications in most environments, ranging from factories to homes [103,104]. Figure 2.3(A-C) shows porous sound absorbing materials and some of the physical models describing their absorbing mechanisms.

However, there are other types of sound absorbing structures such as Helmholtz and plate resonators as well as membrane (micro-perforated) absorbers [103]. Tuned resonators, like Helmholtz resonance absorbers and plate absorbers are those absorbers that their frequency curve of absorption shows a large absorption peak in a narrow band only like materials having holes. The simplest view of a Helmholtz resonator, as shown in Figure 2.3(D), is an empty bottle with a neck on top. A volume of air in and near the open neck vibrates because of the spring behaviour of the air inside the bottle. A mass, either an air mass (Helmholtz absorber) or a solid (plate absorber), are coupled with a soft material or even an air volume acting as spring. When sound excites this system at its particular resonance, it dissipates sound power due to its intrinsic damping. The Helmholtz resonator uses a column of air (cross section S and length l) as mass and volume V as spring, shown in Figure 2.3 (D) [105]. A very common example is a plate containing holes and slits with a layer of porous absorbing material behind it to reduce the stiffness of the spring and increase its damping. In this review article, we see how sound absorption

properties of the silica aerogel materials is different from or similar to those of conventional porous or resonance absorbers.

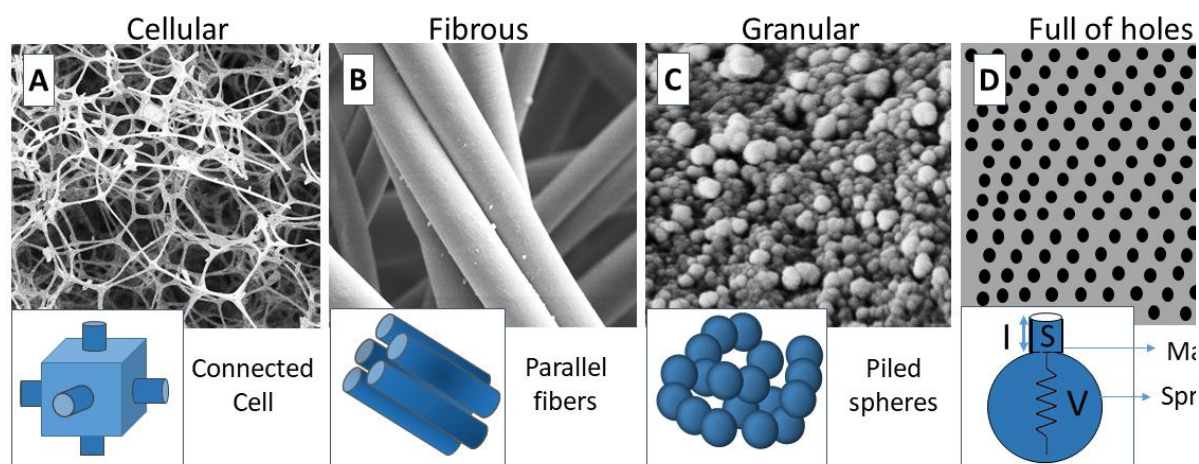


Figure 2.3 (A-C) The three main types of porous absorbing materials and (D) Resonance absorbers of type Helmholtz.

In contrast to sound absorbers, airtight materials, or materials with a high airflow resistance, like steel or composites, are better sound insulators, as sound waves in air have to be coupled to the solid and vice-versa to be transmitted through the layer. In general, the sound insulation effectiveness of a single layer of conventional materials depends upon their stiffness and mass. The mass law states that a material having a high mass per unit area will insulate better. Accordingly, single layers of lightweight materials are not good for sound insulation, but multiple layers of lightweight material with layers of soft material

or of air gaps in-between are more effective sound insulators in this case. Here, as well porous materials, are added in the enclosures between the solid layers to increase sound insulation [4] by reducing the coupling between the solid layers and increase the damping.

However, the open question is whether low-density aerogels can be suitable for acoustic insulation [55,92]. Sound wave propagation occurs in these types of materials in the fluid of the pores and in the solid skeleton or wave propagation if both phases are coupled. The incident wave is slowed down and attenuated because the wave energy is progressively transferred into heat due to a range of physical phenomena such as inter-particle friction, viscous losses in the material pores, thermal, pressure diffusion and sorption effects. The interstitial gas nature, particle bonds, material properties of the solid, geometry, and distribution of the pores, determine which effect is governing for a particular material. For aerogel-based materials, these effects are not fully understood, yet a wide variety of approaches for material preparation exist. The longitudinal speed of sound in the silica aerogel pores is typically of the order of 100 m/s or less [55,61] even though this number for non-porous silica is about 5,000 m/s [68].

2.6.2 Types of acoustic measurements

Sound absorption and insulation are complex functions of intrinsic material properties and extrinsic properties such as surface roughness, sample geometry, and thickness. As a result, collecting accurate acoustical data and their interpretation are more difficult than for data on purely intrinsic properties such as density or thermal conductivity. Many studies that report the acoustic properties of aerogels and aerogel composites do not provide sufficient information of the measurement conditions, intrinsic and extrinsic properties of aerogels to enable a useful evaluation or comparison of their ability to work as a sound absorbers or insulator. Here, we briefly review the techniques, instrumentations, and norms for acoustic measurements.

The impedance tube (ISO 10534-1&2) [106,107] and reverberation room methods (ISO 354) [108] are the most commonly employed technique to measure the sound absorption coefficient. The sound insulation, or airborne sound transmission loss, of material systems, can be measured on small samples via impedance tubes [109] or large samples as a building material or additional lining on them via a standard series of ISO 10140: Part 1-5 [110]. Usually, measurements are made with the high-frequency resolution, but presented in 1/3rd octave bands with the following centre frequencies (Hz): 100, 125, 160, 200, 250, 315, 400, 500, 630, 800, 1000, 1250, 1600, 2000, 2500, 3150, 4000, 5000, as specified in ISO 266 [111].

2.6.3 Sound absorption measurement

The sound absorption coefficient (α) is a dimensionless number ranging from zero to one. It is the proportion of the incident sound energy absorbed by the boundary:

$$\alpha = I_a/I_i \quad (4)$$

where, I_a and I_i are the absorbed and incident sound intensities in W/m^2 , respectively. To be a good sound absorbing material, the value of α should be as close as possible to one which indicates that a high proportion of the energy in the sound wave incident to the material is absorbed (including absorption within the material structure and transmission) [112].

Measurement of the normal incidence acoustic absorption coefficient in the impedance tube is the most common way to determine the ability of a porous material to absorb sound, especially in the research and development stage. An impedance tube is frequently used in the development of new materials because it is a compact set-up that can quickly determine absorption data at relatively low cost and only small samples are required. The apparatus is essentially a cylindrical tube with a test sample holder at one end and a sound source at the other end (Figure 2.4). From the sound pressures in the incident and reflected wave, some of the acoustic properties can be calculated [107].

Impedance tubes typically use one of two methods: (1) the standing wave method (ISO 10534-1) [106] and (2) the transfer function method (ISO 10534-2) [107] (Figure 2.4). The standing wave method is out-dated at present and the transfer function method, which uses the ratio of pressures between two microphone positions, is the most common method to measure the absorption coefficient. The minimum frequency range for a tube is controlled by the microphone spacing, whereas the maximum frequency range is controlled by the tube diameter [107].

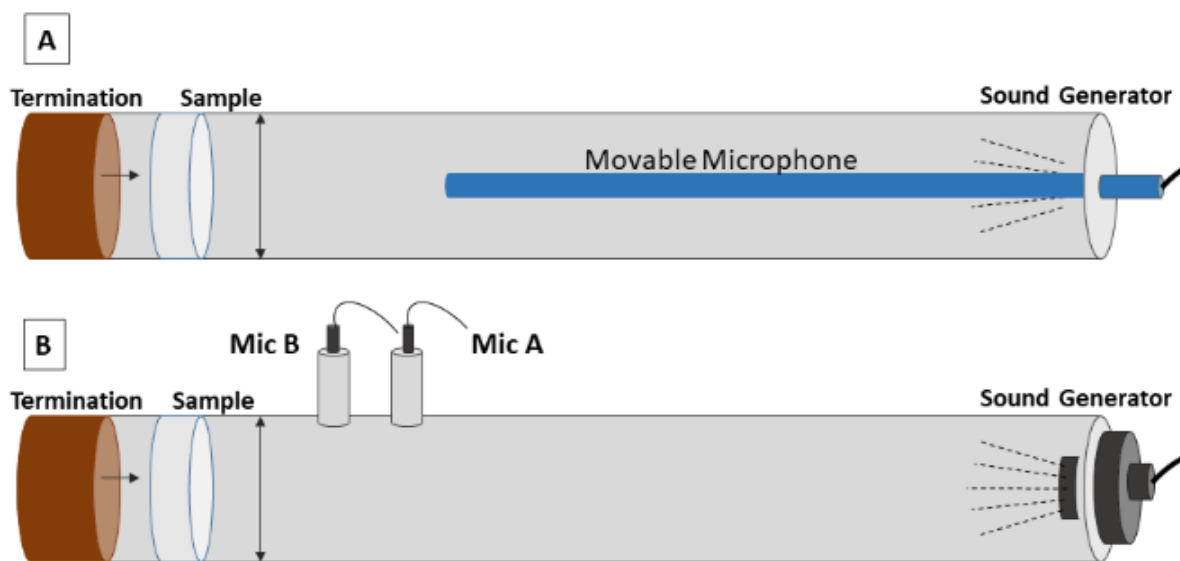


Figure 2.4. Impedance tubes (A) Standing wave method and (B) Transfer function method.

The ISO 10534-2 method [107] directly measures the complex acoustic reflection coefficient at frequency of f (Hz), from which the absorption coefficient spectrum is calculated as:

$$\alpha(f) = 1 - |r(f)|^2 \quad (5)$$

The reflection coefficient is frequency dependent and controlled by material microstructure and geometry [107,113,114].

Measuring reverberation time in a room is another method to determine the random incidence absorption coefficient in which decay of the sound pressure level is measured with several microphones as a function of time after switching off the sound source. Originally the sound pressure level decay curves were directly determined from the sound pressure level spectra measured with a one third octave band analyser in very short time intervals after a broad band noise emitted by a loudspeaker was switched off. In-between more advanced measurement methods are very common. In this case the room response is measured with microphones at several positions, when the room is excited with a known input signal, such as a sine sweep. During post processing first the room impulse responses are determined using deconvolution techniques, band filtered and backward integrated to obtain the decay curves of the sound pressure level for each frequency band, from which the reverberation times are evaluated. When sound is emitted in a reverberant enclosed space in the

presence of a test specimen the rate of decay of this level (reverberation time) after the sound source is switched off depends on the specimen's absorption coefficient and area covered by it. The sound absorption coefficient α_s of the absorbing layer is calculated as

$$\alpha_s = A_T/S \quad (6)$$

where S (m²) is the area covered by the test specimen and A_T (m²) is the equivalent sound absorption area of the test specimen [108]. Often, the reverberation room method is used to estimate the weighted absorption coefficient, α_w , which is calculated through a comparison of the absorption spectra, $\alpha_s(f)$, with a reference curve. Based on the value of α_w , absorbers are classified from A to E, where A corresponds to products with an $\alpha_w \geq 0.90$ [112]. In contrast to the impedance tube methods, the reverberation room is not limited to normal incidence absorption coefficient as it covers all possible angles of incidence, but it does require much larger test samples [107,108].

2.6.4 Sound insulation measurement

The sound insulation performance of a material is defined in terms of the sound reduction index R , which is defined according to eq. 7.

$$R = 10 \log(W_1/W_2) \quad (7)$$

where, W_1 and W_2 are incident sound powers of the incident and transmitted waves, respectively. The sound reduction improvement index ΔR is the difference of the sound reduction indices of a basic element with and without the additional acoustic lining for each third-octave band [109,110]. The frequency-dependent values can be converted into a single number quantity, R_w .

Like for absorption the airborne sound transmission loss (TL) or reduction index (R) in dB for a normal incident sound wave can be measured in the impedance tube using the 'two-load' transfer function method [109], by acquiring the sound pressure in four fixed microphones (two of them between the samples and the sound generator source, and the other two on the back of the sample) positions. Two consecutive acquisitions are carried out for each sample by modifying the characteristics of the tube extremity (a reflective and an absorbing material should be installed) [60]. Unfortunately, this method is only useful for open-cell porous materials with a low to moderate air flow resistance, or limp porous materials with a low bulk modulus or elasticity, where sound propagation in the fluid phase of the material dominates. In most other cases physical effects due to the bending stiffness of the material dominate sound insulation, which cannot be captured correctly with the impedance tube.

For these materials, only the measurement of the diffuse field sound reduction index R , for each frequency, according to the standard test series of ISO 10140

provides the correct estimate of the transmission loss [110]. Here, a large sample of the wall or floor separates two sufficiently big rooms. In the source room sound is generated with a loudspeaker and impinges from all possible directions on the specimen that can undergo vibrations like in a real building. The sound reduction index R is determined from the incident and transmitted sound power by measuring the average sound pressure levels in both rooms and, applying diffuse field assumptions, calculating the associated sound power.

Impact sound insulation/reduction is also an important characteristic of resilient layers. Impact sound insulation reduces the sound of footsteps from people walking or falling objects on a floor structure. It is determined by the impact sound pressure level (L_i) in the room below by using a standard tapping machine for generating an impact sound source. A floating floor system in the upper room or a false ceiling in the lower room can be used to improve the impact sound insulation and therefore reduce the impact sound level [115,116]. The traditional floating floor system can consist of an elastic sound insulation layer and mortar. In addition to the full standardised test, an estimation of the sound insulation performance of a floating floor can be derived from the results of dynamic stiffness measurements performed on small-sized samples (0.04 m²) [117].

2.7 Acoustic properties of silica aerogel and aerogel composites

Conventional sound absorbers such as rock wool and open-cell foams are traditionally used for sound absorption and insulation in buildings, but industry and society are looking for alternative, environmentally friendly materials with advantageous sound absorbing/insulating properties [113] and good thermal insulation. Aerogels present an opportunity to combine good thermal insulation performance with useful acoustical properties. Sound absorption and insulation achieved with aerogels strongly depend on the method of material preparation, aerogel density, and pore structure. The sound attenuation in an aerogel relies on the fraction of energy loss of acoustic waves as they are successively emitted from the gas phase to the solid phase, this reduces the amplitude and velocity of the sound waves, causing it to slow down and dissipate faster. This can make aerogels good materials for acoustic insulation [118].

2.7.1 Sound velocity and impedance in silica aerogels

Silica aerogels [119] display unusual acoustic properties due to their particle network structure, for example extremely low sound velocities in the range of 100-300 m/s for aerogel densities between 0.07-0.3 g/m³, compared to 343 m/s in air and ~5000 m/s for silica glass [120]. Sound velocities as low as 120 m/s

have been reported as early as 1984 [67]. Most literature reports indicate that sound velocity increases with increasing density [119], but other factors may also be important. Gross et al. in 1992 [68] suggested that a simple scaling law for sound velocity $v \propto \rho^\alpha$, with $\alpha=1.3$ is true for densities higher than 0.1 g/m^3 , but at lower density, $\alpha=0.8$ is valid. Longitudinal sound velocity in solids is related to the elastic constants (bulk and shear modulus, correlated to Young's modulus). Heat-treated aerogels display higher sound velocities than untreated aerogels, as heating increases the degree of connectivity of the silica nanoparticle pearl-necklace network structure.

In 1986, Gronauer and Fricke [67] studied if the low sound velocity in aerogels was due to the air-skeleton interactions or low Young's moduli. Such effects are known to be important from conventional sound absorbers, where the fibrous structures are also small compared to the sound wavelengths in the auditory range. They concluded that sound propagation occurs via the skeleton and not through the air within the porous system, hence the low Young's moduli are the root cause for the sound velocities smaller than that of air. Sound propagation of the aerogel is primarily influenced by elastic properties of the skeleton when densities are above 0.100 g/cm^3 , whilst atmospheric pressure in the enclosed air space is important for aerogels with a density of 0.05 g/cm^3 [121,122]. In 1998, Forest et al. presented a comparison of acoustic propagation in alcogels and aerogels and showed an interesting difference: for the high

porosity alcogels, longitudinal wave velocity remains around the same velocity as in alcohol, while in aerogels, the velocity is significantly lower than that in air. They applied the Biot's model for acoustic wave propagation in porous media to study the velocity and attenuation. Biot considered the problem of the acoustical propagation in a porous elastic solid saturated by viscous fluid by deriving the equations for sound waves through the solid and fluid fractions [71].

2.7.2 Sound absorption/insulation in pure/hybrid silica aerogels

A majority of studies reporting on the acoustical properties of aerogels preferred the impedance tube method because of the smaller sample size requirements [63,75-77,80-84,119]. The transmission loss, the ability of aerogel to insulate against incident sound, is usually measured with a four-microphone impedance tube method [123]. Some studies employ their own methods for data evaluation [124], which makes the data comparison difficult. In this section, we focus on the acoustic properties of silica aerogel and its composites with polymers mostly obtained with the impedance tube data. We go through these studies in chronological order.

In 1998, Schmidt et al. [63] reported acoustic properties of pure silica aerogels, hot-press formed plates via dry mixing of silica aerogel with polyvinylbutyrale

(PVB), as well as silica aerogel bound with liquid vinylacetate/ethene. As in the case of a usual porous layer, aerogels display a 1/4 -wavelength resonance peak whose maxima shifts towards lower frequency with increased thickness (see Figure 2.5). An increase in thicknesses in this study was achieved by adding individual layers and the vibration of each layer might have influenced the measurement. The observed absorption coefficient for a $h = 40$ mm thick layer at frequencies above 600 Hz were around 0.6-0.7 which is a promising result [63]. Higher absorption ($\alpha > 0.6$) in thinner layers was achieved at frequencies at which the acoustic wavelength in the material was $d = \lambda/4$ [119]. A thermoplastic bound aerogel produced using a polyvinylbutyrale binder displayed a lower sound absorption value similar to that of expanded and extruded polystyrene with $\alpha < 0.1$ across all frequencies of interest (see Figure 2.6). However, relatively thin layers (e.g., 20 mm) of dispersion bound aerogels, made using aqueous vinylacetate-ethene, show a great improvement in sound absorption coefficient particularly at 500 and 800 Hz (see Figure 2.6).

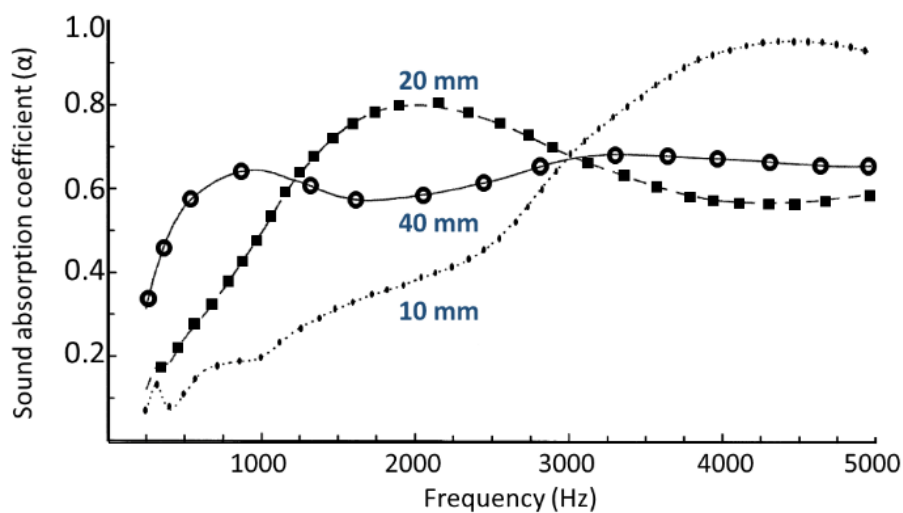


Figure 2.5 Sound absorption coefficient for different heights of an aerogel particle layer. Revised/reproduced with permission from reference [63].

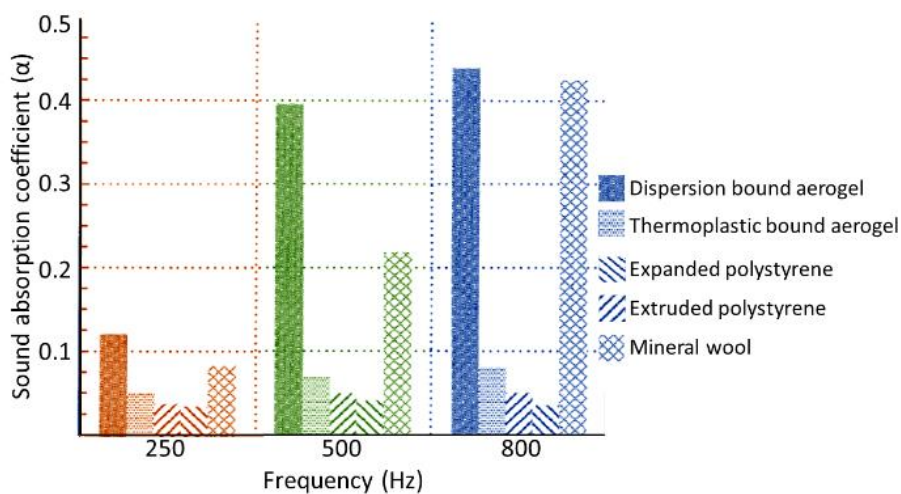


Figure 2.6 Sound absorption coefficient of different insulation materials at a thickness of 20 mm. Revised/reproduced with permission from reference [63].

Schwertfeger and Schmidt, in 2003 [93] patented the use of aerogel-polymer composites for damping of structure-borne or impact sound. In their work, a percentage of aerogel was mixed with PVB or dispersion glue followed with heat treatment which improved impact sound insulation by up to 24 dB for a layer thickness of 18 mm and 90% by volume of hydrophobic aerogel granulate [93]. A substantial acoustic improvement with a relatively low thickness of sound insulation material would be an important tool to solve the significant difficulties of building renovations by separating the mechanical tension of the old building structure from the floor covering [63].

Dong et al. in 2009 [75] produced composite aerogels with variable concentrations of silica and polydimethylsiloxane (PDMS) and evaluated their sound absorption coefficient as a function of composition and average pore size. The acoustic behaviour of aerogels developed in this work differed from that in many commercially available porous acoustic absorbers. The behaviour of these aerogels resembled that of layer membrane which is controlled by the elastic properties of aerogel (Figure 2.7). However, Dong's work did not specify the thickness of the studied commercial materials and aerogel materials. For resonance absorbers, high absorption occurs around a specific frequency, where increasing the amount of PDMS shifts the peak absorption to the higher frequency, ascribed to the reduction in pore size of ormosil aerogel. Dong et al. approximated the porous structure of the aerogels with two models of cavities:

either with a neck (Helmholtz model, eq. 8) or a sphere-like shape. For both models, they claimed that as the cavity size decreases with the increasing PDMS content, resonance-based absorption occurs at higher frequencies, e.g.

$$f_H = \frac{v}{2\pi} \sqrt{\frac{A}{VL}}, \quad (8)$$

where, v , A , V and L , are speed of sound, the cross-sectional area of the neck, volume of the cavity and length of neck, respectively [75].

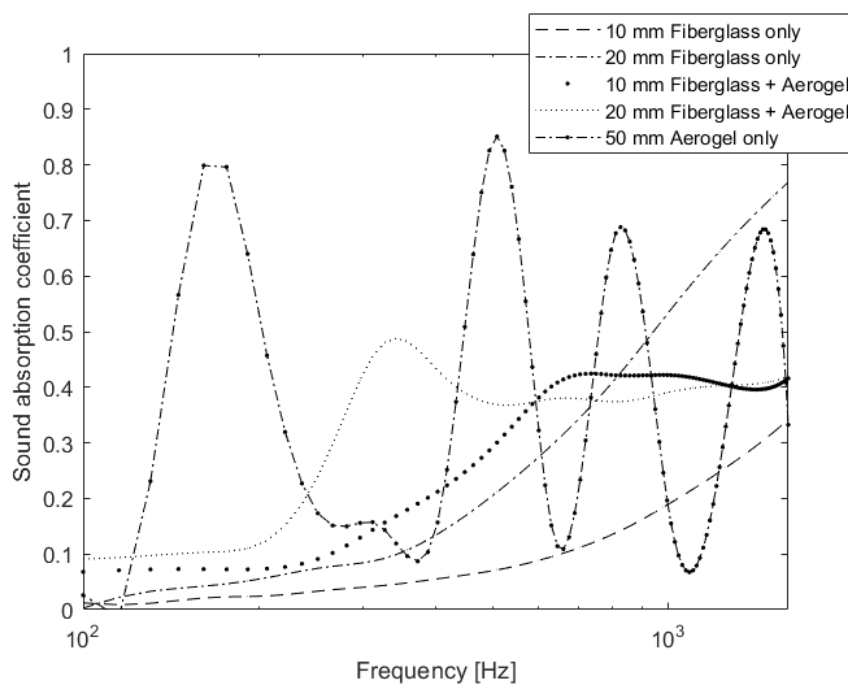


Figure 2.7 Sound absorption coefficient of silica aerogels and silica aerogel blankets with different thickness, compared to fiberglass sound absorbers.

This resonance behaviour is likely to relate to two effects. In the case when the density of aerogel is relatively low and it is granulated to a fine powder (e.g., with particle size much less than 100 μm) the incident sound wave causes fluidisation of the aerogel particles. The aerogel layer behaves like a very light equivalent fluid which causes multiple peaks in the measured absorption spectra. In the case of fibreglass blankets impregnated with aerogel powder, the flow resistivity of the blanket increases dramatically. When exposed to acoustic excitation in the impedance tube, the blanket vibrates. This vibration effect, together with the circumferential air gap effect dominate the measured absorption coefficient spectra which tends to have a single resonance peak and limited absorption coefficient beyond this peak. Figure 2.7 illustrates the sound absorption spectra for a commercial aerogel powder (particle size 2-40 μm , pore diameter 20 nm and particle density 0.12-0.15 g/cm^3) and fibreglass blanket (pore size of 20 μm in the fibres) impregnated with aerogel powder. It also provides a comparison against the absorption coefficient for two conventional fibreglass layers. This data was measured by the authors in a 100 mm diameter impedance tube. Figure 2.8 illustrates the sound absorption spectra for a commercial aerogel powder (particle size 1-20 μm , pore diameter 20 nm and bulk density 0.04-0.10 g/cm^3) with resonance behaviour, and melamine foam (pore size 115 μm) with porous material behaviour, both with a hard-backed layer thickness of 50 mm. The data was measured by the authors

in a 10 mm and 100 mm diameter impedance tube respectively. Comparing Figures 2.7 and 2.8 with previous works [62,73,80], aerogel powder in the micron size range shows continuous peaks across the whole frequency range of 100 to 4000 Hz than aerogels with a larger particle size in the millimetre size range. Resonance behavior of aerogels was also reported by Cai et al. in 2012 [76] for methyltrimethoxysilane (MTMS)-vinyltrimethoxysilane (VTMS) based monolithic aerogels with a thickness of 1.6 cm. Two commercially available acoustic insulation materials, an open-cell polyurethane (PUR) foam with a non-woven scrim (Insulator A, thickness = 2.0) and a non-woven fibre material (Insulator B, thickness = 4.3 cm) were also tested for comparison. Maxima in the absorption coefficient were observed in the frequency range of 540-830 Hz and also at the higher frequency range of 1570-1860 Hz, while insulators A and B exhibit improved acoustic absorption as frequency increases. Strong absorption peaks observed at both low and high-frequency regions may indicate multiple resonances within the aerogel [76].

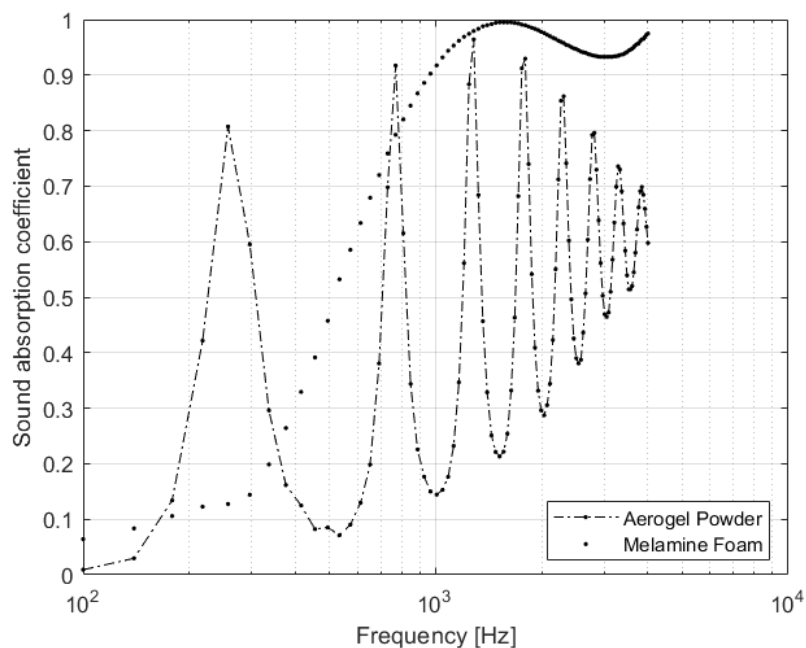


Figure 2.8 Sound absorption coefficient of silica aerogel, compared to a melamine foam (thickness 50 mm).

In 2014 Yan et al. synthesised polyimide-silica aerogel composites and measured their acoustic absorption coefficient in a 16 mm diameter impedance tube [77]. They reported resonance behaviour for the sound absorption coefficient with two to three peaks in the 2.5-10 kHz range (see Figure 2.9). As expected, the positions of the maxima in the absorption coefficient spectra depended on sample thickness: for 10 mm, peaks occur between 5-8 kHz while for a thickness of 30 mm the peaks occur at 2.5, 7, and 10 kHz.

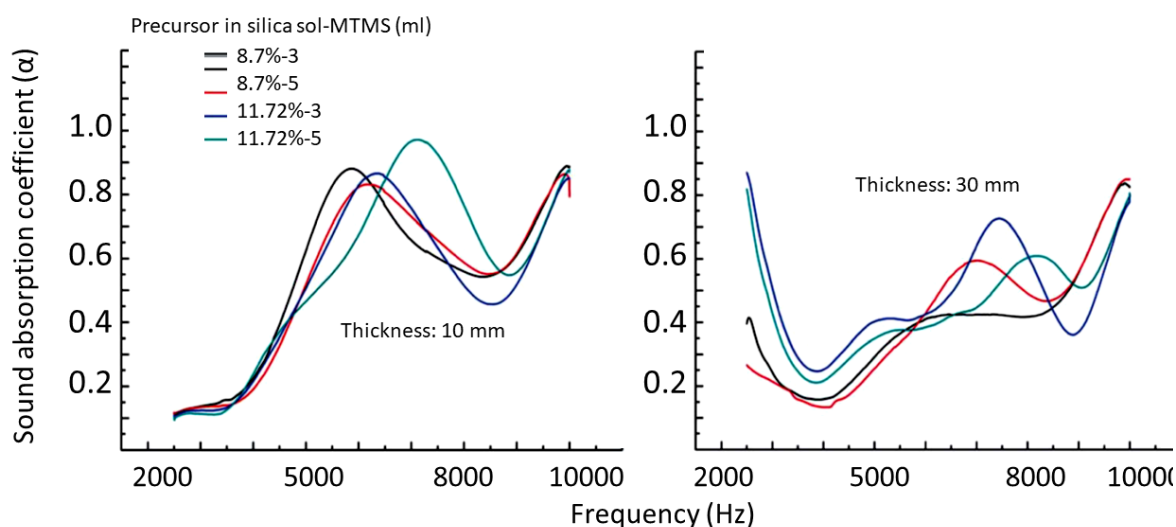


Figure 2.9 Sound absorption coefficient of polyimide-silica aerogels.

Revised/reproduced with permission from reference [77].

Sachithanadam et al. in 2016 [80] measured the acoustic properties of the silica aerogel granules of various sizes from 0.50 to 3.35 mm, and gelatin-silica hybrid aerogels doped with sodium dodecyl sulfate (GSA-SDS) consisting of 1.2 and 1.7 mm granular size. Absorption coefficients varied across grain size. Larger granules exhibited a somewhat lower absorption coefficient than that measured for smaller granules. This result demonstrated the importance of the visco-thermal and pressure diffusion effects which are controlled by the inter-particle pores. The second aspect of their research was the use of the “Inferential Transmission Loss method” (InTLM) to determine the transmission loss using a three-microphone impedance tube. The approach was

a modification to the usual transfer function method by inferring the transmission coefficient with and without the rigid wall. The sound velocity in the GSA-SDS aerogels was found to be very low at 70 to 78 m/s. Both the silica and GSA-SDS aerogels exhibited resonance behaviour in the transmission loss data (see Figure 2.10) and thus, different kind of graphs in comparison with the other research [60] with increasing trend graph with one dip in the resonance frequency.

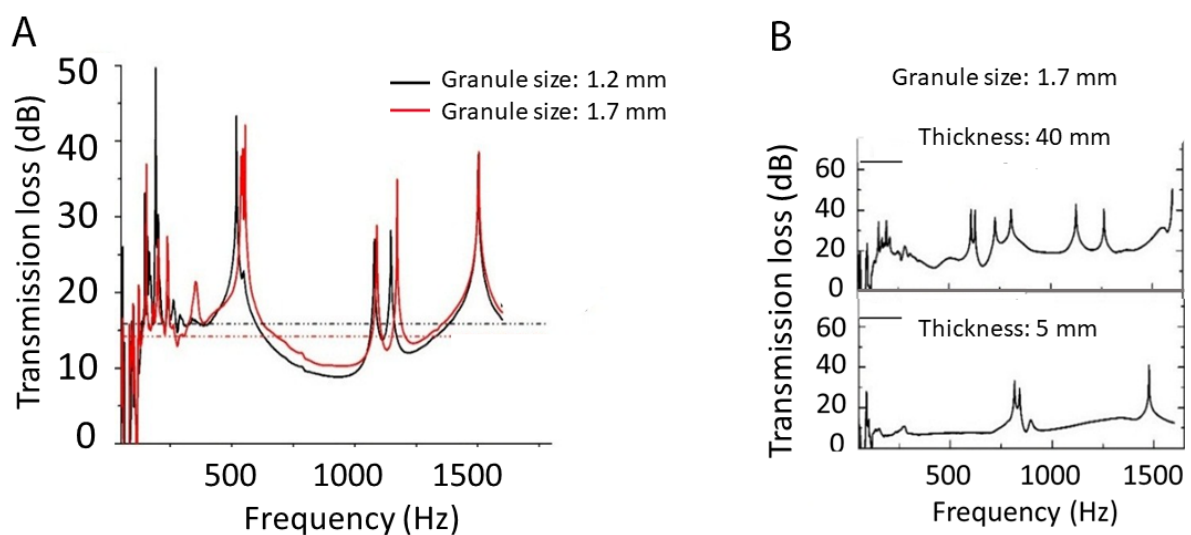


Figure 2.10 Transmission loss for (A) aerogel granules and (B) GSA-AG composites (granular size: 1.7 mm) via the proposed “Inferential Method” using a two-microphone impedance tube. Revised/reproduced with permission from reference [80].

Moretti [60] and Buratti [62] et al., in 2017, experimentally investigated the influence of the granule size of silica aerogels on thermal and acoustic performance. They used a 100 mm diameter, 4-microphone impedance tube to find that smaller grain sizes, which are accompanied by higher densities, and thicker samples improved the sound transmission loss (see Figure 2.11).

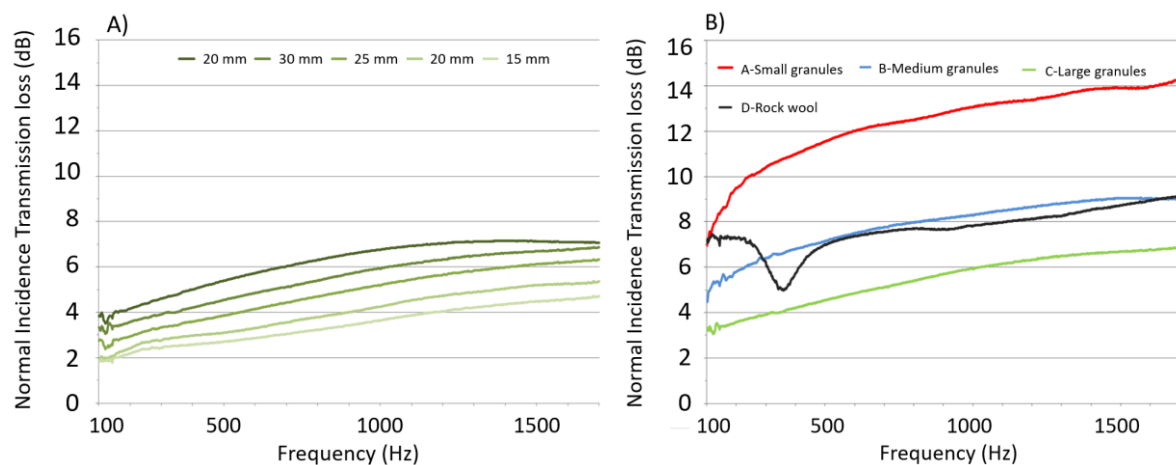


Figure 2.11 (A) Transmission loss of 1-4 mm silica aerogel granule layers for different thicknesses and (B) Comparison between aerogels and rock wool panel in 30 mm thickness. Revised/reproduced with permission from reference [60].

In 2018, Geslain et al. [83] presented a novel signal processing method for retrieving the viscoelastic properties of a silica aerogel clamped plate. This method is based on a genetic algorithm optimisation with two objective

functions resulting from two acoustic configurations, a reflection problem, and a transmission problem in an acoustic impedance tube. The two objective functions are the differences between the experimental and modelled acoustic problems around the plate resonance frequency. The estimated aerogel viscoelastic properties were $\rho=80 \text{ kg/m}^3$, $\nu=0.12$, $E_r=197.92 \text{ kPa}$, where ρ is density, ν is the Poisson ratio and E_r is the real part of the Young's modulus. The absorptive properties of aerogels are encouraging and can be applied to design more complex artificial structures (metasurfaces) for the broadband absorption of sound [83].

Merli et al. in 2018 [118] used 29 mm and 100 mm diameter impedance tubes to study the sound absorption and transmission losses of monolithic and granular aerogels. In their research, they used small aerogel granules of 0.01–1.2 mm (density of 0.08–0.085 g/m^3), intermediate grain size aerogels of 0.7–4.0 mm (density of 0.065–0.075 g/m^3), larger grain size aerogels of 4.0 mm (density of 0.065–0.070 g/m^3) and monolithic aerogel sample thicknesses of 12.7, 19.1 and 25.4 mm. Monolithic aerogels showed peak absorption coefficient values in 0.54 to 0.88 in the frequency range of 1.1 to 1.5 kHz whereas granular aerogels showed peak absorption coefficient values of 0.9 to 1.0 in the frequency range of 1.7 to 4.1 kHz. They found monolithic aerogels to have a transmission loss of 10–15 dB for sound waves attenuating at a frequency of

100-1600 Hz, when compared to granular aerogels which had a lower transmission loss of 5-7 dB [118].

From the limited number of papers reporting the sound absorption and transmission loss of the pure/hybrid silica aerogels, it is clear that silica aerogels, in contrast to the other porous sound absorbers, display a resonance behaviour with one or more resonance frequencies in their sound absorption spectra. The resonance frequencies and width of the resonance peaks depend on their mechanical properties, thickness, sample mounting conditions and potential presence of circumferential air gap. The transmission loss typically rises with an increasing frequency, with a dip in the lower frequency range which corresponds to a layer resonance or resonance in the circumferential air gap. It is possible to qualitatively compare the transmission loss among various aerogels to evaluate the effect of different parameters but relying on the absolute numbers is not recommended from data collected with the impedance tube.

A key problem to good understanding of the acoustical properties of aerogels is to have accurate data on its pore size distribution and pore connectivity. The physics of the effects which control the observed acoustical behaviour is markedly different for different scales of pores. For pores whose size is close to the mean free path (around 70 nm) the sorption effects dominate. For pores whose size is similar or larger than the viscous boundary layer thickness

$\left(\delta = \left(\frac{\eta}{\omega\rho_0}\right)^{0.5}\right)$, where η is the dynamic viscosity and ρ_0 is the ambient density of air) the viscous friction and inertia absorption will dominate. In granulated aerogels with millimetre size particles pressure diffusion absorption can be pronounced. This effect is controlled by the contrast between the relatively large inter-particle pores and relatively small (transport) pores in the surface of aerogel grains. All these effects are difficult to describe in a single theoretical model. Accurate data on the pore size and connectivity are difficult to acquire. As a result, there is a clear lack of publications which study and account for these effects in aerogels.

Last, but not least, there is a clear lack of modelling and simulation of key acoustical properties of monolithic and granulated aerogels. These properties are the complex, frequency-dependent bulk modulus and dynamic density of the air trapped in the material pores and the complex Young's modulus of the frame supporting an aerogel. These properties control the sound speed, attenuation, and acoustical characteristic impedance of the aerogel. Data on these key properties are difficult to find in published literature. This issue is complicated by the liberal use of a range of experimental procedures for measuring the acoustical properties of aerogels which seems to be parochial to a particular layer thickness and experimental setup.

2.7.3 Sound absorption/insulation of silica aerogel-polymer composites

For practical applications, aerogels are usually impregnated in foams or a fibrous matrix. Only a few recent studies have investigated the acoustic properties of foam types of aerogel composites. In 2017, Dourbash et al. [81] prepared and acoustically investigated silica aerogel/PUR foam composites and silica aerogel/elastomeric PU. They showed that adding silica aerogel to the polyol did not improve the thermal and acoustical properties of the PUR foams but did result in elastomeric PU results in better sound insulation characteristics, particularly transmission loss (see Figure 2.12 (B)), which is related to stiffness, absorption potential, and sound attenuation. Increasing the aerogel amount increases the transmission loss in the higher frequency range while adding 1% aerogel material resulted in the highest transmission loss in the frequency range of less than 3 kHz as shown in Figure 2.12(B). Adding more silica aerogel to the polyol substantially reduces the density and increases the number of voids present, this leads to lower values of the transmission loss [81].

Eskandari et al. [82], in 2017, investigated the effect of silica aerogel on Unplasticized Polyvinyl Chloride (UPVC) on acoustic and thermal properties. While a melt procedure was used for mixing, they did not investigate the possibility of (partial) infiltration of polymer into the aerogel pores. Sound absorption values of up to 40% were observed above 2500 Hz. At frequencies below 1000 Hz neat UPVC and all of its composites displayed a downtrend due

to the resonance phenomenon, which causes a reduction in the reflection coefficient and increases transmission [82].

A few studies on the acoustic properties of the other kinds of aerogel materials like recycled polyethylene terephthalate (rPET) aerogels have also been carried out, but this paper focuses on silica-based aerogels and their composites [84].

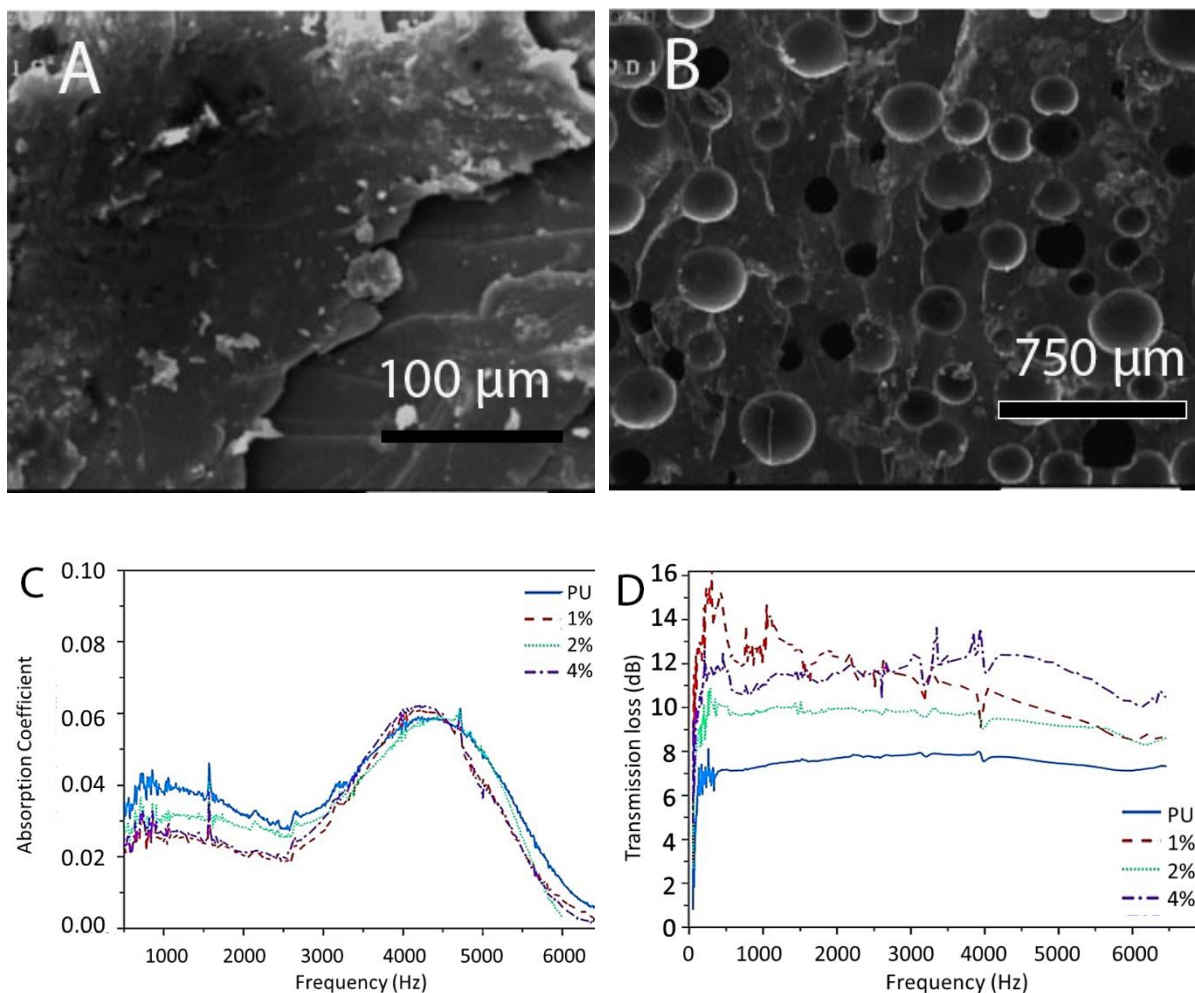


Figure 2.12 (A) SEM image with no aerogel content, (B) SEM image with 2% aerogel content, (C) Sound absorption coefficient, and (D) Transmission loss, for coating grade PU and its composites with 1-4% aerogel.

Revised/reproduced with permission from reference [81].

2.7.4 Sound absorption/insulation of aerogel-textile compounds

There are a few possible ways for how aerogels can be combined with textiles. Nonwovens can be impregnated with a silica aerogel, to produce fibre-reinforced silica aerogel blankets. The often observed dustiness of such blankets motivated investigations on the use of aerogel particles as a porous filler inside the polymer phase, where it is completely protected [64]. Several reports are available where aerogel particles are either mixed with electrospinning PET solution to make aerogel-filled fibres [64], mixed with binder and knife-coated [125], padded [126] or electrospayed [51] onto textiles, or thermally bonded in nonwoven textile [127], but the applications are not related to sound insulation. Here, we review those studies that reported on acoustic properties.

A limited number of reports are available where electrospinning was used to combine aerogel and fibres. A typical approach is to add electrospun nanofibres into a silica precursor before aerogel synthesis to produce aerogel coated fibres

[128, 129]. No literature was available regarding the incorporation of aerogel particles in electrospun polymer fibres, until 2015, when Mazrouei-Sebdani et al. [64] added aerogel particles in a PET electrospinning polymer solution to produce PET-aerogel composite fibres. The addition of silica aerogel particles to the electrospun PET fibres increases the sound absorption coefficient in the frequency range of 250 to 4000 Hz for a sub-millimetre thick layer of fibrous membrane. While 0.5 wt. % aerogel-filled electrospun webs exhibited higher sound absorption at low frequencies of 250 and 500 Hz, 4 wt. % aerogel-filled samples displayed the highest sound absorption coefficient at intermediate frequencies of 1000 and 2000 Hz. Mazrouei et al. suggested that the effects on sound absorption are related not only to the aerogel porous structure itself, but also to the effects of aerogel addition on the fibre structures and properties. Because the lower aerogel content resulted in larger fibre spacings, low-frequency range sound waves could be absorbed more efficiently, as suggested by other researchers [130]. Because the acoustic property of silica aerogel itself is not fully examined (Section 3.2), more experimental and modelling insights on pure silica aerogel are needed before the effect on aerogel-polymer nanofibres can be fully understood.

A nonwoven fabric is a manufactured web of fibres, bonded/entangled together by mechanical, thermal, or chemical processes [131]. Nonwoven fabrics with high bulkiness and resilience, great compressional resistance, and

good filling properties have been extensively studied as one of the most common porous thermal insulating/sound absorbing materials [102,132]. Since both nonwovens and aerogels have impressive thermal and acoustic properties on their own, a combination of these two materials is widely used in various environments because of their flexible structure. When the aerogel blankets are not encapsulated, problems with the migration of the aerogel particles and dust release occur [56]. Despite these potential drawbacks, fibre-reinforced silica aerogel blankets make up well over 50% of the silica aerogel market, and the thermal conductivity of such blankets has been studied extensively. However, it is also essential to understand the sound absorption behaviour of nonwoven-aerogel compounds, which have been studied to a much lesser extent [102].

Oh et al. in 2009 [133] selected two methods for the acoustic optimisation of polyethylene terephthalate (PET) nonwoven-silica aerogel blankets by dipping the nonwoven in a TEOS based sol (method I) or by ultrasonication of a silica hydrogel dispersion (method II), followed by solvent exchange/surface modification with TMCS/n-hexane and ambient pressure drying. All measurements were done for the samples with a thickness of 5 mm. Sound absorption coefficients of the method I and II blankets were low and below 0.1 at frequencies below 1000 Hz. At frequencies above 1000 Hz, the sound absorption coefficient of the method I prepared blankets with a density of 0.184 g/cm³ increased steadily and showed a wide bell-shaped graph (see Figure

2.13) [133] in line with that expected from traditional porous sound absorption materials [8,9,134].

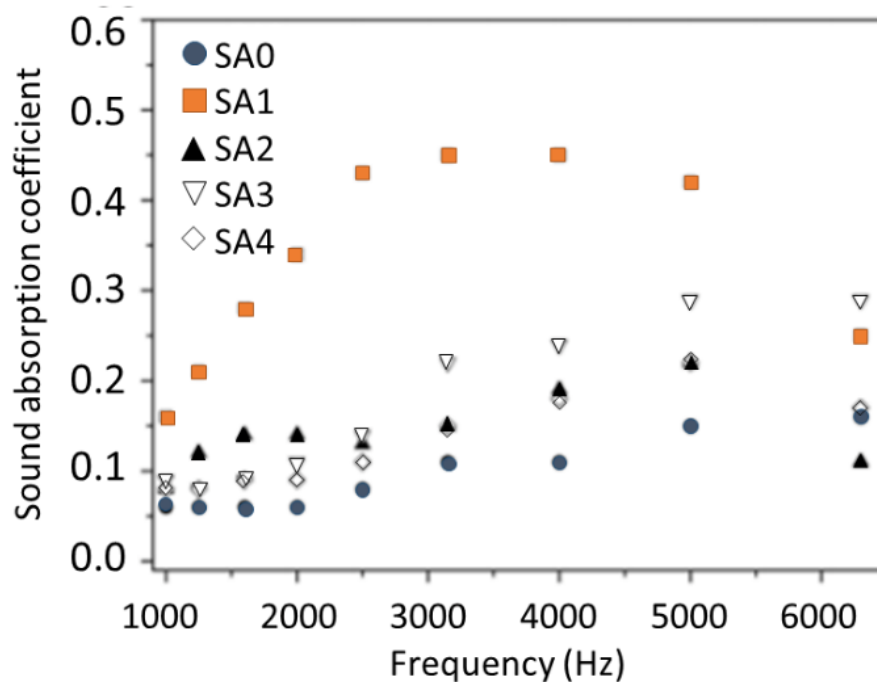


Figure 2.13 Sound absorption coefficient of the 5 mm thickened PET nonwoven-silica aerogel blankets prepared by dipping a PET nonwoven in a TEOS based sol. Revised/reproduced with permission from reference [133].

The presence of silica aerogel had a positive effect on energy absorption. Therefore, PET nonwoven-silica aerogel blankets, prepared under optimum conditions, can be considered as a good sound absorbing material [133] particularly in the frequency range for which the human ear is most sensitive (2.5 to 5 kHz) [9]. However, a majority of conventional porous insulation

materials are also good absorbers in this frequency range. Küçük and Korkmaz, in 2012 [104] investigated the effect of bonding, thickness, composition, permeability, and fibre thickness on sound absorption properties of nonwoven-aerogel composites. They varied the layer thickness from sub-millimetre thick to 35 mm to confirm that the increase in the layer thickness and carefully chosen permeability results in an increase in sound absorption [104].

In another work on PET nonwoven-silica aerogel blankets, Ramamoorthy et al. in 2017 [85] focused on silica aerogel blankets prepared from sol with variable silica content (110 to 28 molar ratio of methanol/TEOS). A molar ratio of 55 was recommended to maximise sound absorption and hydrophobicity. Similar to the work done by Oh et al. (2009) [133], silica aerogel was synthesised with solvent exchange/surface modification with TMCS/n-hexane and ambient pressure drying, but here, structural properties of aerogel composites have also been studied to determine their durability for long term noise control applications [85]. The PET nonwoven-silica aerogel blankets exhibited a higher sound absorption coefficient than the control sample for the entire frequency range of 50–6300 Hz. The silica aerogel present in the nonwoven structures (Figure 2.14) increases the absorption coefficients due to reduced average pore sizes, which cause stronger visco-thermal effects [85]. Also, airflow resistance

has increased in the mesopores due to the presence of aerogel leading to higher sound absorption [85,102].

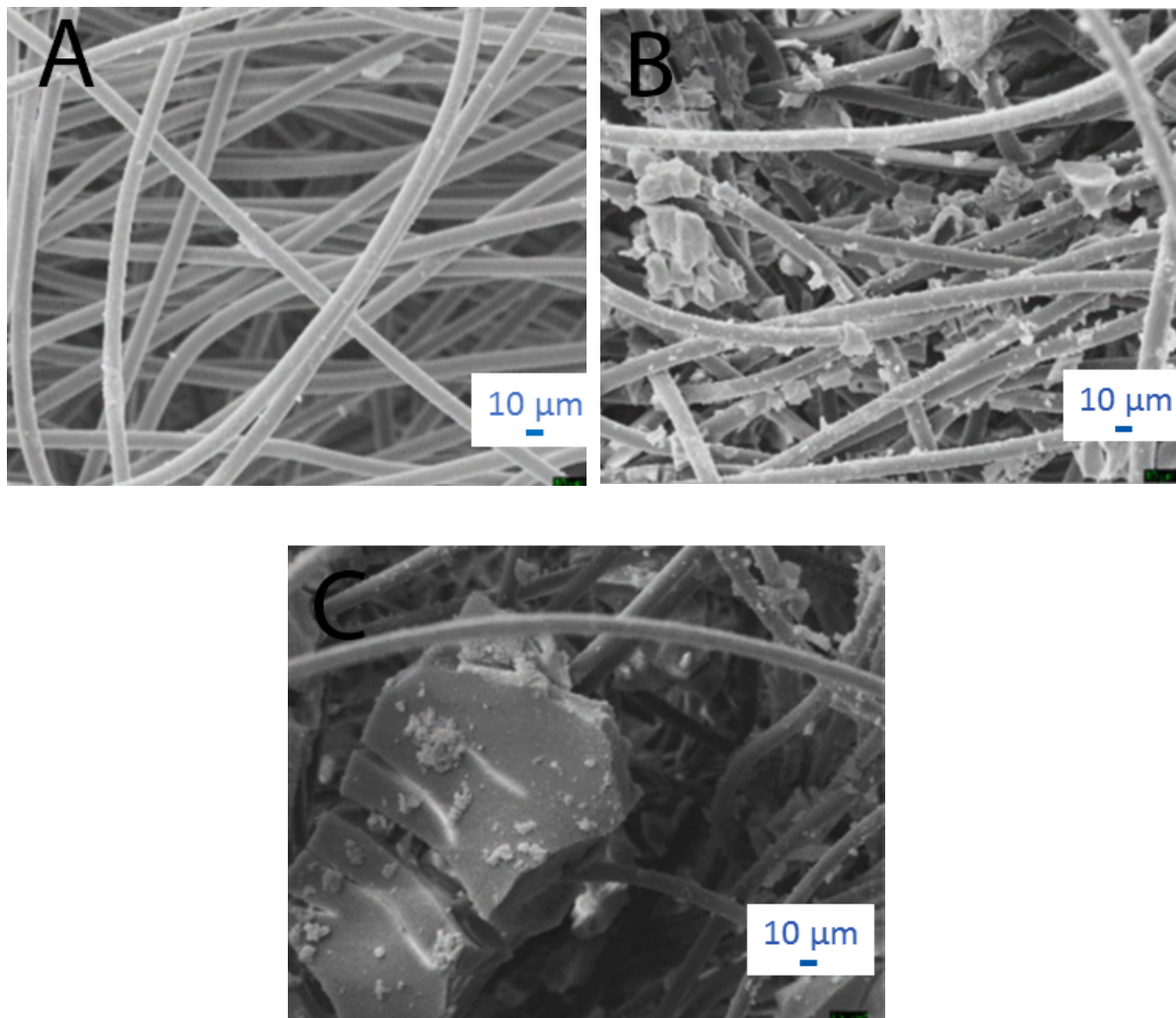


Figure 2.14 SEM images of (A) control PET, (B) PET nonwoven-silica aerogel blankets (MeOH:TEOS molar ratio: 110), and (C) PET nonwoven-silica aerogel blankets (MeOH:TEOS molar ratio: 28). Revised/reproduced with permission from reference [85].

In 2015 Motahari et al. [135] used cotton instead of PET to produce cotton nonwoven (1 cm)-silica aerogel blankets through a single-stage sol-gel process with different MeOH/TEOS molar ratios and aging times, with the aim to produce an efficient sound absorber. The results showed that for high MeOH/TEOS molar ratios (11) and a long aging time (24 hours), significantly higher sound absorption coefficients below 3 kHz can be achieved with blankets with a relatively low bulk density of 0.088 g/cm³. This could be due to the increase of fibre diameter after coating with silica aerogel particles, which decreases the space in between fibres in the mat and increases viscous stress caused by shearing and friction of air across the pores of silica aerogels. A further increase of the MeOH/ TEOS molar ratio to 14 caused an increase in bulk density and speed of sound, and a subsequent reduction in sound absorption. In this work, the thickness of resulted cotton nonwoven-aerogel mats is missing which makes the results incomparable with other research.

In 2019 Yang et al. [102] examined the sound absorption properties of the aerogel-(Polyethylene/polyester) nonwoven bonded blankets, prepared with the method of Venkataramana et al. [127] through the addition of aerogel granules/particles during the thermal bonding of the fibres (see Figure 2.15). The sound absorption coefficient linearly increased with increasing frequency (see Figure 2.16(A)). Although, there was no reference nonwoven sample without aerogel for comparison [102]. Yang et al. concluded that the aerogel

content is not a major factor in determining the sound absorption ability because the sample with the lowest aerogel content showed the higher sound absorption value. Important to note is that the density and the thickness of the samples were different for different aerogel contents, and this may have affected the properties. Lamination of between 2 to 6 sample layers increased the sound absorption coefficient as expected with diminishing returns after more than 3 layers were laminated (see Figure 2.16(B)).

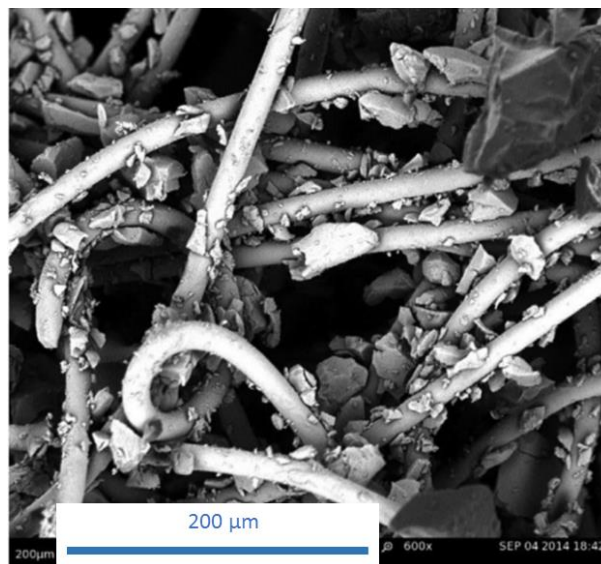


Figure 2.15 SEM images of an aerogel-nonwoven bonded compound.

Revised/reproduced with permission from [102].

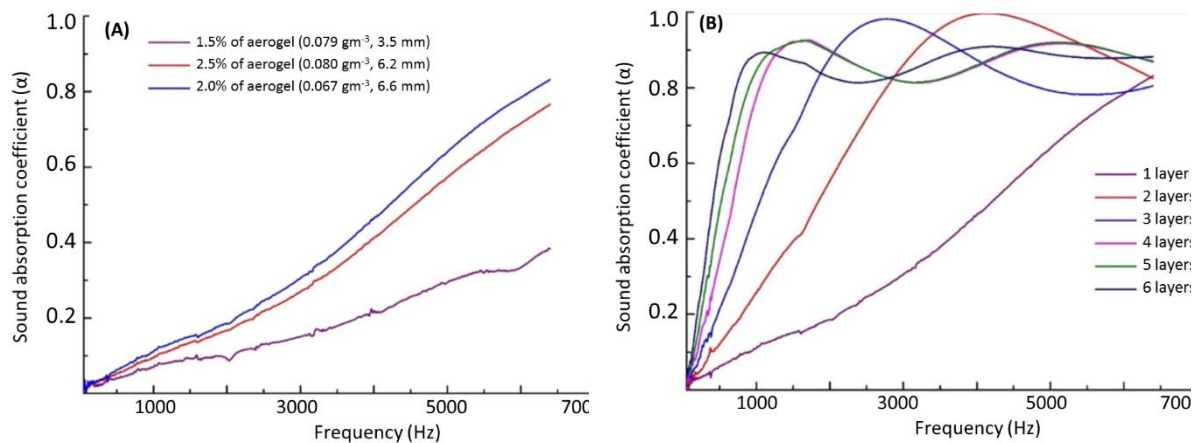


Figure 2.16. Sound absorption coefficient of the aerogel-nonwoven bonded compounds (A) with different aerogel contents and (B) the different number of layers for the sample with 2% of aerogel (0.067 g/m^3 , 6.6 mm).

Revised/reproduced with permission from [102].

In summary, the sound absorption behaviour of nonwoven-silica aerogel blankets depends on silica precursors and synthesis conditions, and different effects are observed in different studies. The addition of silica aerogel generally, but not always, improves the sound absorption, particularly in the medium frequency range, but the extent to which this adds a benefit will depend on the layer thickness and composite arrangement. Nonwovens themselves without silica aerogel are good porous sound absorbers efficient in a broad frequency range. The addition of nonwoven-silica aerogel into a blanket typically results in reduced permeability and increased absorption in a lower frequency range.

Higher concentrations of aerogels in a blanket can result in the resonance behaviour in the absorption coefficient of the composite similar to that seen in neat silica aerogel without fibres (Sections 2.7.2 and 2.7.3).

A summary of works done on the acoustic properties of the silica aerogels and their composition with the polymers can be found in Table 2.2.

Table 2.2. Silica and silica-polymer related aerogels acoustic application related papers.

Material	t (cm)	Method (Device)	Freque ncy (Hz)	Sound Quantity measured	Author (Year)
<i>Silica and silica-polymer derived aerogel</i>					
- SA*		Kundt' s		Absorption	Schmidt [63]
- SA/PVB	1-4	tube	250-	Impact	(1998)
- SA/VAE		(unknown)	5000	insulation	
SA/PVB	1.8	-	-	Impact insulation	Schwertfeger [93]

					(2003)
Silica-PDMS derived aerogel	-	Impedance tube (home- made)	250- 4000	Absorption	Dong [75] (2009)
MTMS-VTMS derived aerogel	1.6	Impedance tube (unknown)	200- 2500	Absorption	Cai [76] (2012)
Polyimide- silica derived aerogel	1-3	Impedance tube (unknown)	2500- 10000	Absorption	Yan [77] (2014)
- SA -GSA-SDS aerogel	1-5	Impedance tube (Brüel & Kjær)	50- 1500	Absorption Transmission loss	Sachithanadam [80] (2016)
SA	1.5-4	Impedance tube	100- 1700	Transmission loss	Moretti [60]

		(Brüel & Kjær)		(2017)
		Signal processing model based on impedance tube	Audible range	Absorption Transmission loss
SA	1.1			Geslain [83] (2018)
Monolithic/granular SA	1.3-2.5	Impedance tube (Brüel & Kjær)	100-4900	Absorption Transmission loss
				Merli [118] (2018)

Silica aerogel-polymer composite

- SA/PUR foams		Impedance tube/		Absorption
- SA/elastomeric PU	1.2-3.7	(Brüel & Kjær)	250-6400	Transmission loss
				Dourbash [81] (2017)

SA/UPVC composites	0.1	Impedance		Absorption Transmission loss	Eskandari [82] (2017)
		tube/ (Brüel & Kjær)	63– 6300		

Silica aerogel-textiles composite

PET nonwoven-SA blankets	0.5	Impedance		Absorption	Oh [133] (2009)
		tube (unknown)	250– 6400		
Cotton nonwoven (1 cm)-SA blankets	-	Impedance		Absorption	Motahari [135] (2015)
		tube (Brüel & Kjær)	100– 6300		
SA-filled superfine PET fibers	0.02– 0.024	Impedance		Absorption	Mazrouei [130] (2015)
		tube/ Home- made	250– 4000		

PET nonwoven-SA blankets	0.5-0.6	Impedance tube/ (Brüel & Kjær)	50- 6300	Sound absorption	Ramamoorthy [85] (2017)
SA-(PE/PET) nonwoven bonded blankets	0.4-0.7 (1-6 layers)	Impedance tube/ (Brüel & Kjær)	50- 6400	Sound absorption	Yang [102] (2019)
PET nonwoven-SA blankets	2.7 and 6.4 (non- woven)	Impedance tube/(BSW A)	50- 6100	Sound absorption	Talebi [90] (2019)

*SA: Silica aerogel, PVB: Polyvinylbutyrane, VAE: vinylacetate/ethene, PDMS: polydimethylsiloxane, MTMS: Methyltrimethoxysilane, VTMS: Vinyltrimethoxysilane, GSA: gelatin-silica aerogels, SDS: Sodium dodecyl sulfate, PU: Polyurethane, UPVC: Unplasticized Polyvinyl Chloride, PE: Polyethylene.

2.7.5 Sound absorption/insulation of aerogel renders

Recently aerogels granules have been incorporated into high-performance concrete and render for building applications [56, 79, 136]. Silica aerogel filled renders in particular have established themselves in the market place particularly for thermal insulation during the renovation of historical buildings [137]. Aerogel-based insulating renders, which can be applied to external and interior walls, are manufactured by mixing the conventional ingredients, additives and water with granular aerogel and coated on the wall (Figure 2.17) [78,79].

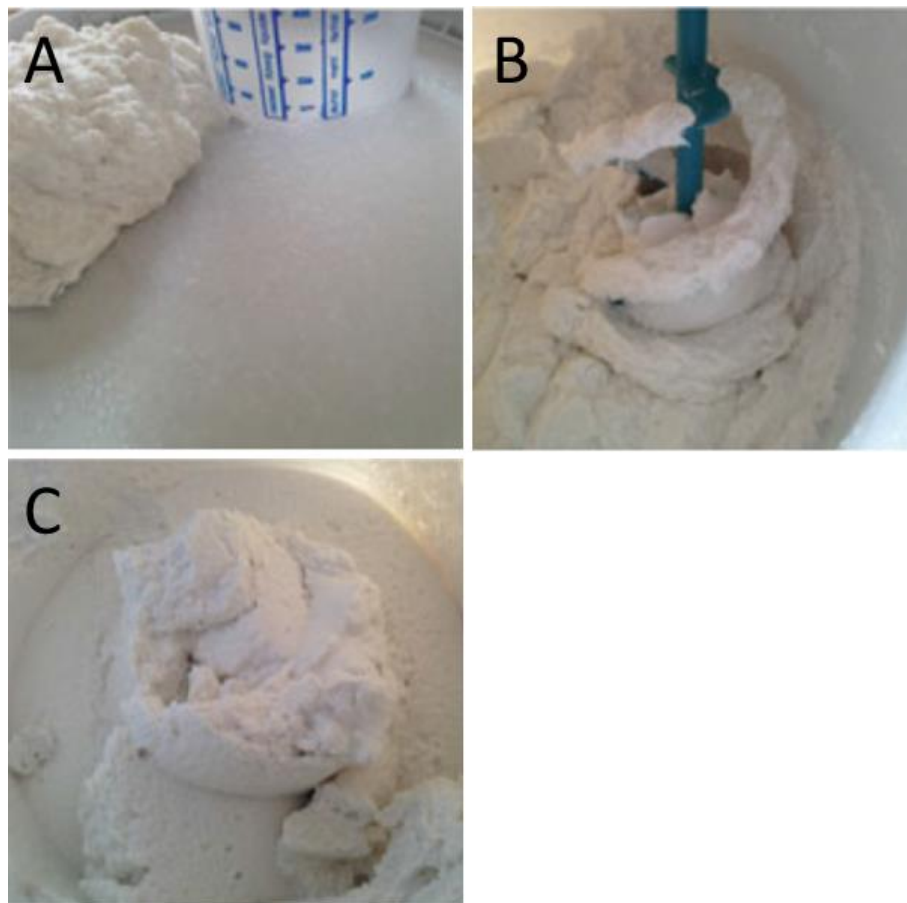


Figure 2.17 Mixing and applying of an aerogel-based plaster. (A) original components, (B) mixing phase, (C) final composition, and (D) in situ application on the wall. Revised/reproduced with permission from [78].

In 2014 Buratti et al. [78] reported the sound absorption coefficient of the two samples composed of plasterboard support, an aerogel insulation plaster with aerogel of two different thicknesses and a final plaster coat (2 mm). Tests were carried out on small samples with an impedance tube. The results showed a strong dependence on the acoustic behaviour on the final coat, which

negatively influenced the acoustic properties. The acoustic absorption coefficients of the aerogel embedded samples were not very high for the proposed plasters [78].

Preikss et al. [138] in 2018 applied silica aerogel granules in a foamed gypsum (5-30%) and attached an aerogel blanket to one side of the foamed gypsum intending to improve the thermal and acoustic properties. However, no significant increase of the sound absorption coefficient in the 1 kHz frequency could be obtained for the foamed gypsum itself. On the other hand, attaching the silica aerogel blanket to one side of the solid gypsum specimen did lead to an increase of the sound absorption coefficient from 0.05 to 0.3 [56, 138].

In summary, very few studies investigated the acoustic properties of silica aerogel filled renders and products. These preliminary studies did not observe a clear acoustic benefit of adding silica aerogel to renders and boards, but this question cannot be settled with the currently available data. Also, this points out that the aerogels pores that are filled and/or cloaked with the plaster should be discussed here.

2.7.6 Sound absorption/insulation of aerogel glazing systems

Because of their ultra-low thermal conductivity and high translucency and good solar-optical properties, silica aerogels have been investigated for their application in window systems. It is thus also of interest to study the sound insulation behaviour of aerogel-based glazing systems. As early as 1991 Narang provided a detailed study of the diffuse field sound-transmission behaviour of aerogel-based glazing systems with different glass thicknesses and interspace, and compared the results to those of conventional double glazing [139].

Two kinds of frequencies, considerable in the study of acoustic properties of the glazing systems, windows, and walls in the buildings, are critical frequency and resonance frequency. When the wavelength of sound air projected on the plate equals the wavelength of the bending waves, the movement of the panel increases, leading to low sound insulation. The lowest frequency at which this wave coincidence occurs for flat homogenous plates is the critical frequency and can be approximated with

$$f_c = \frac{c^2}{1.81h} \sqrt{\frac{\rho(1 - \nu^2)}{E}}, \quad (9)$$

where, c , h , ρ , ν , and E are the sound velocity in the air, thickness, the density of the material, Poisson's ratio, and Young's modulus, respectively. The resonance dip due to the coincident effect usually begins about an octave below the

critical frequency. Below the frequency range of the coincidence, the mass law determines the sound reduction index. Above the coincidence zone, the sound reduction index depends on the frequency only for double systems. For a temperature of 20°C and normal sound incidence, the resonance frequency is

$$f_{res} = 59.8 \sqrt{\frac{1}{d} \left(\frac{1}{m_1} + \frac{1}{m_2} \right)}, \quad (10)$$

where, d is the distance between the inner surfaces of the glazing, and m_1 and m_2 (kg) are the mass of each pane. If the frequency of the sound incident on a double element is higher than the resonance frequency, the air chamber absorbs part of the sound energy, resulting in greater acoustic insulation than is observed in a single element with the same mass [139, 140].

Because mass-air-mass resonance is a major drawback in conventional double-glazed windows for insulation against traffic noise, it appears that by choosing appropriate physical parameters of an aerogel filling of the interspace of the double-glazed system, one should be able to design a suitable window system free of the undesirable resonance dip in the low to the medium frequency range. Figure 2.18 shows that the transmission loss increases for an aerogel filled double glazing system [139]. However, compromises with respect to aerogel layer thickness may need to be made concerning acoustic/thermal performance versus cost, transparency, and solar gains.

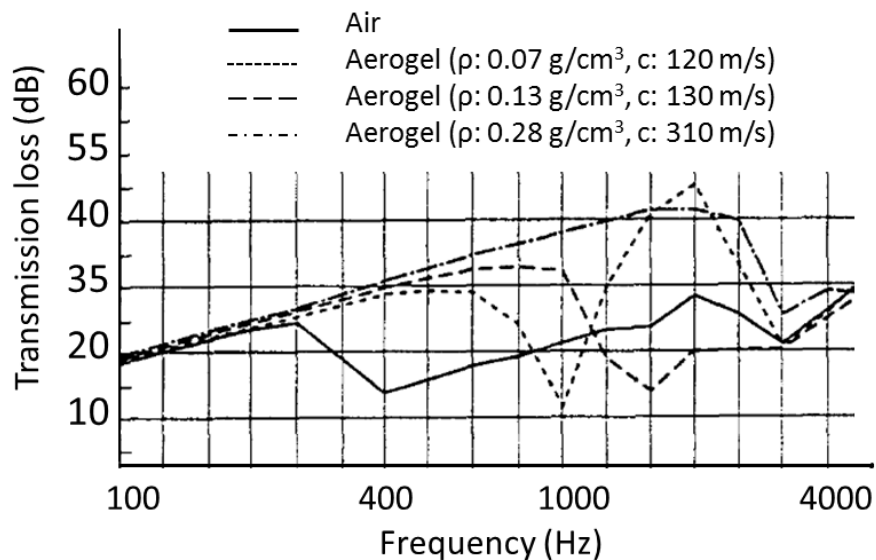


Figure 2.18 Sound transmission loss for a glazing system (glass-aerogel-glass of 4-6-4 mm). Revised/reproduced with permission from [139].

Buratti et al. in 2012 evaluated a prototype of an aluminium frame window with granular aerogel in the interspace [141]. Not only was thermal transmittance of the innovative glazing system lower than 1 W/m^2 , but also the acoustic properties were improved with $R_w=37 \text{ dB}$ which is 3 dB higher than that of a conventional window with air in the interspace [141]. Importantly, this number was achieved according to the standard series of ISO 10140 which is the test used on large-scale samples, a test more reliable than the impedance tube method. To improve further the acoustic performance of the window ($R_w>40 \text{ dB}$), the granular aerogel could be assembled into laminated glasses with a special acoustic polyvinyl butyral layer. Figure 2.19 shows the R-curve of the

samples with and without aerogel [125]. In 2014 these systems were tested in-field monitoring campaigns to validate the capability of aerogels in improving the acoustic performance of the glazing systems [142].

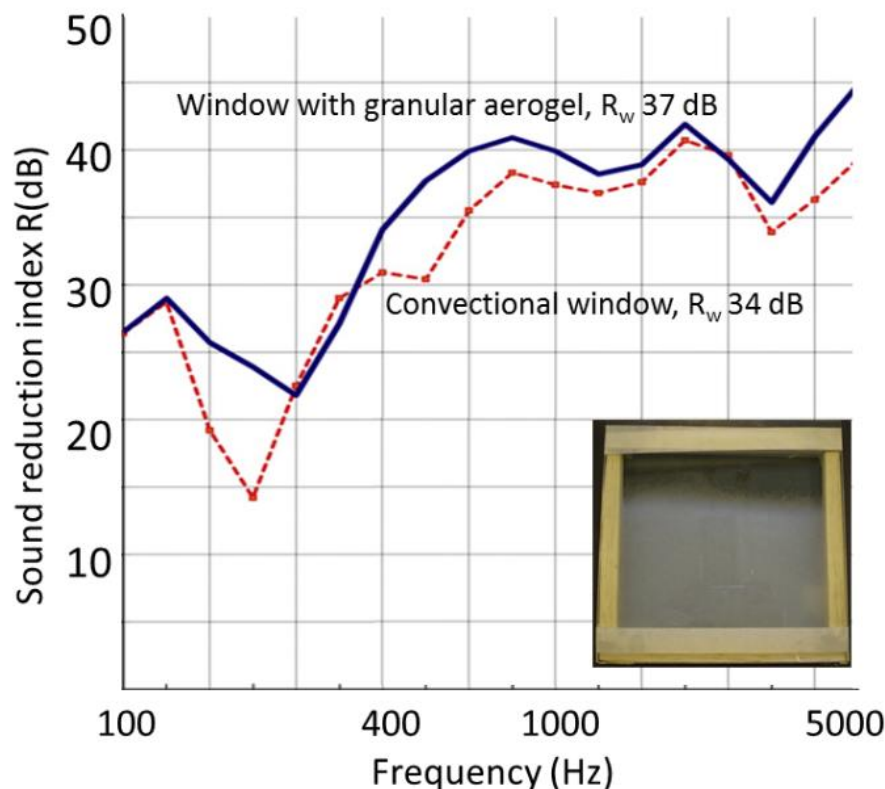


Figure 2.19 Sound reduction index (R) for the conventional window and the glazing prototype with aerogel in the interspace. Revised/reproduced with permission from [141].

2.8 Aerogel-based products versus conventional acoustic materials

In this section, we compare silica aerogel-based materials to four classes of conventional acoustic materials. This comparison is complicated by the wide

variability of aerogel-based products (describe in Section 2.7.6) and perhaps more critically, the wide knowledge gaps about their acoustic properties. As discussed in the previous sections, silica aerogel can be incorporated in a wide variety of composite materials (fibre mats, polymers, inorganic renders and concrete, glazing systems) and the nature of the composite can be the dominant control on the acoustic properties, sometimes more so than the properties of the aerogel itself. In addition, sound absorption properties depend on the composition, thickness and surface pattern of the absorbers, method of mounting (air gap) and frequency of the incident sound are also very important.

Table 2.3 compares the most important, application-relevant physical properties of aerogel-based materials to conventional acoustic materials. In terms of sound absorption, porous, fibrous and foamed materials display absorption over a wide range of frequency, while perforated materials show high sound absorption, but in a narrow frequency range. The pore size of foamed materials, and holes' size and holes' surface density for perforated systems determines their frequency range and percentage of absorption. Silica aerogels on their own resemble more closely the behaviour of the perforated materials with resonance absorption in a narrow frequency range, but in combination with fibres and textiles behave more similarly to fibrous materials and foams.

Table 2.3 Comparison of conventional and aerogel-based acoustic insulation materials

Material	Fibrous mats Mineral wool	Polymeric fibres	Polymer foams	Perforated panels	Silica aerogel
Density (kg/m ³)	Low (30–150)	Low-medium (50–1200)	Low (8–400)	Medium- high	Low (20– 200)
Pore size	Macroporous	Macroporous	Macro- /mesoporous	Macroporous	Mesoporous
Hydrophobicity	Low-medium	Low-medium	Low-medium	Low-medium	High (tunable)
Fire resistance	Good	Poor	Poor	Poor to good	Good
Structure	Fibrous	Fibrous	Cellular (open/closed)	Perforations	Nanoparticle networks
Λ (mW m ⁻¹ K ⁻¹)	Low (30–36)	Low (30–36)	Low (20–36)	High	Ultra-lowow (12–36)
Cost	Low	Low-medium	Low-high	High	High
Acoustic	Absorption	Absorption vibration isolation	Absorption insulation	Resonant	Absorption insulation

Applications	Insulation	Less	Vibration	Absorbers	
Absorption frequency	Wide range	Wide range	Wide range	Narrow range	Narrow range (wide if combined with textiles)

All tabulated materials, aside from the perforated plates, display low densities and low thermal conductivities. Among the conventional materials, closed-cell, pentane and/or CO₂ filled polymer foams (often polyurethane based) have the lowest thermal conductivity, but closed-cell foams tend to perform worse acoustically compared to open-cell foams because these materials do not allow for viscous, inertia and thermal absorption effects to develop in the material pores. Silica aerogels have even lower thermal conductivities due to their mesoporous structures. Silica aerogels also stand out for their hydrophobicity. In the absence of fire retardants, polymer based materials (foams and fibrous materials) naturally display worse fire properties compared to mineral wool or silica aerogel. Silica aerogel based products are more expensive by up to one order of magnitude compared to fibrous mats and most polymer foams, although high performance polyurethane foams engineered for impact noise control and vibration isolation can also be very expensive. Perforated materials are usually used for very specific applications, e.g., as ceiling tiles in auditoria,

theatres or concert halls, while fibrous and foamed materials are used in standard applications, such as residential, commercial and public buildings, automotive and other transportation thanks to their low cost and ease of installation. Mineral wool is particularly cost-effective, but cannot be used as a final cover or design in terms of their health and environmental problems, whereas other materials can target the acoustical/architectural designs, particularly foams for internal designs and perforated systems for internal/external designs. Aerogels, when mixed with other materials, have the potential of being used as the final coating related to their minimised dust releasing behaviour.

2.9 Summary, open questions, and road to market

From the literature survey above it is clear that the physics of how sound propagates through silica aerogel is poorly understood. Although there is literature on the absorption and transmission properties of aerogels and effects of thickness [63, 77, 93], pore size [75], and granule size [60, 80], these studies lack mathematical modelling to understand key physical mechanisms which can explain the observed acoustical behaviour of aerogels. A majority of these works are particular to the adopted layer thickness and do not discuss any generic acoustical quantities such as frequency-dependent bulk modulus of the air trapped in an aerogel, its dynamic density and complex Young' s modulus

of the aerogel' s frame which can exhibit viscoelastic behaviour. These properties are frequency-dependent and should be related to the aerogel' s chemistry and pore morphology. There is a wide variation in how experimental data were collected and interpreted. Therefore, systematic efforts are necessary to fully discern and realise the potential of silica aerogel and its composites as acoustic materials.

Since the physics of sound absorption/transmission is not fully understood even for pure silica aerogel, the situation for composites is much more dramatic. Because of the wide variety of composites (polymers, textiles, renders), each type of composite will require its own detailed experimental and theoretical investigations, but the effect of silica aerogel on the acoustic properties of the final products is typically investigated as a side-thought, and only a few studies focus on this matter. In contrast to neat silica aerogel, aerogel-fibre blankets typically display smoother dependencies of the sound absorption coefficient on frequency, with broad bell-shaped curves reminiscent of the aerogel-free nonwovens [102, 133, 135]. Although thermal insulation and fire resistance remain the market driver for aerogel blankets for pipeline and industrial insulation, commercial products have passed the industry' s acoustic standards, e.g., ISO 15665 [143]. These systems are offered by Armacell (Germany) and ULVA Insulation Systems (UK). The main users are in the oil, gas, and petrochemical sectors. For other building materials other than aerogel

blankets, sound an improvement in sound transmission loss was observed for the aerogel-filled double glazing systems in some case studies [139, 141], but there is no clear data if an improvement is possible for aerogel filled renders and gypsums. From the limited available data, it is clear that the combination of aerogels with other building materials can significantly affect the aerogel's acoustic performance even in an adverse way [138]. Hence, the method used for the integration of the aerogel with other aqueous/liquid phase materials should be considered carefully and the effect on acoustic properties evaluated through rigorous measurements.

In the current marketplace, silica aerogels' unique selling point is the ultra-low thermal conductivity, which enables thinner thermal insulation layers. Based on the current state-of-the-art, it is clear that silica aerogels and its derivative products often have good acoustic properties, but they do not necessarily outperform conventional materials and products. Only a few studies have targeted acoustic properties as a selling point for silica aerogel [93]. As large-scale production is concerned, only limited data are available on the use of the transparent silica aerogel in the interspace of the double glazing systems in the pilot-scale which showed the sound transmission loss was increased in comparison with the glazing system with the air in the interspace [139, 141]. However, also in the field of transparent insulation, it is not clear if the benefits

are sufficient to offset the added cost of an aerogel solution. Whether acoustics can become a market driver for silica aerogel remains an open question, particularly from the viewpoint of silica aerogel's high cost and low mechanical properties, compared to conventional materials. Additionally, the combination of aerogels with polymers and other materials should be carried out thoughtfully to prevent infiltration of the aerogel mesoporosity and to avoid adverse effects on the acoustic performance.

Silica aerogels' absorption behaviour has the potential for interior room acoustics to absorb specific frequencies (e.g., absorbing layer combined with typical porous absorbers of rock wool and foam). In addition, the relatively high sound absorption coefficients and transmission loss, especially at low to intermediate frequencies, combined with the low density and thickness can play an important role in reducing the weight and thickness of construction elements. However, the silica aerogel-based products currently on the market have been developed for thermal insulation as their main application. Hence, the composite properties have been optimised to minimise thermal conductivity with mechanical strength, durability and ease of installation as important secondary parameters. The acoustic performance has at best been considered of minor importance, or more commonly, has not been considered at all. The question of how well an aerogel-based product can perform as

acoustic insulation, if it were to be optimised for its acoustic properties first and foremost, thus remains open.

The silica aerogel thermal insulation market is rapidly growing. The use of thinner insulation layers, compared to mineral wool, inevitably has consequences for the acoustic performance of the façade. Lingering uncertainty on the direction and size of the effects could negatively impact this market. Thus, although the feasibility of acoustics as a market driver remains an open question, it is clear that a better understanding of the acoustic performance of silica aerogel and its products is imperative to support the main thermal insulation application.

Acknowledgments

This work was supported by a Bridge - Proof of Concept Fellowship (grant No. 193700 to Z. M.-S.). The authors are also grateful the EPSRC-sponsored Centre for Doctoral Training in Polymers, Soft Matter and Colloids (EP/L016281/1) at the University of Sheffield for their financial support of this work. We would also like to thank our industry partner Armacell and Dr. Mark Swift and Mr. Pavel Holub for their continued support throughout this research study.

References

1. S.S. Kistler, "Coherent expanded aerogels and jellies," *Nature*, 127, p. 741, 1931. <https://doi.org/10.1038/127741a0>
2. N. Hüsing, U. Schubert, "Aerogels-Airy Materials: Chemistry, Structure, and Properties," *Angew. Chem. Int. Ed.*, 37, pp. 22–45, 1998. [https://doi.org/10.1002/\(SICI\)1521-3773\(19980202\)37:1/2 <22::AID-ANIE22 >3.0.CO;2-I](https://doi.org/10.1002/(SICI)1521-3773(19980202)37:1/2 <22::AID-ANIE22 >3.0.CO;2-I)
3. A.C. Pierre, A. Rigacci, "SiO₂ aerogels, in: N. Leventis, M.M. Koebel (Eds.), *Aerogel' s handbook*," *Springer, New York*, pp. 21–45, 2011. https://doi.org/10.1007/978-1-4419-7589-8_2
4. J.P. Arenas, M.J. Crocker, "Recent trends in porous sound-absorbing materials," *Sound Vib.*, 44(7), pp. 12–18, 2010.
5. G. Carlson, D. Lewis, K. McKinley, J. Richardson, T. Tillotson, "Aerogel commercialization: technology, markets and costs," *J. Non-Cryst. Solids*, 186, pp. 372–379, 1995. [https://doi.org/10.1016/0022-3093\(95\)00069-0](https://doi.org/10.1016/0022-3093(95)00069-0)
6. A.M. Anderson, M.K. Carroll, "Hydrophobic silica aerogels: review of synthesis, properties and applications, in: N. Leventis, M.M. Koebel (Eds.), *Aerogels handbook*, *Springer, New York*, pp. 47–77, 2011. https://doi.org/10.1007/978-1-4419-7589-8_3

-
7. A.-M. Siouffi, "Silica gel-based monoliths prepared by the sol-gel method: facts and figures, *J. Chromatogr. A*, 1000, pp. 801–818, 2003.
[https://doi.org/10.1016/S0021-9673\(03\)00510-7](https://doi.org/10.1016/S0021-9673(03)00510-7)
8. S. Salimian, A. Zadhoush, M. Naeimirad, R. Kotek, S. Ramakrishna, "A review on aerogel: 3D nanoporous structured fillers in polymer-based nanocomposites," *Polym. Compos.*, 39(10), pp. 3383–3408, 2018.
<https://doi.org/10.1002/pc.24412>
9. G.M. Pajonk, "Some applications of silica aerogels," *Colloid. Polym. Sci.*, 281(7) pp. 637–651, 2003.
<https://doi.org/10.1007/s00396-002-0814-9>
10. S. Teichner, G. Nicolaon, M. Vicarini, G. Gardes, "Inorganic oxide aerogels" , *Adv. Colloid Interface Sci.*, 5(3), pp. 245–273, 1976.
[https://doi.org/10.1016/0001-8686\(76\)80004-8](https://doi.org/10.1016/0001-8686(76)80004-8)
11. F. Schwertfeger, A. Zimmermann, "Process for the preparation of modified aerogels, and their use," US Patent 5888425, 1999.
12. M.M. Koebel, L. Huber, S. Zhao, W.J. Malfait, "Breakthroughs in cost-effective, scalable production of superinsulating, ambient-dried silica aerogel and silica-biopolymer hybrid aerogels: from laboratory to pilot scale," *J. Sol-Gel Sci. Technol.*, 79(2), pp. 308–318, 2016.
<https://doi.org/10.1007/s10971-016-4012-5>

-
13. A. Stojanovic, S. Zhao, E. Angelica, W.J. Malfait, M.M. Koebel, "Three routes to superinsulating silica aerogel powder," *J. Sol-Gel Sci. Technol.* 90(1), pp. 57–66, 2019.
<https://doi.org/10.1007/s10971-018-4879-4>
14. Y. Huang, H. Song, C. Guangnan, D. Huaming, Y. Bihe, C. Xianfeng, Y. Xiaobing, "Fast preparation of glass fiber/silica aerogel blanket in ethanol & water solvent system," *J. Non-Cryst. Solids*, 505, pp. 286–291, 2019.
<https://doi.org/10.1016/j.jnoncrysol.2018.11.003>
15. Y. Huang, H. Song, F. Mengmeng, D. Huaming, P. Yueleij, C. Xudong, "Organic solvent-saving preparation of water glass-based aerogel granules under ambient pressure drying," *J. Non-Cryst. Solids*, 521, pp. 119507–119513, 2019.
<https://doi.org/10.1016/j.jnoncrysol.2019.119507>
16. J.C. Wong, H. Kaymak, S. Brunner, M.M. Koebel, "Mechanical properties of monolithic silica aerogels made from polyethoxydisiloxanes," *Microporous Mesoporous Mater.*, 183, pp. 23–29, 2014.
<https://doi.org/10.1016/j.micromeso.2013.08.029>
17. K.J. Lee, Y.H. Kim, J.K. Lee, H.J. Hwang, "Fast synthesis of spherical silica aerogel powders by emulsion polymerization from water glass," *Chem. Sel.*, 3(4), pp. 1257–1261, 2018.

<https://doi.org/10.1002/slct.201703000>

18. Z. Mazrouei-Sebdani, S. Salimian, A. Khoddami, F. Shams-Ghahfarokhi, "Sodium silicate based aerogel for absorbing oil from water: the impact of surface energy on the oil/water separation," *Mater. Res. Express*, 6(8), p. 085059, 2019.

<https://doi.org/10.1088/2053-1591/ab1eed>

19. S. Zhao, A. Stojanovic, E. Angelica, O. Emery, D. Rentsch, R. Pauer, M.M. Koebel, W.J. Malfait, "Phase transfer agents facilitate the production of superinsulating silica aerogel powders by simultaneous hydrophobization and solvent-and ion-exchange," *Chem. Eng. J.*, 381, p. 122421, 2020.

<https://doi.org/10.1016/j.cej.2019.122421>

20. G.M. Pajonk, E. Elaloui, P. Achard, B. Chevalier, J.-L. Chevalier, M. Durant, "Physical properties of silica gels and aerogels prepared with new polymeric precursors," *J. Non-Cryst. Solids*, 186, pp. 1–8, 1995.

[https://doi.org/10.1016/0022-3093\(95\)00210-3](https://doi.org/10.1016/0022-3093(95)00210-3)

21. A.P. Rao, A.V. Rao, G. Pajonk, "Hydrophobic and physical properties of the two step processed ambient pressure dried silica aerogels with various exchanging solvents," *J. Sol-Gel Sci. Technol.*, 36(3), pp. 285–292, 2005.

<https://doi.org/10.1007/s10971-005-4662-1>

22. A.V. Rao, G. Pajonk, "Effect of methyltrimethoxysilane as a co-precursor on the optical properties of silica aerogels," *J. Non-Cryst. Solids*, 285, pp. 202–209, 2001.
[https://doi.org/10.1016/S0022-3093\(01\)00454-9](https://doi.org/10.1016/S0022-3093(01)00454-9)
23. K. Kanamori, M. Aizawa, K. Nakanishi, T. Hanada, "New transparent methylsilsesquioxane aerogels and xerogels with improved mechanical properties," *Adv. Mater.*, 19(12), 1589–1593, 2007.
<https://doi.org/10.1002/adma.200602457>
24. D.Y. Nadargi, S.S. Latthe, A.V. Rao, "Effect of post-treatment (gel aging) on the properties of methyltrimethoxysilane based silica aerogels prepared by two-step sol–gel process," *J. Sol-Gel Sci. Technol.*, 49(1), pp. 53–59, 2009.
<https://doi.org/10.1007/s10971-008-1830-0>
25. K. Kanamori, "Organic–inorganic hybrid aerogels with high mechanical properties via organotrialkoxysilane-derived sol–gel process," *J. Ceram. Soc. Jpn.*, 119(1385), pp. 16–22, 2011.
<https://doi.org/10.2109/jcersj2.119.16>
26. M.-A. Einarsrud, M.B. Kirkedelen, E. Nilsen, K. Mortensen, J. Samseth, "Structural development of silica gels aged in TEOS," *J. Non-Cryst. Solids*, 231, pp. 10–16, 1998.
[https://doi.org/10.1016/S0022-3093\(98\)00405-0](https://doi.org/10.1016/S0022-3093(98)00405-0)

27. J.L. Gurav, I.-K. Jung, H.-H. Park, E.S. Kang, D.Y. Nadargi, "Silica aerogel: synthesis and applications," *J. Nanomater.*, 2010, pp. 1–11, 2010.
<https://doi.org/10.1155/2010/409310>
28. W.J. Malfait, R. Verel, M.M. Koebel, "Hydrophobization of silica aerogels: insights from quantitative solid-state NMR spectroscopy," *J. Phys. Chem. C*, 118(44), pp. 25545–25554, 2014.
<https://doi.org/10.1021/jp5082643>
29. A. Stojanovic, S.P. Comesaña, D. Rentsch, M.M. Koebel, W.J. Malfait, "Ambient pressure drying of silica aerogels after hydrophobization with mono-, di- and tri-functional silanes and mixtures thereof," *Microporous Mesoporous Mater.*, 284, pp. 289–295, 2019.
<https://doi.org/10.1016/j.micromeso.2019.04.038>
30. S.D. Bhagat, Y.-H. Kim, K.-H. Suh, Y.-S. Ahn, J.-G. Yeo, J.-H. Han, "Superhydrophobic silica aerogel powders with simultaneous surface modification, solvent exchange and sodium ion removal from hydrogels," *Microporous Mesoporous Mater.*, 112, pp. 504–509, 2008.
<https://doi.org/10.1016/j.micromeso.2007.10.03>
31. L. Huber, S. Zhao, W.J. Malfait, S. Vares, M.M. Koebel, "Fast and Minimal-Solvent Production of Superinsulating Silica Aerogel Granulate," *Angew. Chem. Int. Ed.*, 56(17), pp. 4753–4756, 2017.
<https://doi.org/10.1002/anie.201700836>

-
32. Z. Mazrouei-Sebdani, A. Khoddami, H. Hadadzadeh, M. Zarrebini, A. Karimi, F. Shams-Ghahfarokhi, "The effect of the nano-structured aerogel powder on the structural parameters, water repellency, and water vapor/air permeability of a fibrous polyester material," *Mater. Chem. Phy.*, 177, pp. 99–111, 2016.
<https://doi.org/10.1016/j.matchemphys.2016.04.002>
33. G.W. Scherer, J. Gross, L.W. Hrubesh, P.R. Coronado, "Optimization of the rapid supercritical extraction process for aerogels," *J. Non-Cryst. Solids*, 311(3), pp. 259–272, 2002.
[https://doi.org/10.1016/S0022-3093\(02\)01379-0](https://doi.org/10.1016/S0022-3093(02)01379-0)
34. T.B. Roth, A.M. Anderson, M.K. Carroll, "Analysis of a rapid supercritical extraction aerogel fabrication process: Prediction of thermodynamic conditions during processing," *J. Non-Cryst. Solids* 354(31), pp. 3685–3693, 2008.
<https://doi.org/10.1016/j.jnoncrysol.2008.04.003>
35. A.M. Anderson, C.W. Wattle, M.K. Carroll, "Silica aerogels prepared via rapid supercritical extraction: effect of process variables on aerogel properties," *J. Non-Cryst. Solids* 355(2), pp. 101–108, 2009.
<https://doi.org/10.1016/j.jnoncrysol.2008.10.005>

-
36. J.F. Poco, P.R. Coronado, R.W. Pekala, L.W. Hrubesh, "A rapid supercritical extraction process for the production of silica aerogels," MRS Online Proceedings Library Archive, 431, 1996.
37. B.M. Gauthier, S.D. Bakrania, A.M. Anderson, M.K. Carroll, "A fast supercritical extraction technique for aerogel fabrication," *J. Non-Cryst. Solids*, 350, pp. 238–243, 2004.
<https://doi.org/10.1016/j.jnoncrysol.2004.06.044>
38. A.M. Anderson, C.W. Wattlely, M.K. Carroll, "Silica aerogels prepared via rapid supercritical extraction: effect of process variables on aerogel properties," *J. Non-Cryst. Solids*, 355(2), pp. 101–108, 2009.
<https://doi.org/10.1016/j.jnoncrysol.2008.10.005>
39. D.B. Mahadik, Y.K. Lee, N.K. Chavan, S.A. Mahadik, H.H. Park, "Monolithic and shrinkage-free hydrophobic silica aerogels via new rapid supercritical extraction process," *J. Supercrit. Fluids*, 107, pp. 84–89, 2016.
<https://doi.org/10.1016/j.supflu.2015.08.020>
40. J. Fricke, T. Tillotson, "Aerogels: production, characterization, and applications," *Thin solid films*, 297, pp. 212–223, 1997.
[https://doi.org/10.1016/S0040-6090\(96\)09441-2](https://doi.org/10.1016/S0040-6090(96)09441-2)

-
41. S.S. Prakash, C.J. Brinker, A.J. Hurd, S.M. Rao, "Silica aerogel films prepared at ambient pressure by using surface derivatization to induce reversible drying shrinkage," *Nature*, 374(6521), pp. 439–443, 1995.
<https://doi.org/10.1038/374439a0>
42. S. Iswar, W.J. Malfait, S. Balog, F. Winnefeld, M. Lattuada, M.M. Koebel, "Effect of aging on silica aerogel properties," *Microporous Mesoporous Mater.*, 241, pp. 293–302, 2017.
<https://doi.org/10.1016/j.micromeso.2016.11.037>
43. G. Reichenauer, "Structural characterization of aerogels, in: N. Leventis, M. M. Koebel (Eds.), *Aerogels Handbook*," *Springer, New York*, pp. 449–498, 2011.
<https://doi.org/10.1016/j.micromeso.2016.11.037>
44. M. Koebel, A. Rigacci, P. Achard, "Aerogel-based thermal superinsulation: an overview," *J. Sol-Gel Sci. Technol.*, 63(3), pp. 315–339, 2012.
<https://doi.org/10.1007/s10971-012-2792-9>
45. N. Leventis, H. Lu, "Polymer-crosslinked aerogels, in: N. Leventis, M.M. Koebel (Eds.), *Aerogels Handbook*," *Springer, New York*, pp. 251–285, 2011.
https://doi.org/10.1007/978-1-4419-7589-8_13

46. M.A.B. Meador, "Improving elastic properties of polymer-reinforced aerogels, in: N. Leventis, M.M. Koebel (Eds.), *Aerogels Handbook*," *Springer, New York*, pp. 315–334, 2011.
https://doi.org/10.1007/978-1-4419-7589-8_15
47. J.P. Randall, M.A.B. Meador, S.C. Jana, Tailoring mechanical properties of aerogels for aerospace applications," *ACS Appl. Mater. Interfaces*, 3(3), pp. 613–626, 2011. <https://doi.org/10.1021/am200007n>
48. G. Churu, B. Zupančič, D. Mohite, C. Wisner, H. Luo, I. Emri, C. Sotiriou-Leventis, N. Leventis, H. Lu, "Synthesis and mechanical characterization of mechanically strong, polyurea-crosslinked, ordered mesoporous silica aerogels," *J. Sol-Gel Sci. Technol.*, 75(1), pp. 98–123, 2015.
<https://doi.org/10.1007/s10971-015-3681-9>
49. G. Hayase, K. Kanamori, K. Abe, H. Yano, A. Maeno, H. Kaji, K. Nakanishi, "Polymethylsilsesquioxane–cellulose nanofiber biocomposite aerogels with high thermal insulation, bendability, and superhydrophobicity," *ACS Appl. Mater. Interfaces*, 6(12), pp. 9466–9471, 2014.
<https://doi.org/10.1021/am501822y>
50. S. Zhao, W.J. Malfait, A. Demilecamps, Y. Zhang, S. Brunner, L. Huber, P. Tingaut, A. Rigacci, T. Budtova, M.M. Koebel, "Strong, thermally superinsulating biopolymer–silica aerogel hybrids by cogelation of silicic acid with pectin," *Angew. Chem. Int. Ed.*, 54(48), pp. 14282–14286, 2015.

<https://doi.org/10.1002/ange.201507328>

51. F. Shams-Ghahfarokhi, A. Khoddami, Z. Mazrouei-Sebdani, J. Rahmatinejad, H. Mohammadi, "A new technique to prepare a hydrophobic and thermal insulating polyester woven fabric using electro-spraying of nano-porous silica powder," *Surf. Coat. Technol.*, 366, pp. 97–105, 2019.

<https://doi.org/10.1016/j.surfcoat.2019.03.025>

52. R. Baetens, B.P. Jelle, A. Gustavsen, "Aerogel insulation for building applications: a state-of-the-art review," *Energy Build.*, 43(4), pp. 761–769, 2011.

<https://doi.org/10.1016/j.enbuild.2010.12.012>

53. J. Ryu, "Flexible aerogel superinsulation and its manufacture," US Patent 6068882, 2000.

54. R. Trifu, N. Bhobho, Flexible coherent insulating structures, US Patent US20070173157A1, 2007.

55. Y.K. Akimov, "Fields of application of aerogels," *Instrum. Exp. Tech.*, 46(3), pp. 287–299, 2003.

<https://doi.org/10.1023/A:1024401803057>

56. S. Hoffele, S.J. Russell, D.B. Brook, "Light-weight nonwoven thermal protection fabrics containing nanostructured materials," *Int. Nonwovens J.*, 14(4), pp. 10–16, 2005.

-
57. A. Neugebauer, K. Chen, A. Tang, A. Allgeier, L.R. Glicksman, L.J. Gibson, "Thermal conductivity and characterization of compacted, granular silica aerogel," *Energy Build.*, 79, pp. 47–57, 2014.
<https://doi.org/10.1016/j.enbuild.2014.04.025>
58. B.P. Jelle, R. Baetens, A. Gustavsen, "Aerogel insulation for building applications, in Levy, D., Zayat, M., (Eds)," *The Sol-Gel Handbook*, Wiley-VCH Verlag GmbH & Co. KGaA, pp. 1385-1412, 2015.
59. M. Jabbari, D. Åkesson, M. Skrifvars, M.J. Taherzadeh, "Novel lightweight and highly thermally insulative silica aerogel-doped poly (vinyl chloride)-coated fabric composite," *J. Reinf. Plast. Compos.*, 34(19), pp. 1581–1592, 2015.
<https://doi.org/10.1177/0731684415578306>
60. E. Moretti, F. Merli, E. Cuce, C. Buratti, "Thermal and acoustic properties of aerogels: preliminary investigation of the influence of granule size," *Energy Procedia*, 111, pp. 472–480, 2017.
<https://doi.org/10.1016/j.egypro.2017.03.209>
61. L.W. Hrubesh, J.F. Poco, "Thin aerogel films for optical, thermal, acoustic and electronic applications," *J. Non-Cryst. Solids*, 188, pp. 46–53, 1995.
[https://doi.org/10.1016/0022-3093\(95\)00028-3](https://doi.org/10.1016/0022-3093(95)00028-3)

62. C. Buratti, F. Merli, E. Moretti, "Aerogel-based materials for building applications: Influence of granule sizes on thermal and acoustic performance," *Energy Build.*, 152, pp. 472–482, 2017.
<https://doi.org/10.1016/j.enbuild.2017.07.071>
63. M. Schmidt, F. Schwertfeger, "Applications for silica aerogel products," *J. Non-Cryst. Solids*, 225, pp. 364–368, 1998.
[https://doi.org/10.1016/S0022-3093\(98\)00054-4](https://doi.org/10.1016/S0022-3093(98)00054-4)
64. Z. Mazrouei-Sebdani, A. Khoddami, H. Hadadzadeh, M. Zarrebini, "Synthesis and performance evaluation of the aerogel-filled PET nanofiber assemblies prepared by electro-spinning," *RSC Adv.*, 5(17), pp. 12830–12842, 2015.
<https://doi.org/10.1039/C4RA15297B>
65. A. Shaid, L. Wang, R. Padhye, M.R. Bhuyian, "Aerogel nonwoven as reinforcement and batting material for firefighter's protective clothing: a comparative study," *J. Sol-Gel Sci. Technol.*, 87(1), pp. 95–104, 2018.
<https://doi.org/10.1007/s10971-018-4689-8>
66. M. Venkataraman, R. Mishra, J. Militky, X. Xiong, J. Marek, J. Yao, G. Zhu, "Electrospun nanofibrous membranes embedded with aerogel for advanced thermal and transport properties," *Polym. Adv. Technol.*, 29(10), pp. 2583–2592, 2018. <https://doi.org/10.1002/pat.4369>

-
67. M. Gronauer, J. Fricke, "Acoustic properties of microporous SiO₂-aerogel," *Acta Acust. united Acust.* 59(3), pp. 177–181, 1986.
68. J. Gross, J. Fricke, L. Hrubesh, "Sound propagation in SiO₂ aerogels," *J. Acoust. Soc. Am.* 91(4), pp. 2004–2006, 1992.
<https://doi.org/10.1121/1.403684>
69. R. Gerlach, O. Kraus, J. Fricke, P.-C. Eccardt, N. Kroemer, V. Magori, "Modified SiO₂ aerogels as acoustic impedance matching layers in ultrasonic devices," *J. Non-Cryst. Solids*, 145, pp. 227–232, 1992.
[https://doi.org/10.1016/S0022-3093\(05\)80461-2](https://doi.org/10.1016/S0022-3093(05)80461-2)
70. V. Gibiat, O. Lefeuvre, T. Woignier, J. Pelous, J. Phalippou, "Acoustic properties and potential applications of silica aerogels," *J. Non-Cryst. Solids*, 186, pp. 244–255, 1995.
[https://doi.org/10.1016/0022-3093\(95\)00049-6](https://doi.org/10.1016/0022-3093(95)00049-6)
71. L. Forest, V. Gibiat, T. Woignier, "Biot' s theory of acoustic propagation in porous media applied to aerogels and alcogels," *J. Non-Cryst. Solids*, 225, pp. 287–292, 1998.
[https://doi.org/10.1016/S0022-3093\(98\)00325-1](https://doi.org/10.1016/S0022-3093(98)00325-1)
72. J.F. Conroy, B. Hosticka, S.C. Davis, A.N. Smith, P.M. Norris, "Microscale thermal relaxation during acoustic propagation in aerogel and other porous media," *Microscale Thermophys. Eng.*, 3(3), pp. 199–215, 1993.
<https://doi.org/10.1080/108939599199756>

73. L. Forest, V. Gibiat, A. Hooley, "Impedance matching and acoustic absorption in granular layers of silica aerogels," *J. Non-Cryst. Solids*, 285, pp. 230–235, 2001.
[https://doi.org/10.1016/S0022-3093\(01\)00458-6](https://doi.org/10.1016/S0022-3093(01)00458-6)
74. N. Bheekhun, A. Talib, A. Rahim, M.R. Hassan, "Aerogels in aerospace: an overview," *Adv. Mater. Sci. Eng.*, 2013, pp. 1–18, 2013.
<https://doi.org/10.1155/2013/406065>
75. W. Dong, T. Faltens, M. Pantell, D. Simon, T. Thompson, W. Dong, "Acoustic properties of organic/inorganic composite aerogels," in: Y. Brechet, J.D. Embury, P.R. Onck (Eds.), *Materials Research Society Symposium Proceedings*, p. 1188, 2009. <https://doi.org/10.1557/PROC-1188-LL07-02>
76. J.Y. Cai, S. Lucas, L.J. Wang, Y. Cao, "Insulation properties of the monolithic and flexible aerogels prepared at ambient pressure," *Adv. Mat. Res., Trans. Tech. Publ.*, 391–392, pp. 116–120, 2011.
<https://doi.org/10.4028/www.scientific.net/AMR.391-392.116>
77. P. Yan, B. Zhou, A. Du, "Synthesis of polyimide cross-linked silica aerogels with good acoustic performance," *RSC Adv.*, 4(102), pp. 58252–58259, 2014.
<https://doi.org/10.1039/C4RA08846H>

78. C. Buratti, E. Moretti, E. Belloni, F. Agosti, "Development of innovative aerogel-based plasters: preliminary thermal and acoustic performance evaluation," *Sustainability*, 6(9), pp. 5839–5852, 2014.
<https://doi.org/10.3390/su6095839>
79. C. Buratti, E. Moretti, E. Belloni, "Aerogel plasters for building energy efficiency," in: F. Pacheco Torgal, C. Buratti, S. Kalaiselvam, C.G. Granqvist, V. Ivanov (Eds.), *Nano and Biotech Based Materials for Energy Building Efficiency*, Springer, Cham. pp. 17–40, 2016.
https://doi.org/10.1007/978-3-319-27505-5_2
80. M. Sachithanadam, S.C. Joshi, "Effect of granule sizes on acoustic properties of protein-based silica aerogel composites via novel inferential transmission loss method," *Gels* 2(1), p.11, 2016.
<https://doi.org/10.3390/gels2010011>
81. A. Dourbash, C. Buratti, E. Belloni, S. Motahari, "Preparation and characterization of polyurethane/silica aerogel nanocomposite materials," *J. Appl. Polym. Sci.*, 134(8), p. 44521, 2017.
<https://doi.org/10.1002/app.44521>
82. N. Eskandari, S. Motahari, Z. Atoufi, G. Hashemi Motlagh, M. Najafi, "Thermal, mechanical, and acoustic properties of silica-aerogel/UPVC composites," *J. Appl. Polym. Sci.*, 134(14), p. 44685, 2017.
<https://doi.org/10.1002/app.44685>

-
83. Geslain, J.-P. Groby, V. Romero-García, F. Cervera, J. S´anchez-Dehesa, "Acoustic characterization of silica aerogel clamped plates for perfect absorption," *J. Non. Cryst. Solids*, 499, pp. 283–288, 2018.
<https://doi.org/10.1016/j.jnoncrysol.2018.07.021>
84. H.W. Koh, D.K. Le, G.N. Ng, X. Zhang, N. Phan-Thien, U. Kureemun, H.M. Duong, "Advanced recycled polyethylene terephthalate aerogels from plastic waste for acoustic and thermal insulation applications," *Gels*, 4(2), p. 43, 2018.
<https://doi.org/10.3390/gels4020043>
85. M. Ramamoorthy, A. Pisal, R. Rengasamy, A.V. Rao, "In-situ synthesis of silica aerogel in polyethylene terephthalate fibre nonwovens and their composite properties on acoustical absorption behavior," *J. Porous Mater.*, 25(1), pp. 179–187, 2018. <https://doi.org/10.1007/s10934-017-0431-0>
86. Buratti, E. Moretti, "Silica nanogel for energy-efficient windows, Nanotechnology in eco-efficient construction," in: F. Pacheco-Torgal, M. V. Diamanti, A. Nazari, C-G. Granqvist (Eds.), *Nanotechnology in Eco-Efficient Construction*, Materials, Processes and Applications, Woodhead Publishing Series in Civil and Structural Engineering, pp. 207–235, 2013.
<https://doi.org/10.1533/9780857098832.2.207>

-
87. Buratti, E. Moretti, Nanogel windows, in: F. Pacheco Torgal, M. Mistretta, A. Kaklauskas, C.G. Granqvist, L.F. Cabeza (Eds.), "Nearly zero energy building refurbishment," *Springer, London*, pp. 555–582, 2013.
https://doi.org/10.1007/978-1-4471-5523-2_20
88. T. Linhares, M.T.P. de Amorim, L. Durães, "Silica aerogel composites with embedded fibres: a review on their preparation, properties and applications," *J. Mater. Chem. A.*, 7, pp. 22768–22802, 2019.
<https://doi.org/10.1039/C9TA04811A>
89. A.A. Fernández-Marín, N. Jiménez, J.P. Groby, J. Sánchez-Dehesa, V. Romero- García, "Aerogel-based metasurfaces for perfect acoustic energy absorption," *Appl. Phys. Lett.*, 115(6), p. 061901, 2019.
<https://doi.org/10.1063/1.5109084>
90. Z. Talebi, P. Soltani, N. Habibi, F. Latifi, "Silica aerogel/polyester blankets for efficient sound absorption in buildings," *Constr. Build. Mater.*, 220, pp. 76–89, 2019.
<https://doi.org/10.1016/j.conbuildmat.2019.06.031>
91. G.G. Kaya, H. Deveci, "Synergistic effects of silica aerogels/xerogels on properties of polymer composites: A review," *J. Ind. Eng. Chem.*, 89, pp. 13–27, 2020.
<https://doi.org/10.1016/j.jiec.2020.05.019>

-
92. A.C. Pierre, G.M. Pajonk, "Chemistry of aerogels and their applications," *Chem. Rev.*, 102(11), pp. 4243–4266, 2002.
<https://doi.org/10.1021/cr0101306>
93. F. Schwertfeger, M. Schmidt, D. Frank, "Use of aerogels for deadening structure-borne and/or impact sounds," US Patent 6598358B1, 2003.
94. K. Schaumburg, E. Wallstrom, "Aerogel compositions," US Patent 9827296, 2017.
95. S.M. Jones, J. Sakamoto, "Applications of aerogels in space exploration, in: N. Leventis, M.M. Koebel (Eds.), *Aerogels Handbook*," *Springer, New York*, pp. 721–746, 2011. https://doi.org/10.1007/978-1-4419-7589-8_32
96. G. Kim, S. Hyun, "Effect of mixing on thermal and mechanical properties of aerogel-PVB composites," *J. Mater. Sci.*, 38(9), pp. 1961–1966, 2003.
<https://doi.org/10.1023/A:1023560601911>
97. M.K. Williams, T.M. Smith, L.B. Roberson, F. Yang, G.L. Nelson, "Flame Retardant Effect of Aerogel and Nanosilica on Engineered Polymers" , 2010.
<https://ntrs.nasa.gov/api/citations/20110002953/downloads/20110002953.pdf>
98. H.M. Kim, Y.J. Noh, J. Yu, S.Y. Kim, J.R. Youn, "Silica aerogel/polyvinyl alcohol (PVA) insulation composites with preserved aerogel pores using

interfaces between the superhydrophobic aerogel and hydrophilic PVA solution," *Compos. Part A: Appl. Sci. Manuf.*, 75, pp. 39–45, 2015.

<https://doi.org/10.1016/j.compositesa.2015.04.014>

99. S. Motahari, G.H. Motlagh, A. Moharramzadeh, "Thermal and flammability properties of polypropylene/silica aerogel composites," *J. Macromol. Sci. B*, 54(9), pp. 1081–1091, 2015.

<https://doi.org/10.1080/00222348.2015.1078619>

100. M. Afrashi, D. Semnani, Z. Talebi, P. Dehghan, M. Maherolnaghsh, Comparing the drug loading and release of silica aerogel and PVA nano fibers, *J. Non. Cryst. Solids*, 503, pp. 186–193, 2019.

<https://doi.org/10.1016/j.jnoncrysol.2018.09.045>

101. P.M. Norris, S. Shrinivasan, "Aerogels: unique material, fascinating properties and unlimited applications," *Annual Review of Heat Transfer*, 14, pp. 385–408, 2005.

<https://doi.org/10.1615/AnnualRevHeatTransfer.v14.220>

102. T. Yang, X. Xiong, M. Venkataraman, R. Mishra, J. Novák, J. Militký, "Investigation on sound absorption properties of aerogel/polymer nonwovens," *J. Text. I.*, 110(2), pp. 196–201, 2019.

<https://doi.org/10.1080/00405000.2018.1472540>

103. T.J. Cox, P. D'antonio, "Acoustic absorbers and diffusers: theory, design and application," *J. Acoust. Soc. Am.*, 117(3), p. 988, 2005.

<https://doi.org/10.1121/1.1861060>

104. M. Küçük, Y. Korkmaz, "The effect of physical parameters on sound absorption properties of natural fiber mixed nonwoven composites, *Text. Res. J.*, 82(20), pp. 2043–2053, 2012.

<https://doi.org/10.1177/0040517512441987>

105. L. Kela, "Resonant frequency of an adjustable Helmholtz resonator in a hydraulic system," *Arch. Appl. Mech.*, 79(12), pp. 1115–1125, 2009.

<https://doi.org/10.1007/s00419-008-0279-5>

106. ISO 10534-1, Acoustics: Determination of sound absorption coefficient and impedance in impedance tubes-Part 1: method using standing wave ratio, 1996

107. ISO 10534-2, Acoustics: Determination of sound absorption coefficient and impedance in impedance tubes-Part 2: transfer-function method, 2001

108. ISO 354, Acoustics: Measurement of sound absorption in a reverberation room, 2003

109. ASTM E2611-17, Standard Test Method for Normal Incident Determination of Porous Material Acoustical Properties Based on the Transfer Matrix Method, 2017. 10.1520/E2611-17.

-
110. ISO 10140-2, Acoustics: Laboratory measurement of sound insulation of building elements-Part 2: measurement of airborne sound insulation, 2010.
111. ISO 266, Acoustics: Preferred Frequencies, 1997.
112. ISO 11654, Acoustics: Sound Absorbers for Use in Buildings-Rating of Sound Absorption, 1997.
113. J. Chandradass, S. Kang, D.-s. Bae, "Synthesis of silica aerogel blanket by ambient drying method using water glass-based precursor and glass wool modified by alumina sol," *J. Non. Cryst. Solids*, 354(34), pp. 4115–4119, 2008.
<https://doi.org/10.1016/j.jnoncrysol.2008.03.039>
114. D. Pilon, R. Panneton, F. Sgard, "Behavioral criterion quantifying the effects of circumferential air gaps on porous materials in the standing wave tube," *J. Acoust. Soc. Am.*, 116(1), 344–356, 2004.
<https://doi.org/10.1121/1.1756611>
115. B.N. Gover, J. Bradley, S. Schoenwald, B. Zeitler, "Subjective ranking of footstep and low-frequency impact sounds on lightweight wood-framed floor assemblies," in: *Proceeding of Forum Acusticum, Aalborg, Denmark*, 2011 c7a4eb4d-aaf7-4990-93f7-3573bc0a1406

-
116. F. Asdrubali, S. Schiavoni, K. Horoshenkov, "A review of sustainable materials for acoustic applications," *Build. Acoust.*, 19(4), pp. 283–311, 2012.
<https://doi.org/10.1260/1351-010X.19.4.283>
117. ISO 9052-1, Acoustics: Determination of dynamic stiffness-Part 1: Materials used under floating floors in dwellings, 1989.
118. F. Merli, A.M. Anderson, M.K. Carroll, C. Buratti, "Acoustic measurements on monolithic aerogel samples and application of the selected solutions to standard window systems," *J. Appl. Acoust.*, 142, pp. 123–131, 2018.
<https://doi.org/10.1016/j.apacoust.2018.08.008>
119. J.C. Wang, J. Shen, X.Y. Ni, B. Wang, X.D. Wang, J. Li, "Acoustic properties of nanoporous silica aerogel," *Rare Metal Mat. Eng.*, 39, pp. 14–17, 2010.
120. M. Gronauer, A. Kadur, J. Fricke, "Mechanical and acoustic properties of silica aerogel, in: J. Fricke (Ed.)," *Aerogels, Springer*, Berlin, pp. 167–173, 1986.
https://doi.org/10.1007/978-3-642-93313-4_1
121. J. Gross, J. Fricke, R. Pekala, L. Hrubesh, "Elastic nonlinearity of aerogels," *Phys. Rev. B.*, 45(22), p. 12774, 1992.
<https://doi.org/10.1103/PhysRevB.45.12774>

-
122. J. Gross, G. Reichenauer, J. Fricke, "Mechanical properties of SiO₂ aerogels," *J. Phys. D: Appl. Phys.*, 21(9), p. 1447,1988.
<https://doi.org/10.1088/0022-3727/21/9/020>
123. B.H. Song, J.S. Bolton, "A transfer-matrix approach for estimating the characteristic impedance and wave numbers of limp and rigid porous materials," *J. Acoust. Soc. Am.*, 107(3), pp. 1131–1152, 2000.
<https://doi.org/10.1121/1.428404>
124. J. Feng, D. Le, S.T. Nguyen, V.T.C. Nien, D. Jewell, H.M. Duong, "Silica cellulose hybrid aerogels for thermal and acoustic insulation applications," *Colloids Surf. A.*, 506, pp. 298–305, 2016.
<https://doi.org/10.1016/j.colsurfa.2016.06.052>
125. Shaid, L. Wang, R. Padhye, "The thermal protection and comfort properties of aerogel and PCM-coated fabric for firefighter garment," *J. Ind. Text.* 45(4), pp. 611–625, 2016.
<https://doi.org/10.1177/1528083715610296>
126. L. Jin, K. Hong, K. Yoon, "Effect of aerogel on thermal protective performance of firefighter clothing," *J. Fiber Bioeng. Inf.*, 6(3), pp. 315–324, 2013.
<https://doi.org/10.3993/jfbi09201309>

127. M. Venkataraman, R. Mishra, D. Jasikova, T. Kotresh, J. Militky, "Thermodynamics of aerogel-treated nonwoven fabrics at subzero temperatures," *J. Ind. Text.*, 45(3), pp. 387–404, 2015.
<https://doi.org/10.1177/1528083714534711>
128. L. Li, B. Yalcin, B.N. Nguyen, M.A.B. Meador, M. Cakmak, "Flexible nanofiber-reinforced aerogel (xerogel) synthesis, manufacture, and characterization," *ACS Appl. Mater. Interfaces*, 1(11), pp. 2491–2501, 2009.
<https://doi.org/10.1021/am900451x>
129. H. Wu, Y. Chen, Q. Chen, Y. Ding, X. Zhou, H. Gao, "Synthesis of flexible aerogel composites reinforced with electrospun nanofibers and microparticles for thermal insulation," *J. Nanomater.*, 375093, 2013.
<https://doi.org/10.1155/2013/375093>
130. H. Bahrambeygi, N. Sabetzadeh, A. Rabbi, K. Nasouri, A.M. Shoushtari, M. R. Babaei, "Nanofibers (PU and PAN) and nanoparticles (Nanoclay and MWNTs) simultaneous effects on polyurethane foam sound absorption," *J. Polym. Res.*, 20(2), p. 72, 2013.
<https://doi.org/10.1007/s10965-012-0072-6>
131. K. Singha, S. Maity, M. Singha, P. Paul, D.P. Gon, "Effects of fiber diameter distribution of nonwoven fabrics on its properties," *Int. J. Text. Sci.*, 1, pp. 7–14, 2012. <https://doi.org/10.5923/j.textile.20120101.02>

-
132. H.S. Seddeq, "Factors influencing acoustic performance of sound absorptive materials," *Aust. J. Basic Appl. Sci.*, 3(4), pp. 4610–4617, 2009.
133. K.W. Oh, D.K. Kim, S.H. Kim, "Ultra-porous flexible PET/Aerogel blanket for sound absorption and thermal insulation," *Fibers Polym.*, 10(5), pp. 731–737, 2009.
<https://doi.org/10.1007/s12221-010-0731-3>
134. A.S. Dorcheh, M. Abbasi, "Silica aerogel; synthesis, properties and characterization," *J. Mater. process. technol.*, 199, pp. 10–26, 2008.
<https://doi.org/10.1016/j.jmatprotec.2007.10.060>
135. S. Motahari, H. Javadi, A. Motahari, "Silica-aerogel cotton composites as sound absorber," *J. Mater. Civ. Eng.*, 27(9), 04014237, 2015.
[https://doi.org/10.1061/\(ASCE\)MT.1943-5533.0001208](https://doi.org/10.1061/(ASCE)MT.1943-5533.0001208)
136. U. Berardi, "Aerogel-enhanced systems for building energy retrofits: Insights from a case study," *Energy Build.*, 159, pp. 370–381, 2018.
<https://doi.org/10.1016/j.enbuild.2017.10.092>
137. M. Ganobjak, S. Brunner, J. Wernery, "Aerogel materials for heritage buildings: Materials, properties and case studies," *J. Cult. Heritage*, 42, pp. 81–98, 2019.
<https://doi.org/10.1016/j.culher.2019.09.007>

-
138. I. Preikšs, J. Skujāns, U. Iljins, "Possibilities of silica aerogel application for foam gypsum compositions," in: 3rd International Scientific Conference. Proceedings (Latvia). Latvia University of Agriculture, 2011.
139. P. Narang, "A theoretical study of sound transmission through aerogel glazing systems," *Appl. Acoust.*, 34(4), pp. 249–259, 1991.
[https://doi.org/10.1016/0003-682X\(91\)90008-3](https://doi.org/10.1016/0003-682X(91)90008-3)
140. M.D. Guild, V.M. García-Chocano, J. Sánchez-Dehesa, T.P. Martin, D.C. Calvo, G. J. Orris, "Aerogel as a soft acoustic metamaterial for airborne sound," *Phys. Rev. Appl.*, 5(3), 034012, 2016
<https://doi.org/10.1103/PhysRevApplied.5.034012>
141. C. Buratti, E. Moretti, "Experimental performance evaluation of aerogel glazing systems," *Appl. Energy*, 97, pp. 430–437, 2012.
<https://doi.org/10.1016/j.apenergy.2011.12.055>
142. F. Cotana, A.L. Pisello, E. Moretti, C. Buratti, "Multipurpose characterization of glazing systems with silica aerogel: In-field experimental analysis of thermal-energy, lighting and acoustic performance," *Build. Environ.*, 81, pp. 92–102, 2014.
<https://doi.org/10.1016/j.buildenv.2014.06.014>
143. ISO 15665, Acoustics – Acoustic insulation for pipes, valves and flanges, 2003.

Chapter 3:

The acoustical absorption by air-saturated aerogel powders

This chapter is published as:

H. Begum, Y. Xue, J.S. Bolton, K.V. Horoshenkov, "The acoustical absorption by air-saturated aerogel powders" , *J. Acoust. Soc. Am.*, 151(3), 1502–1515, 2022.

<https://doi/10.1121/10.0009635>

Authorship statement:

The principal author of the paper is H. Begum. The contribution of H. Begum is the research investigation, experimental data collection and participation in the data interpretation.

3.1 Abstract

The acoustical behaviour of air-saturated aerogel powders in the audible frequency range is not well understood. It is not clear, for example, which physical processes control the acoustic absorption and/or attenuation in a very light, loose granular mix in which the grain diameter is on the order of a micron.

The originality of this work is the use of a Biot-type poro-elastic model to fit accurately the measured absorption coefficients of two aerogel powders with particle diameters in the range 1–40 μm . It is shown that these materials behave like a viscoelastic layer and their absorption coefficient depends strongly on the root mean square pressure in the incident wave. Furthermore, it was found that the loss factor controlling the energy dissipation due to the vibration of the elastic frame is a key model parameter. The value of this parameter decreased progressively with both frequency and sound pressure. In contrast, other fitted parameters in the Biot-type poro-elastic model, e.g., the stiffness of the elastic frame and pore size, were found to be relatively independent of the frequency and amplitude of the incident wave. It is shown that these materials absorb acoustic waves very efficiently around the frequencies of the frame resonance.

Keywords: Acoustics; aerogels; modelling; particles; porous materials

3.2 Introduction

The desire to develop a diverse class of lightweight, porous and cost-effective materials for acoustic applications has been the focus of industrialists for the past few decades [1]. Traditionally, a large selection of these materials were fibrous layers and reticulated foams [2]. Companies are invested in the use of foams or fibrous materials due to their high percentage of open pore availability (e.g., section 13.9 in reference [2]) and their versatile nature, which makes it possible to incorporate them in the form of layered composites. Their porous nature allows them to be effective absorbers, which can dissipate the acoustic energy of propagating sound waves, and some may have viscoelastic properties, which control structure-borne noise by attenuating structural vibrations through near-field damping (NFD) [3], achieved *via* viscous interaction between the porous medium and evanescent acoustical near-field of a vibrating structure. There may be additional dissipation caused by the elastic nature of the frame if it is sufficiently stiff, i.e., when using poro-elastic media instead of limp porous media as near-field dampers [4]. The acoustical damping multifunctionality of porous media has been investigated for several years, and the study is summarised in reference [5], which also provides the theoretical fundamentals of the study introduced in this article. The most important macroscopic physical characteristics (also referred to as bulk properties), which determine the acoustical properties of foams and fibrous

media are: (i) airflow resistivity/effective pore size, (ii) porosity, (iii) pore tortuosity, and (iv) elastic modulus of the frame [6]. Granular media are also of popular interest because of their useful sound absorption and sound insulating properties [7,8]. Materials such as flint particles [9], hemp [10] and expanded clays [11,12] have already been extensively studied. In particular, classical acoustics theory such as the Biot theory for poro-elastic media has proven to be capable of modelling sound absorption and insulation resulting from granular media which have complex and hierarchical micro-structures such as granular activated carbon stacks [13].

Granular aerogels are gaining more interest as an acoustic product due to their unique microstructural properties, i.e., porosities of approximately 95%, very low bulk densities (e.g., 0.0120 g/cm^3) and large surface area values in the range from 700 to 900 m^2/g [14]. The global aerogel market was evaluated at $\$701 \times 10^6$ USD in 2019 and is projected to reach $\$1395.5 \times 10^6$ USD by 2027 with a reported compound annual growth rate (CAGR) of 9.3%. Its primary development is in the building, oil and gas industries. Because of their chemical inertness and low thermal conductivity, aerogels are sought after products for pipe insulation and protection [15]. The main drawbacks, however, are their high-cost production (specifically for monolithic aerogels) and ever-changing economic barriers [16]. Nonetheless, their exciting acoustical properties still create the potential for profitable gain for industries. Sound waves have been

observed to propagate through silica aerogels at one-third the speed of sound in air or less: i.e., at about 100 m/s [17]. Forest *et al.* [18] have also found that sound velocities in aerogels can be as low as 60–70 m/s. The latter property results in rather high acoustic attenuation in aerogels since it effectively increases a given layer depth as a fraction of the wavelength.

In general, there is a lack of combined experimental data and analytical models that are available to predict the acoustical properties of granular aerogels. There is some literature by Begum *et al.* [19] which focus on analytical models and experimental data of the acoustical properties of granular silica aerogels. However, that work was performed using material with millimetric grain sizes, and by using a triple porosity model, where only pore size and particle size were taken into consideration, and not the elastic properties of the material frame. Xue *et al.* [20] have observed non-linear acoustical behaviour of aerogel particle stacks consisting of relatively small particles (i.e., 2–40 micron), and that the non-linearity being dependent on the frequency and depth of the sample stack. Further evidence of non-linearity is presented in this article. A majority of other related research exclusively focuses on much denser granular media with millimetric grain mixes using a Padé approximation approach, e.g., Horoshenkov and Swift [19] and Horoshenkov *et al.* [21].

Earlier research by Song and Bolton [22] was directed at using a four-microphone standing wave tube and the transfer matrix method (TMM) to

determine the fundamental acoustical properties, such as wave number and characteristic impedance of limp or rigid porous materials: i.e., materials that can be modelled as effective fluids. Based on that information arbitrarily shaped porous material domains can then be modelled by providing data, such as complex density and complex sound speed to finite element models, for example. In contrast, here, the two-microphone standing wave tube method was used to measure the normal incidence absorption coefficients of the aerogels layers [23], and the material was modelled as a poro-elastic layer, hence, allowing for both frame and airborne waves within the aerogel layers [2].

Because a majority of the literature has focused on millimetric [2,11] grain mixes with sub-millimeter pore sizes [24], there is a gap in the understanding of the acoustical behaviour of powder aerogels, whose particle sizes are close to a micron. The modelling of such small particles with different excitation sound pressures will help to understand the non-linear effects, which typically develop in lightweight materials such as aerogels. An approach like this will also build the connection between the material' s bulk properties, such as material density and particle size, and key acoustical characteristics such as the normal incidence absorption coefficient.

Thus, there are two primary motivations for the present work. First, based on fitting the experimental data, the connections developed in that way can help to inversely characterise the aerogel' s acoustical-related bulk properties, thus,

quantifying each bulk property' s contribution to the material' s sound absorption performance. Second, and consequently, it becomes possible to optimise the acoustical performance of this type of aerogel by designing or specifying these bulk properties appropriately. However, this is not the main interest of the research here as we are primarily trying to understand the connection between the acoustical-related bulk properties and the materials' sound absorption performance.

The structure of this chapter is as follows. In Section 3.3, the experimental methods and characterisation techniques used to measure the physical material properties of aerogel powders are described. Presented in Section 3.4 are the acoustical theories and the approach to modelling of the acoustics of the aerogel granules. The results and related discussion are described in Section 3.5 in which the data are interpreted with a mathematical model that can be used to characterise the acoustical-related bulk properties. The concluding remarks, which summarise the characterisation process and the main result, are presented in Section 3.6.

3.3 Materials and Methods

3.3.1 Materials characterisation

Microstructural observations of the particle size distribution of the silica aerogels studied here – Enova IC3100 produced by Cabot Corporation, Alpharetta Georgia, USA (denoted as type 1), and JIOS AeroVa D20 produced by JIOS Aerogel, Korea (denoted as type 2) were made by using scanning electron microscopy (SEM). The instrument used was an FEI Inspect F50 FEG SEM (Eindhoven, The Netherlands). The samples were mounted as per the manufacturer' s guidelines and were initially carbon coated using a Quorum Technologies Q150T coater (Quorum, Sussex, UK). However, that coating proved to be insufficient to prevent sample charging even at 5 kV and, therefore, the samples were subsequently given a 5 nm gold coat using a Quorum Technologies Q150R gold sputter coater.

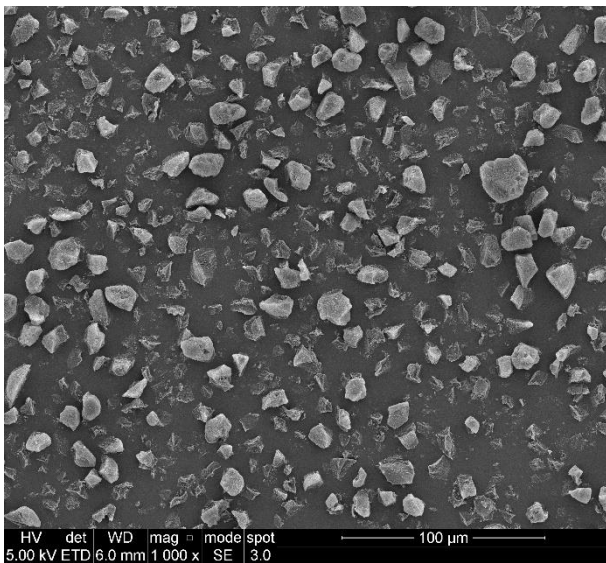
Secondary Electron Images (SE) were obtained at a range of the accelerating voltages (kV) as indicated on the micrographs. The spot size three was used with the 20 μm final lens aperture (smallest for the highest resolution) inserted. For the highest magnification images, the working distance (WD) was reduced to 6 mm from the standard 10 mm for type 1.

Figures 3.1 (a)–(f) includes SEM images of type 1 and type 2 aerogel powders. These images were used to identify the aerogel particle distribution and

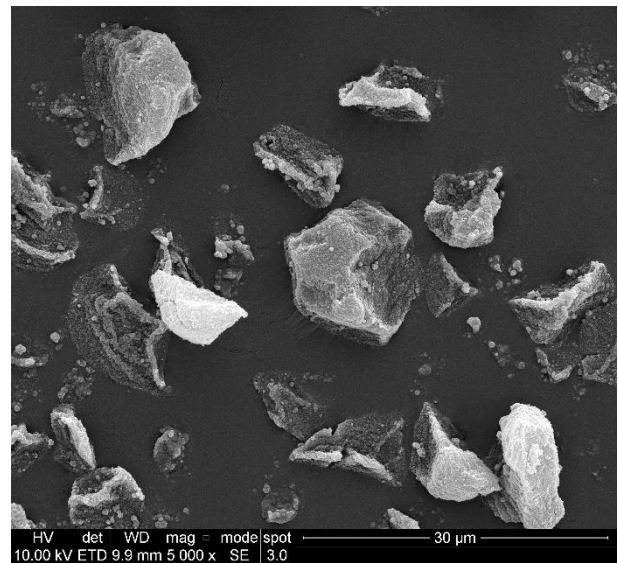
structure of the pore sizes. A Java-based image processing program, ImageJ, was used to manually measure the size of 100 individual type 1 and type 2 particles in the images that were obtained at a high magnification (1000 \times) at a scale bar of 100 μm . The data was collated to determine the normal approximation of the particle size distribution: see THE supplementary material in reference [25]. The average type 1 particle size was found to be 13.69 μm , with minimum and maximum values of 7.91 μm and 24.83 μm , respectively, and the average type 2 particle size was 14.20 μm with minimum and maximum values of 5.54 μm and 41.78 μm respectively. These average particle size values correspond to those that were used for the 3P-Biot-TMM/ACM modelling of the acoustical properties (detailed in Sections 3.4 and 3.5), and the measured minimum and maximum values of the type 1 and type 2 aerogel powders also corresponded to the values given in the manufacturers' technical data sheets.

Note that the SEM magnification scale in each of the images in Figure 3.1 changes between 100 μm , 30 μm , 1 μm and 500 nm to provide a better insight into the particle microstructure. The 100 μm magnification was used to determine the mean particle size and standard deviation. The 30 μm magnification illustrates the angular nature of these particles. The 1 μm and 500 nm magnifications show that these particles are not solid but are nanoporous. We note that SEM image analysis is sensitive to the detail of the loading of samples onto the carbon stub: i.e., when a large amount is deposited, the

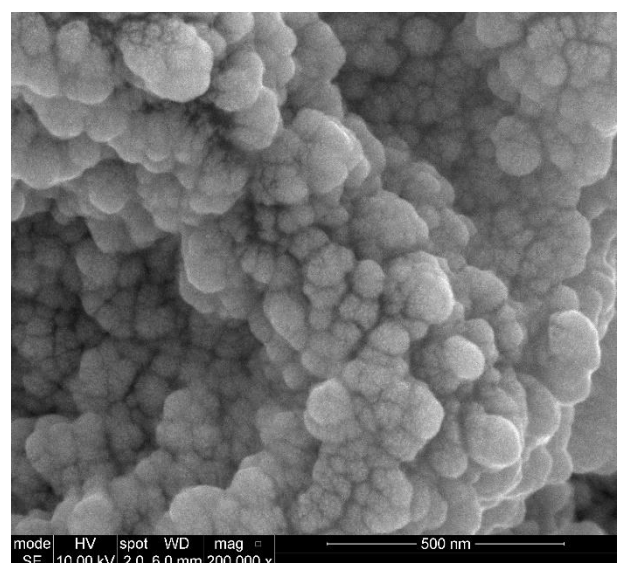
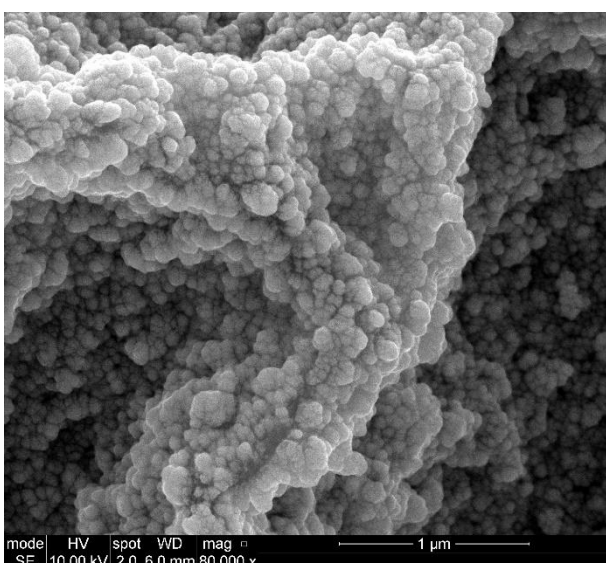
coating is affected, and this may fracture the image surfaces. Furthermore, there may be sampling bias causing the contrast/brightness settings to be adjusted and this may also affect the results [19].



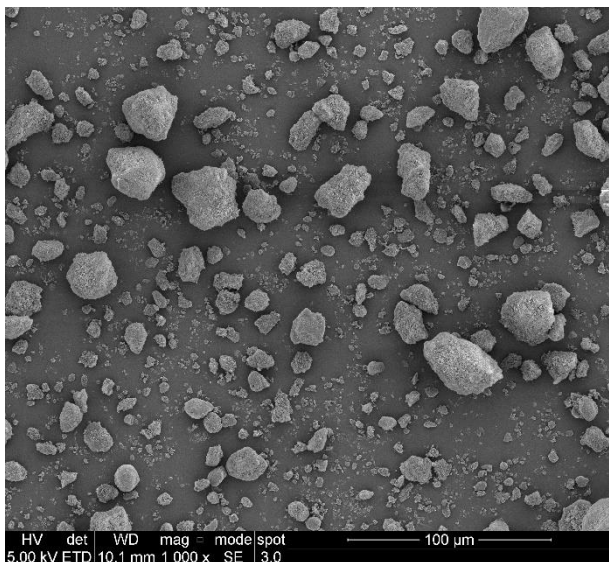
a) Type 1 – SEM image at 100 μm



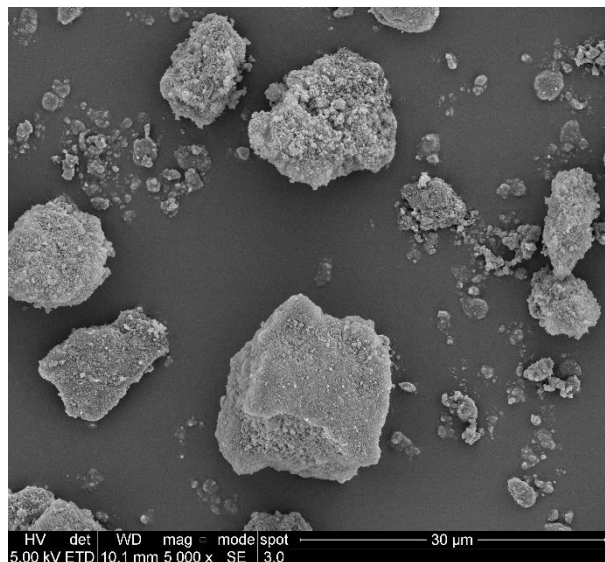
b) Type 1 – SEM image at 30 μm



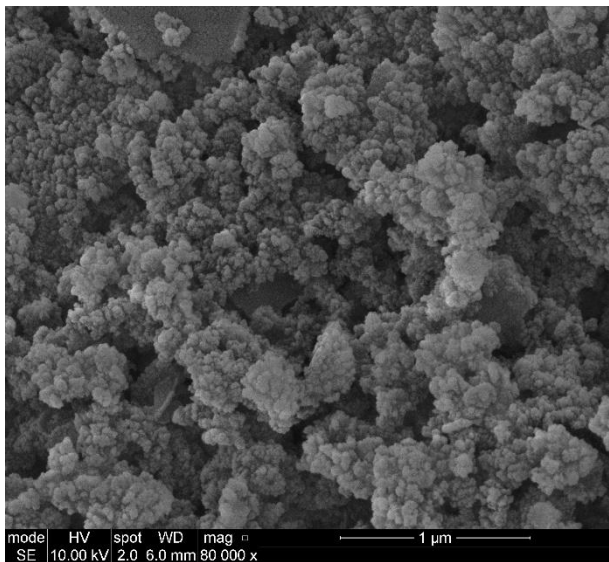
c) Type 1 – SEM image at 1 μm



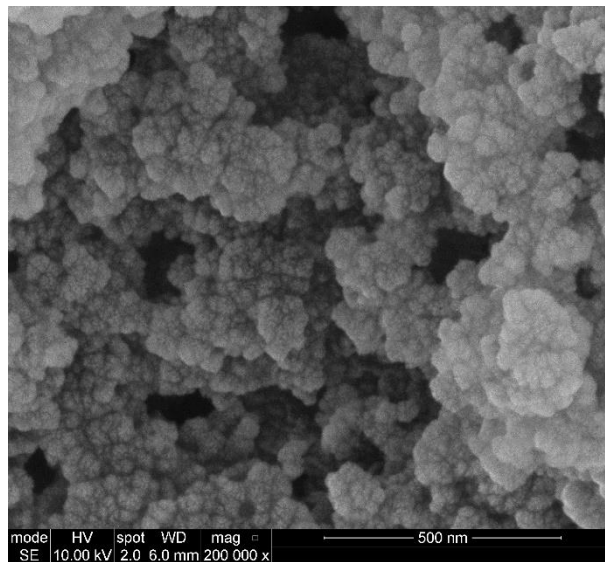
d) Type 1 – SEM image at 500 nm



e) Type 2 – SEM image at 100 μm



f) Type 2 – SEM image at 30 μm



g) Type 2 – SEM image at 1 μm

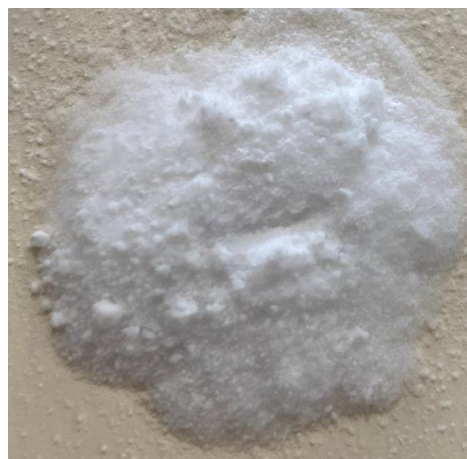
h) Type 2 – SEM image at 500 nm

Figure 3.1 The SEM images of type 1 and 2 aerogels taken at increasing magnifications (1000 x (a) and (e), 5000 x (b) and (f), 80,000 x (c) and (g) and 200,000 (d) and (h)).

The skeletal material density was calculated from the mass and volume combined with the volume-pressure relationship of Boyle' s law measured using the gas displacement method (Micrometrics AccuPyc 1330 Helium Pycnometer used at 20 °C, Lincoln, England). The result was 2430 kg/m³ for type 1 and 1710 kg/m³ for type 2. The bulk densities of these materials, ρ_b , were determined using calibrated scales: they were 38.71 kg/m³ \pm 0.18 and 104.91 kg/m³ \pm 1.26 for aerogel particle types 1 and 2, respectively.



Type 1 – Enova IC3100



Type 2 – JIOS AeroVa D20

Figure 3.2 Photographs of the powder samples used in the impedance tube experiments.

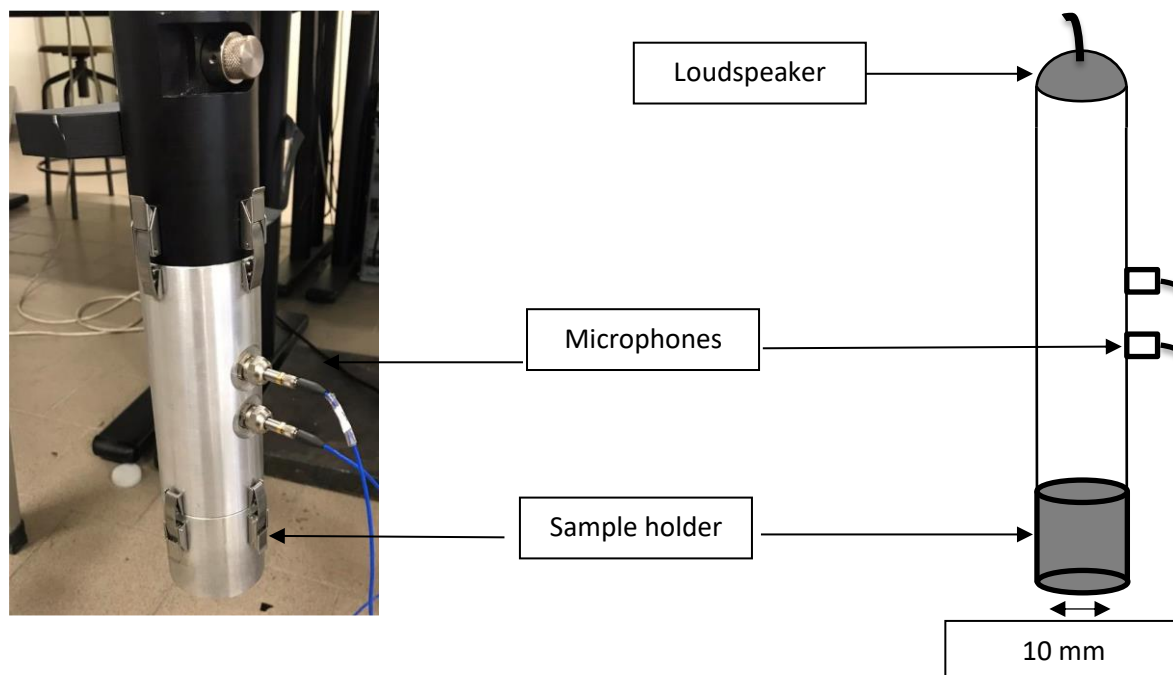


Figure 3.3 The 2-microphone impedance tube setup to measure the surface impedance of a porous layer (taken with permission from reference [26]).

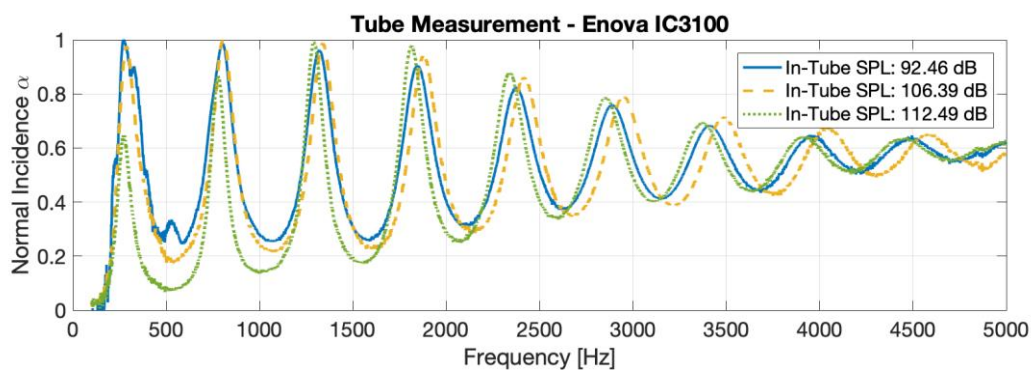
The acoustical properties of the aerogel stacks were measured in a 10 mm diameter standing wave tube which was custom made by Materiacustica (Ferrara, Italy) [27]. This two-microphone tube setup was developed to test small material specimens, such as granular media and powders in accordance with the ISO standard 10534-2:2001 [23]. This setup enabled the measurement

of the normalised surface acoustic impedance, complex reflection coefficient, and sound absorption coefficient of a hard-backed porous layer in the frequency range from 100 to 4999 Hz. The spacing between the two microphones was 30 mm, which is usual for this frequency range as recommended in the ISO standard [23]. The distance from the sample surface to the first microphone was 85.9 mm. The thickness of all the samples used in the acoustic experiments was 50 mm. Figure 3.2 shows the type 1 and type 2 aerogel powders which were used in the acoustic experiments. Finally, Figure 3.3 shows a photograph and sketch of the vertical standing wave tube that was used in these experiments. Note that all sound pressure levels (SPL) quoted here refer to the sound wave incident on the sample, integrated over the frequency range 100–4999 Hz.

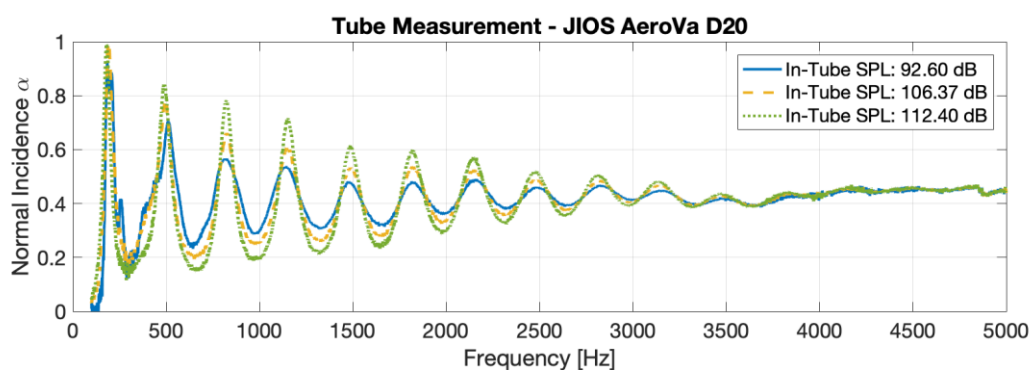
3.4 Modelling of aerogel granule stacks

It was observed from the experimental data that the acoustical absorption coefficients of the tested aerogel granule stacks differed significantly from those that would be expected from a conventional sound absorber such as a layer of polymeric fibres. The acoustic absorption coefficient of the aerogel layers showed multiple, lightly damped depth resonances: as an example, the normal incidence sound absorption coefficients measured at different incident,

broadband SPL (dB) for the two types of materials are shown in Figure 3.4. Notably, large peak values of absorption appear at unusually low frequencies. It was also found that the heights of these peaks decreased with increasing SPL, which provides the main evidence that the aerogel sample stacked in the tube behave non-linearly. As well, there appears to be a slight frequency shift for the type 1 material (Enova IC3100, Cabot Corporation, Alpharetta, GA) as the level changes which also suggests a nonlinear response. It was also clear when conducting the experiments that the granules comprising the powder samples vibrated under acoustic excitation. That vibration caused some dispersion of powder particles over the area of the impedance tube adjacent to the sample holder. The sample thickness occasionally reduced by as much as 0.5 mm after the first time that the acoustic stimulus was applied. When that shrinkage occurred, more material was added to compensate for this change. There was little or no subsequent change in the sample thickness when the experiment was repeated without touching the sample. At this stage, the experimental data were recorded and used for the comparison with the models.



a)



b)

Figure 3.4 The normal incidence sound absorption coefficients, measured at different in-tube SPL in the standing wave tube experiments for (a) type 1 (Enova IC3100, Cabot Corporation, Alpharetta, GA) and (b) type 2 material (JIOS AeroVa D20, JIOS Aerogel, Korea). In the legend SPL corresponds to the incident, broadband SPL measured with the two microphones in accordance with reference [23].

3.4.1 Acoustical theories for predicting sound absorption

In the present work, two models were used to predict the frequency-dependent equivalent density, ρ_e , and bulk modulus, K_f of the fluid phase (i.e., air) in the aerogel granule stacks: (i) the 5-parameter Johnson-Champoux-Allard (JCA) model [28,29]; and (ii) the 3-parameter Páde approximation (3P) model [30]. The Biot theory [31] (also see Chapter 11 in reference [2]) was then applied to account for the frame elasticity in the presence of air.

(*Note – the section below is not included in the original published paper)

The Biot theory was originally developed by Maurice Anthony Biot [31] and he states that all porous media can be divided into three general types: rigid-porous, limp-porous and elastic-porous, where rigid and limp are the extreme cases of an elastic porous medium when the bulk elasticity of the frame is extremely large or small respectively.

To understand this in detail, if the solid phase of the target material is like plastic foam or stacked granules then it can be modelled as rigid-framed; with a longitudinal wave propagating within the porous medium, with the complex wavenumber calculated as [5]

$$k_c = \omega(\rho_{eff}/K_f)^{1/2} = \omega(\rho'_{eff}/K'_f)^{1/2} \quad (1)$$

and the complex density of the rigid porous medium expressed as

$$\rho_c = \rho'_{eff} = \rho_{eff}/\phi. \quad (2)$$

If the solid phase of the material is lightweight like a polymeric, fibrous layer then it can be modelled as limp-framed with only one longitudinal wave propagating within the limp, porous medium. The complex wavenumber can be calculated as

$$k_c = \left[\frac{\omega^2(\rho_{11}^*\rho_{22}^* - \rho_{12}^{*2})}{\rho_{11}^*R - 2\rho_{12}^*Q + \rho_{22}^*P} \right]^{1/2}, \quad (3)$$

and the complex density of the limp-porous medium can be expressed as

$$\rho_c = \frac{k_c^2(\rho + Q_a + Q + Ra)}{\omega^2(1 - \phi + \phi a)}, \quad (4)$$

with

$$a = \frac{\rho_{12}^*Q - \rho_{11}^*R}{\rho_{12}^*R - \rho_{22}^*Q}, \quad (4)$$

where P , Q , and R are the simplified elastic coefficients, equivalent to

$$P = \frac{K_f(1 - \phi)^2}{\phi} = K'_f(1 - \phi)^2, \quad (5)$$

$$Q = K_f(1 - \phi) = K'_f\phi(1 - \phi), \quad (6)$$

$$R = K_f\phi = K'_f\phi^2, \quad (7)$$

and Biot's modified mass density coefficients: ρ_{12}^* , ρ_{11}^* , and ρ_{22}^* are expressed as

$$\rho_{12}^* = -\phi\rho_0(\alpha_\infty - 1) + i\sigma\phi^2 \frac{Gj(\omega)}{\omega} = \rho_0\phi - \rho_{22}^*, \quad (8)$$

$$\rho_{11}^* = \rho_b + \phi\rho_0(\alpha_\infty - 1) - i\sigma\phi^2 \frac{Gj(\omega)}{\omega} = \rho_b - \rho_{12}^*, \quad (9)$$

$$\rho_{22}^* = \phi\rho_0\alpha_\infty - i\sigma\phi^2 \frac{Gj(\omega)}{\omega} = \phi\rho_{eff} = \phi^2\rho'_{eff}, \quad (10)$$

where ρ_b is the bulk density of the porous medium and is calculated using the equation $\rho_b = \rho_s(1 - \phi)$, where ρ_s is the density of the solid material and ϕ is the porosity.

If the solid phase of the material has a finite elasticity, like a layer of polyurethane foam then it can be modelled as elastic-framed with two longitudinal and one transverse wave that can propagate through a poro-elastic medium. The complex wavenumber of the two longitudinal waves, k_1 and k_2 and the transverse wave, k_3 can be calculated as

$$k_1 = \left[\frac{\omega^2(P\rho_{22}^* + R\rho_{11}^* - 2Q\rho_{12}^* - \sqrt{\Delta})}{2(PR - Q^2)} \right]^{1/2}, \quad (11)$$

$$k_2 = \left[\frac{\omega^2(P\rho_{22}^* + R\rho_{11}^* - 2Q\rho_{12}^* + \sqrt{\Delta})}{2(PR - Q^2)} \right]^{1/2} \quad '' \quad (12)$$

$$k_3 = \left[\frac{\omega^2(\rho_{11}^*\rho_{22}^* - \rho_{12}^{*2})}{N\rho_{22}^*} \right]^{1/2}, \quad (13)$$

where Δ is given by

$$\Delta = (P\rho_{22}^* + R\rho_{11}^* - 2Q\rho_{12}^*)^2 - 4(PR - Q^2)(\rho_{11}^*\rho_{22}^* - \rho_{12}^{*2}), \quad (14)$$

the sheer modulus, N of the poro-elastic medium can be expressed in terms of Young' s modulus, E_1 , Poisson' s ratio, ν , and mechanical loss factor, η_m as

$$N = \frac{E_1(1 + i\eta_m)}{2(1 + \nu)}. \quad (15)$$

The elasticity coefficient P can be expressed as

$$P = \frac{3}{4}N + K_b + \frac{K_f(1 - \phi)^2}{\phi} = \frac{3}{4}N + K_b + K'_f(1 - \phi)^2. \quad (16)$$

where K_b is the bulk modulus given by

$$K_b = \frac{2N(1 + \nu)}{3(1 - 2\nu)}. \quad (17)$$

3.4.2 Bulk modulus and equivalent density predictions with the JCA model

The original JCA model requires five non-acoustic parameters as inputs: (i) airflow resistivity, σ ; (ii) porosity, ϕ ; (iii) tortuosity, α_∞ ; (iv) viscous characteristic length, Λ ; and (v) thermal characteristic length, Λ' . Note that the static thermal permeability, k'_0 [32] (denoted as q'_0 on pages 84–85 in reference [2]), is also considered as a thermal-effects contributor to the bulk modulus in the extended Johnson-Champoux-Allard-Lafarge (JCAL) model, but it was not used as an input to the JCA model that was applied in the current study. Also, note

that for fibrous media as described in reference [5], Λ and Λ' are usually calculated as functions of σ , ϕ , α_∞ [30] and the shape factors are c (usually equal to 1 for fibres) and c' (i.e., $c' = \Lambda/\Lambda'$). In contrast, σ , ϕ , α_∞ , Λ and Λ' were used in the current study to calculate ρ_e and K_f based on the JCA model (eqs. (3) and (18) in reference [28]). Other ambient parameters needed for the modelling process included the dynamic viscosity of air, $\eta = 1.82 \times 10^{-5}$ Pa s, the speed of sound in air, $c_0 = 343$ m/s, the density of air, $\rho_0 = 1.21$ kg/m³, the Prandtl number, $B^2 = 0.71$, and the specific heat ratio, $\gamma = 1.402$.

(*Note – the section below is not included in the original published paper)

To characterise the bulk properties of a porous medium, the effective density, ρ_e and bulk modulus, K_f of a fluid phase (i.e., air) must be calculated by quantifying the viscous and thermal effects in the pores [5]. To calculate the effective density, ρ_e , we use the equation

$$\rho_{eff} = \alpha_\infty \rho_0 \left[1 + \frac{\sigma}{i\omega \rho_0 \alpha_\infty} G_J(\omega) \right], \quad (18)$$

and to calculate the bulk modulus, K_f we use the equation

$$K_f = \gamma \rho_0 / \left[\gamma (\gamma - 1) \left[1 + \frac{\sigma' \phi}{iB^2 \omega \rho_0 \alpha_\infty} G'_J(\omega) \right]^{-1} \right], \quad (19)$$

where

$$G_J(\omega) = \left(1 + \frac{4i\alpha_\infty^2 \eta \rho_0 \omega}{\sigma^2 \Lambda^2 \phi^2} \right)^{1/2}, \quad (20)$$

and

$$G'_J(B^2\omega) = \left(1 + \frac{4i\alpha_\infty^2 \eta \rho_0 B^2 \omega}{\sigma'^2 \Lambda^2 \phi^2} \right)^{1/2}. \quad (21)$$

To understand the JCA model, we must understand this individually. The dynamic tortuosity, α , is the function used to express the dynamic viscous permeability. It is given in the work by Johnson *et al* [33]. by:

$$\alpha(\omega) = \frac{\nu\phi}{j\omega q_0} \left[1 + \left(\frac{2\alpha_\infty q_0}{\phi\Lambda} \right)^2 \frac{j\omega}{\nu} \right]^{1/2} + \alpha_\infty \quad (22)$$

Eq. 5 was important to describe the sound propagation in porous media and justifies the asymptotic behaviour. He has shown that the effective density can be written at high frequencies at first-order approximation in $1/\sqrt{\omega}$ for large ω

$$\rho = \alpha_\infty \rho_0 \left[1 + (1 - j) \frac{\delta}{\Lambda} \right] \quad (23)$$

and for small ω the limit is given by

$$\rho(\omega) = \rho_0 \alpha_\infty \left(1 + \frac{2\alpha_\infty q_0}{\Lambda^2 \phi} \right) + \frac{\eta\phi}{j\omega q_0}, \quad (24)$$

Directly measuring the static thermal permeability is not easy. The Lafarge model which uses

$$\alpha'(\omega) = \frac{\nu' \phi}{j\omega q'_0} \left[1 + \left(\frac{2\alpha_\infty q'_0}{\phi \Lambda'} \right)^2 \frac{j\omega}{\nu'} \right]^{1/2} + 1 \quad (25)$$

Where q'_0 is replaced by the permeability $q'_0 = \phi \Lambda'^2 / 8$ of a porous medium with circular cylindrical pores having a radius $R = \Lambda'$ leading to

$$\alpha'(\omega) = \frac{8\nu'}{j\omega \Lambda'^2} \left[1 + \left(\frac{\Lambda'}{4} \right)^2 \frac{j\omega}{\nu'} \right]^{1/2} + 1 \quad (26)$$

This arbitrary choice for q'_0 can lead to a large area in the localisation of the transition frequency where the imaginary part of the bulk modulus reaches its maximum. This does not lead to a large error in the determination of the surface impedance because the damping is mainly created by the viscosity via the effective density.

3.4.3 Bulk modulus and equivalent density predictions with the 3-parameter model

The three-parameter (3P) model described in reference [30] was also adopted as a simpler alternative to the JCA model to predict the aerogel's bulk modulus and effective density. These properties were then used in the Biot model [31] to account for the response of the poro-elastic nature of the aerogel stacks. The 3P model makes use of the median pore size, \bar{s} , porosity, ϕ , and standard deviation of the pore size, σ_s . It is assumed that the median pore size,

standard deviation of the pore size, two characteristic lengths, flow resistivity and tortuosity are inter-related [30]: i.e.,

$$\Lambda = \bar{s} e^{-5/2(\sigma_s \log 2)^2} \quad (27)$$

$$\Lambda' = \bar{s} e^{3/2(\sigma_s \log 2)^2} \quad (28)$$

$$\alpha_\infty = e^{4(\sigma_s \log 2)^2} \quad (29)$$

$$\sigma = \frac{8\eta\alpha_\infty}{\bar{s}^2\phi} e^{6(\sigma_s \log 2)^2} \quad (30)$$

The parameters defined by eqs. (27)-(30) were then used as inputs to calculate the effective density, ρ_G , and bulk modulus, K_ρ , of the equivalent fluid representation [28,29] of the aerogel granule stack. Alternative equations for calculating these two properties can be found in the original paper by Horoshenkov et al. (reference [30], eqs. (13) and (16)).

3.4.4 Effective density and bulk modulus as inputs in the Biot poro-elastic model

The JCA model outputs, ρ_e and K_f could be used together with the aerogel' s σ , ϕ , α_∞ , its bulk density, ρ_b , and/or its elasticity parameters {mechanical loss factor, η_m , and longitudinal stiffness, $D = E_1(1 - \nu)/[(1 + \nu)(1 - 2\nu)]$ }, where E_1 is Young' s modulus and ν is Poison' s ratio} as bulk property inputs for the Biot-poro-elastic theory (originally introduced in reference [31], and whose

formulations are summarised in Section 2.3 of reference [5]). On the other hand, when the 3P model was applied, its outputs, ρ_c and K_p , were translated into effective density, ρ_e , and bulk modulus, K_f , of the fluid phase of the poro-elastic material to make them configurable as inputs for the subsequent calculations involving the Biot poro-elastic theory: i.e.,

$$\rho_e = \phi \rho_c^*, \quad (31)$$

$$K_f = \phi K_p^*, \quad (32)$$

where "*" denotes the complex conjugate, which is required owing to the difference in the adopted $e^{\pm i\omega t}$ convention in the two models (see reference [29] and [30]).

It should be noted that, here, the Biot-poro-elastic theory was preferred instead of the Biot-limp-porous theory (also summarised in Section 2.3 of reference [5]) which makes it possible to introduce a small, but finite value of D for the aerogel stack's elastic frame. In that case, a frequency-dependent η_m can be used to quantify the non-linearity of the material's loss mechanism in the low frequency regime shown in the experimental data. Finally, the layer depth, d , was used as a bulk property to calculate the sound absorption of a finite depth layer by using either the TMM [34] or the arbitrary coefficient method (ACM) [35], both of which functioned equivalently.

3.5 Results & Discussion – Characterisation of acoustical-related bulk properties

3.5.1 Fitting the measured sound absorption coefficient spectra

The characterisation of the bulk properties was performed by fitting the two models described in Section 3.4 to the measured frequency-dependent absorption coefficients for the type 1 and type 2 aerogels. This fitting process was based on the MATLAB built-in numerical optimisation function “particleswarm” (The MathWorks, Natick, MA). To be more specific, the parameters σ , ϕ , α_∞ , Λ , Λ' , ρ_b , and D were also fitted as frequency-independent values by using the 3P-JCA-Biot-poro-elastic-TMM/ACM model for type 1 and type 2 aerogel granule stacks. The criteria for this fitting step were first the good fits of the peak locations and amplitudes to the measured data, and that the fitted dynamic density, ρ_b because the latter was the dominant parameter controlling the peak locations. These parameters were not dominant, i.e., most significant, in the fitting process. η_m was manually adjusted from constant to frequency-dependent at each in-tube sound pressure level for both types of aerogels, with all the other bulk properties fixed to previously fitted values. The criteria for this fitting step were the good fits of the peak locations to the measured data and that the fitted dynamic density, ρ_b was close to the measured ρ_b , because the latter was the dominant parameter controlling the peak locations. Furthermore, η_m was fitted as a frequency-dependent

parameter at each in-tube sound pressure level for both types of aerogels, with all the other bulk properties fixed to previously fitted values. Note that the loss factor was a dominant parameter in this fitting step to ensure a good fit of peak amplitude over a broad range of frequencies especially at low frequencies. Also note that the detailed process of the development of frequency-dependent ("dynamic") loss factor groups is described in a later part of this section. Both E_1 and ν were estimated values in order to represent a finite, but small, elasticity of the aerogel stack's solid frame, so that the frequency-dependent η_m could then be introduced to capture the acoustical non-linearity at low frequencies. The origin of that non-linearity is yet to be identified. Nonetheless, the frequency-dependent η_m (i.e., dynamic loss factor) provides an effective means of representing the non-linearity quantitatively.

These parameters controlled the frequency of the maxima in the absorption coefficient spectra. It was also noted that these parameters and the frequencies of the peaks were relatively independent of the excitation level. Furthermore, η_m was fitted as a frequency-dependent parameter at each in-tube SPL for both types of aerogels, with all of the other bulk properties fixed to the previously determined values. The sensitivity analysis suggests that the loss factor was a dominant parameter in this fitting step to ensure a good fit of the peak amplitudes over a broad range of frequencies, and excitation levels, and also note that the detailed process of the development of the frequency-dependent

(“dynamic”) loss factor groups is described in a later part of this section. We finally note that D was specifically introduced to represent the finite, but small, elasticity of the aerogel stack’s solid frame, so that the frequency-dependent η_m could then be introduced via the complex modulus of elasticity to capture the acoustical non-linearity at low frequencies. The origin of that non-linearity is yet to be identified; nonetheless, the frequency-dependent η_m (i.e., dynamic loss factor) provides an effective means of representing the non-linearity quantitatively.

Tables 3.1 and 3.2 present the summary of the input parameters identified inversely by using the JCA and 3P models. The measured and predicted normal incidence absorption coefficients for type 1 and type 2 aerogel powders are shown in Figures 3.5(a) and 3.6(a), respectively. Figures 3.5(a) and 3.6(a) present the results for the range of incident SPL used in these tests. Recall that the broadband SPL was calculated by combining the narrow band SPL measured at the frequency points from 100 to 4999 Hz for which the absorption coefficient data were measured. This information was available as a standard report generated for each measurement taken with the Materiacustica impedance tube. The narrow band SPL was calculated using the Fourier spectrum for the sound pressure with the two-microphone procedure detailed in reference [23,26]. By comparing the JCA-based (orange) and 3P-based (green) simulations of the sound absorption spectra, it can be seen that both models

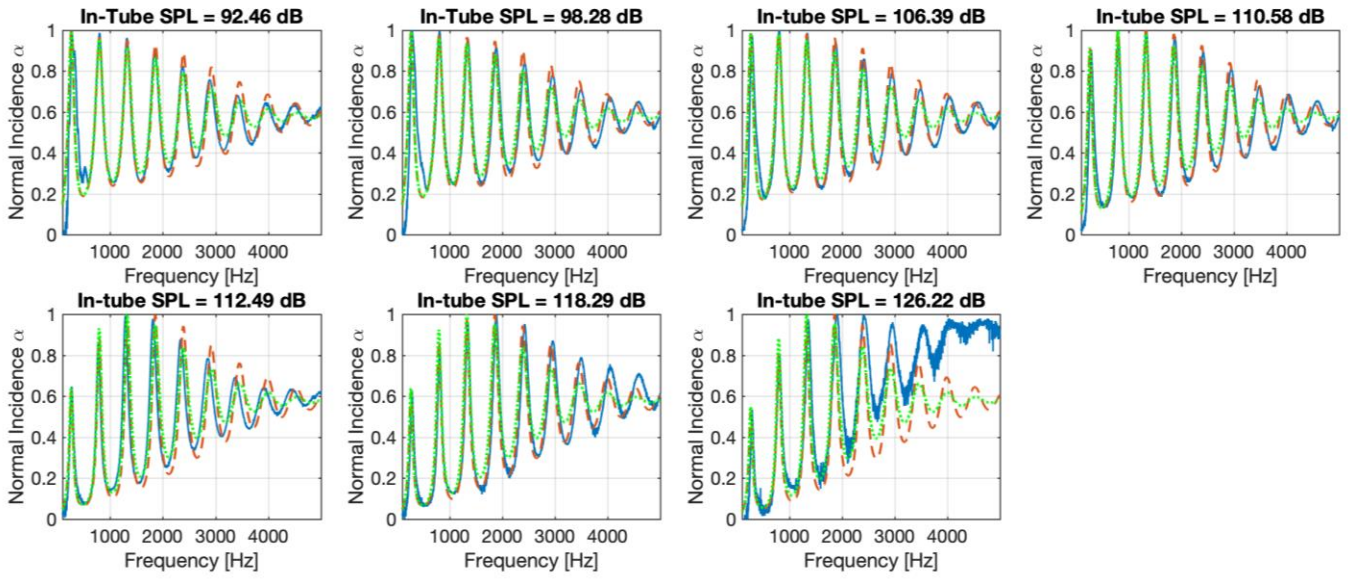
can very accurately predict the sound absorption performance for the target aerogel materials, especially in the low and medium frequency range below 2000 Hz. To further evaluate the prediction accuracy, the spectra of cumulative squared error, from 100 Hz to 4999 Hz, between model-predicted and experiment-measured sound absorption are plotted in Figures 3.5(b) and 3.5(c) for the type 1 and 3.6(b) and 3.6(c) for the type 2 materials, respectively, with the total root mean squared errors, $\sqrt{\bar{x}^2}$ marked in the legends. It can be seen that the two models represent the experimental result with very similar accuracy.

Table 3.1 Bulk properties characterised by fitting the JCA-Biot-TMM/ACM [29,33,34] with the measurements and used to predict sound absorption coefficient spectra.

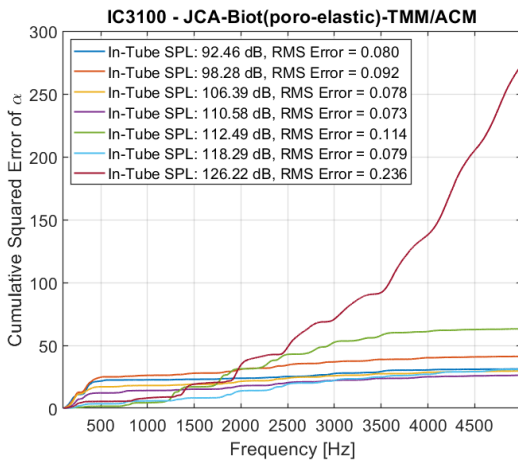
Material	σ [Rayls/m MKS]	ϕ	α_∞	Λ [μm]	Λ' [μm]	ρ_b [kg/m^3]	E_1 [Pa]	ν	η_m
Type 1	10.5×10^6	0.999	3.0	36.1	36.1	35.5	775	0.396	Eq. (7) and Table 3.3
Type 2	10.5×10^6	0.999	3.0	36.1	36.1	94.0	775	0.396	Eq. (7) and Table 3.3

Table 3.2 Bulk properties used for the 3P-Biot-TMM/ACM [30,33,34] to predict sound absorption coefficient spectra.

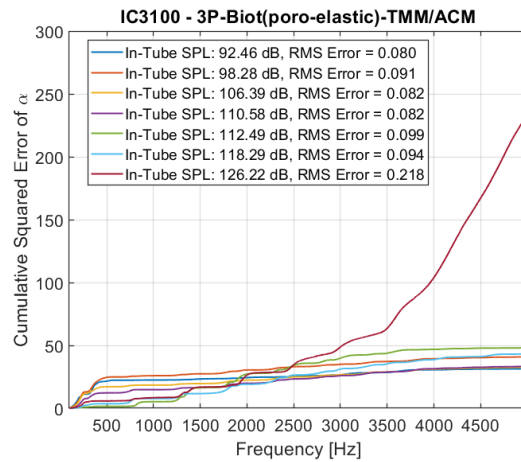
Material	ϕ	s_b [μm]	σ_s	ρ_b [kg/m^3]	E_1 [Pa]	ν	η_m
Type 1	0.999	14.7	0.756	35.5	775	0.396	Eq. (7) and Table 3.3
Type 2	0.999	14.7	0.756	94.0	775	0.396	Eq. (7) and Table 3.3



a)



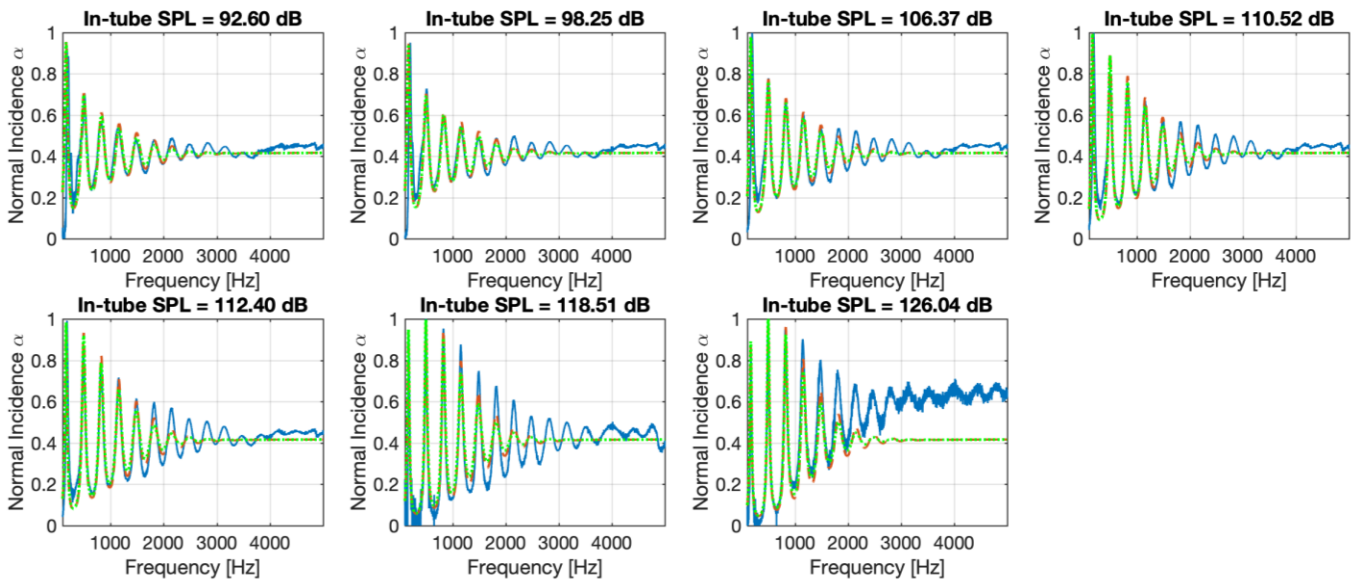
b)



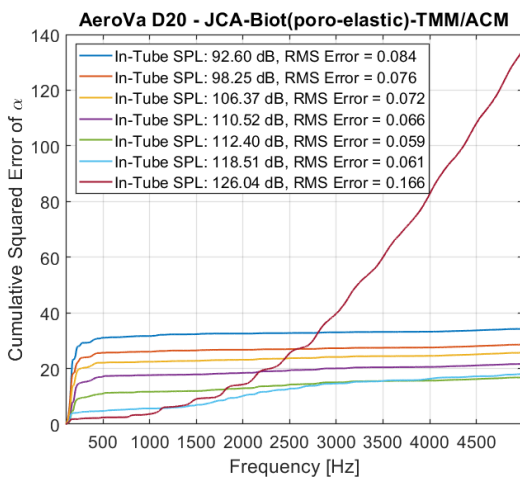
c)

Figure 3.5 (a) The normal incidence absorption coefficients, α' s, of Enova IC3100 (type 1); Cabot Corporation, Alpharetta, GA) at different incident SPL by experimental measurement (blue-solid lines), the JCA-Biot(poro-elastic)-TMM/ACM model

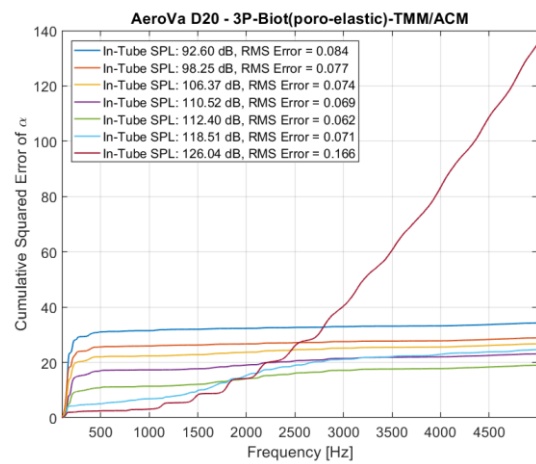
prediction (orange-dashed lines), the 3P-Biot(poro-elastic)-TMM/ACM model prediction (green-dotted lines), (b) cumulative squared error between the JCA-Biot(poro-elastic)-TMM/ACM model prediction and experimental measurement, and (c) cumulative squared error between the 3P-Biot(poro-elastic)-TMM/ACM model prediction and experimental measurement are shown.



a)



b)



c)

Figure 3.6 (a) The normal incidence absorption coefficients, α' s, of JIOS AeroVa D20 (type 2; JIOS Aerogel, Korea) at different incident SPL by experimental measurement (blue-solid lines), the JCA-Biot(poro-elastic)-TMM/ACM model prediction (orange-

dashed lines) and the 3P-Biot(poro-elastic)--TMM/ACM model prediction (green-dotted lines), (b) cumulative squared error between the JCA-Biot(poro-elastic)-TMM/ACM model prediction and experimental measurement, and (c) cumulative squared error between the 3P-Biot(poro-elastic)-TMM/ACM model prediction and experimental measurement are shown.

The predicted sound absorption coefficient spectra (Figs. 3.5(a) and 3.6(a)) were calculated at the 4900 equally spaced frequencies ranging from 100 to 4999 Hz in the fitting process to match the frequency step in the measured data. That congruence allowed the introduction of a 4900-step loss factor that decreased logarithmically with increasing frequency, f , i.e.,

$$\log_{10} \eta_m = af + b. \quad (33)$$

Eq. (33) is a regression to the frequency-dependence obtained from the model fitting. That form of dependence was the most significant factor that enabled good fitting of the model to the measured absorption coefficient spectra, especially at low frequencies for both materials, and it allowed the non-linearity of both materials' acoustical performance to be numerically captured. Particularly, it was found that the coefficients a and b in Eq. (33) depend on the incident sound pressure incident on the sample: their values are given in Table 3.3. The dependence of these coefficients, a and b in Eq. (33) on the SPL is

plotted in Figures 3.7 and 3.8 for type 1 and type 2 aerogels, respectively, to illustrate this behaviour graphically. These coefficients have a clear physical meaning. The absolute value of coefficient a is the rate with which the loss factor decreases with an increasing frequency. The value of the coefficient b is the low-frequency limit of the loss factor, i.e., the greater it is, the greater the losses associated with the frame vibration excited by the incident sound wave when the frequency of sound is relatively low. These data suggest that the dependence of the loss factor on the frequency for the relatively low bulk density type 1 aerogel is not strongly affected by the SPL (see Figure 3.7). In the case of type 2 aerogel, however, there is a rapid increase in the absolute value of a when the SPL reaches 110 dB. This means that the dependence of the loss factor on the frequency becomes much more pronounced.

The behaviour of the coefficient b on the sound pressure level is rather similar for the two aerogels as illustrated in Figure 3.8. Below 105 dB, the value of this coefficient does not depend very significantly on the type of aerogel or the SPL. Above this threshold however, the value of b drops suddenly and then continues to reduce slowly with an increasing SPL. This behaviour suggests that there is a sudden drop in the loss factor near the level of 105 dB. The absolute value of this drop was considerably greater in the case of the lighter aerogel (type 1), suggesting that the drop in the losses caused by a more intense incident sound wave is greater when the bulk material density is lighter.

Table 3.3 The coefficients in the equation for the dynamic loss factor (Eq. (33)) for the two aerogels.

Type 1			Type 2		
In-tube SPL [dB]	<i>a</i>	<i>b</i>	In-tube SPL [dB]	<i>a</i>	<i>b</i>
92.46	-5.511×10^{-4}	1.353	92.60	-5.307×10^{-4}	1.333
98.28	-5.520×10^{-4}	1.335	98.25	-5.720×10^{-4}	1.358
106.39	-6.328×10^{-4}	1.318	106.37	-6.328×10^{-4}	1.277
110.58	-6.328×10^{-4}	1.141	110.52	-6.736×10^{-4}	1.071
112.49	-6.328×10^{-4}	0.761	112.40	-7.144×10^{-4}	1.017
118.29	-6.736×10^{-4}	0.768	118.51	-1.470×10^{-3}	1.046
126.22	-6.940×10^{-4}	0.649	126.04	-1.674×10^{-3}	0.969

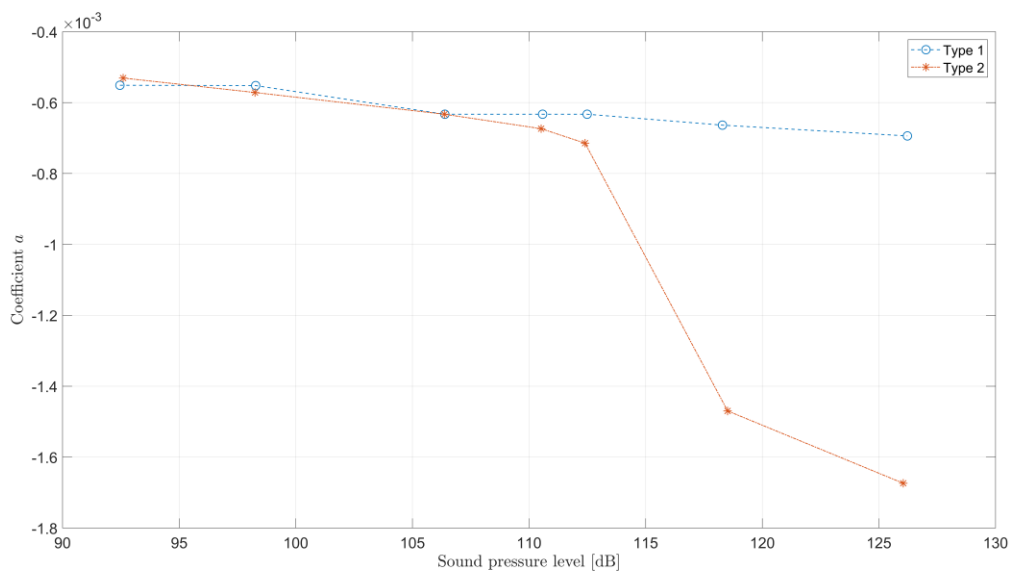


Figure 3.7 The dependence of the coefficient α in Eq. (33) on the sound pressure level.

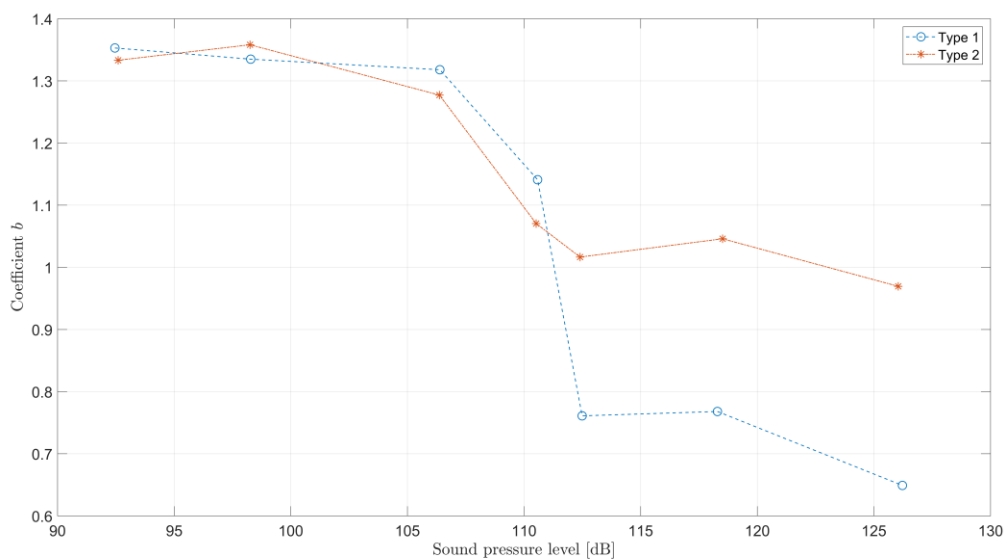


Figure 3.8 The dependence of the coefficient b in Eq. (33) on the SPL.

When a sound wave is incident on a spec of particles whose density is low and comparable with that of air, it is likely to generate a drag force on each of the particles. Because the particles are light in terms of the density, the drag force can be comparable to the gravity force which holds these particles in place. As the material is not consolidated i.e., the particles are loose, the drag force can cause the particles to oscillate. In view of these results, it may be of interest to estimate the radiation pressure acting on the aerogel particles. In the presence of an oscillatory flow, e.g., an incident sound wave, the drag force acting on an isolated aerogel particle with radius R is in reference [36]

$$F = 6\pi\mu R \left(1 + \frac{R}{\delta}\right) u + 3\pi R^2 \sqrt{\frac{2\mu\rho_0}{\omega}} \left(1 + \frac{2R}{9\delta}\right) \frac{\partial u}{\partial t} \quad (34)$$

where $\delta = \eta/(\rho_0\omega)$ is the viscous layer depth, $\nu = \eta/\rho_0$ is the kinematic viscosity of air, ω is the angular frequency, and u is the acoustic particle velocity in the incident sound wave. In the case of harmonic excitation, $u = u_0 \sin(\omega t)$ so that the derivative in eq. (34) is $\frac{\partial u}{\partial t} = \omega u_0 \cos \omega t$. Figure 3.9 shows the frequency-dependent, normalised drag force amplitude, $|F|$, acting on a particle with $2R = 14 \mu\text{m}$ diameter at the broadband SPL of 112 dB. This diameter is similar to the mean particle diameter measured from the SEM images for the type 1 and type 2 aerogels studied in this work. The drag force predicted by eq. (34) was normalised against the particle gravity force, $F_g = 4/3R^3\rho_b g$, where g is the gravity acceleration. The acoustic velocity amplitude, u_0 , in eq. (34) was estimated by using the narrow band incident SPL measured at the sample

surface and surface impedance of the sample. The data shown in Figure 3.9 (particularly at the peaks) suggest that for type 1 aerogel the drag force almost always exceeds the gravity force at this level of excitation, i.e., the aerogel particles are likely to be forced into motion by viscous drag frequencies. These resonance frequencies in the $|F/F_g|$ spectra coincide with the maxima in the absorption coefficient spectra shown in Figure 3.5(a). In the case of type 2 aerogel, the normalised drag force is close to one near the resonance peaks which occur below 1000 Hz. Further increase in the SPL will make this force exceed one, which means that the particles of this aerogel will begin to vibrate under acoustic excitation. Similarly, for a powder with a particle size distribution, it would be expected that this ratio can exceed one for particles whose size is less than the adopted mean.

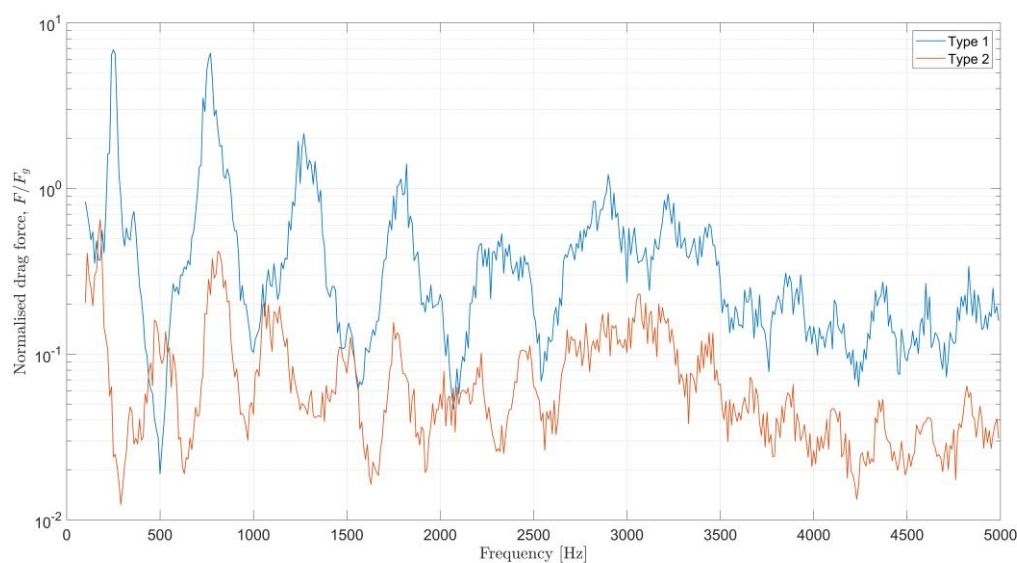


Figure 3.9 The spectra for the normalised drag force acting on a particle of type 1 and type 2 aerogel in the case of 112 dB broadband SPL incident on the surface of the aerogel specimen in the impedance tube.

Figure 3.10 shows the estimates of the displacement spectra for the air particle displacement, (u/ω) in the incident sound wave at 112 dB. Under the particle displacement we assume the amplitude of the oscillatory movement of the air molecules is caused by the passing of acoustic waves. The collective behaviour of these molecules is random, however when averaged, the motion of air molecules is superimposed on top of the random motion. Figures 3.9 and 3.10 can explain the change in the absorption coefficient spectra with the increased SPL. When the sound pressure level is relatively small, e.g., 92 dB (broadband), then the displacement in the incident sound wave is well below that of the particle diameter. The relatively light particles in type 1 aerogel can begin to be excited by the vibrating air, particularly in the lower frequency range. However, their movements are likely to be much smaller than their diameters. In this way, they interact mechanically with each other, losing energy through contact friction so that the acoustic absorption coefficient reaches peaks close to one at frequencies below 1000 Hz (see Figure 3.5 for 92 dB). As the level of excitation increases, the amplitude of the particle movement increases progressively. This amplitude generally reduces with the increased frequency. When this amplitude

becomes comparable with the particle diameter, e.g., 1 μm at 250 Hz for 112 dB excitation (see Figure 3.10), the particle contact can begin to separate, i.e., they lose contact with each other, so that the losses reduce below 1000 Hz as illustrated by the standing wave tube data in Figure 3.5. At this level, the amplitude of the displacement of air molecules in the medium and high frequency regime (1000–3000 Hz) is close to the 1-10 nm range (around 1/1000th of the particle diameter), which seems ideal to result in an increase in the absorption coefficients, particularly around the resonance peaks as shown in Figure 3.5.

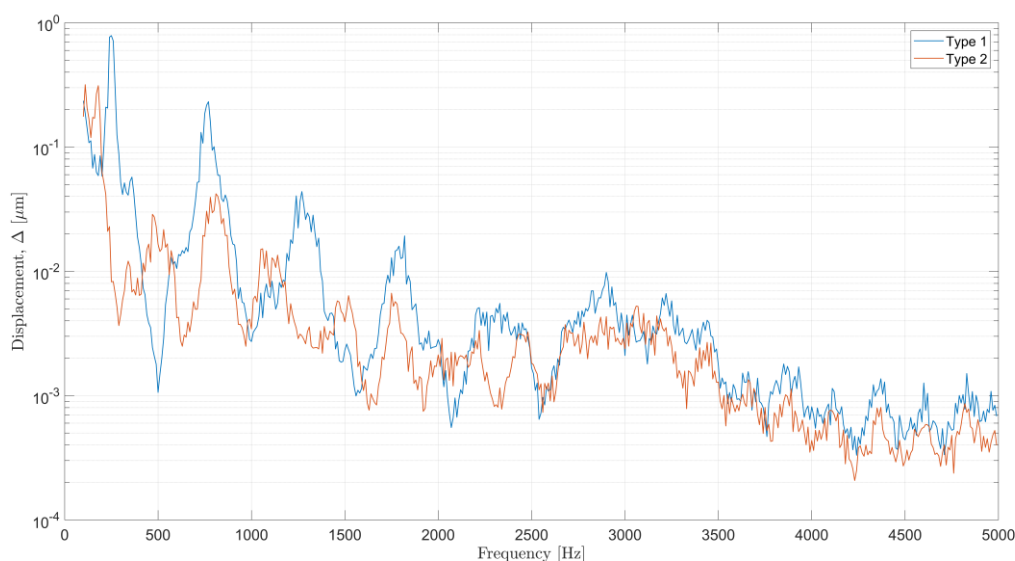


Figure 3.10 The spectra for the displacement of the air molecules in the sound wave incident on the surface of Type 1 and Type 2 aerogel specimen in the impedance tube.

Similar behaviour can be seen in the case of the type 2 aerogel (see Figure 3.6). However, this is a much denser material, so this behaviour is much less pronounced because this denser material would require a much greater drag force to make its particles lose contact with each other, hence, changing the dissipation mechanism as shown in Fig. 3.9. Nevertheless, it appears from the data that the amplitude, of the peaks in the absorption coefficient in the frequency range of 1000–2000 Hz almost doubles as the broadband SPL increases from 92 to 126 dB (see Figure 3.6). The adopted models do not predict this accurately.

Furthermore, to prove that the dynamic loss factor groups in the Biot-poro-elastic theory are required to provide good fittings/predictions of the target aerogel granule stacks' sound absorption performance, especially at the low frequency region, both Biot-limp-porous theory and Biot-poro-elastic theory with constant loss factor (i.e., independent of frequency or in-tube SPL) were used to predict the normal incidence sound absorption coefficients, and the predicted results are shown as comparisons with measured results in Appendix A. Neither of these models can predict the absorption coefficients as accurately as the poro-elastic model with frequency-dependent loss factor.

3.6 Conclusions

In the present work the acoustic absorption offered by two powder-form aerogels with particle sizes in the range of 5.54–41.78 μm were studied. Two theoretical models were fitted to the measured data. The 5-parameter Johnson-Champoux-Allard model [28,29] and an alternative three-parameter [30] model have been used in combination with the Biot poro-elastic model [31] to predict the acoustical properties of the aerogel layers and, therefore, to explain the measured data. A summary of the main conclusions is:

- (1) A relatively thin (e.g., 50 mm thick) layer of a light aerogel powder can provide a very high (almost 100%) acoustic absorption at relatively low frequencies, e.g., below 250 Hz;
- (2) the behaviour of these materials is non-linear, i.e., it depends on the amplitude of the incident sound pressure;
- (3) the agreement between the predicted and measured absorption coefficient obtained with the adopted models was close, with root mean squared errors, $\sqrt{\bar{x}^2}$ below 0.1, for most of the in-tube SPL and with the given quoted set of input parameters;
- (4) Reasonable bulk densities were captured by the numerical fitting function, which showed that the type 2 (94 kg/m^3) aerogel had a density more than twice that of type 1 (35.5 kg/m^3), but both bulk densities characterised by the models were smaller than the values directly

measured using material samples (type 1: 38.7 kg/m³, type 2: 104.9 kg/m³) This indicated that the aerogel's mass density might vary under different in-tube SPL and loading conditions (i.e., standing wave tube input voltages) due to non-linearity;

- (5) a finite elasticity expressed in terms of the longitudinal stiffness is a key parameter to predict the frequencies of the peaks in the measured absorption coefficient spectra;
- (6) different sets of dynamic loss factors (see Table 3.3) were needed to yield "best fits" at different in-tube SPL, which indicates that the non-linearities of both materials quantified in terms of the dynamic loss factor are dependent on the frequency and incident SPL;
- (7) additional sound absorption mechanisms related to the non-linearity and, potentially, effects from submicron pores, cannot be captured by the Biot-type poro-elastic model and needs to be considered to provide better fits in the high frequency region (i.e., above 2000 Hz) especially when the incident SPL is relatively large;
- (8) the loss factor required to fit the measured data at low frequencies (i.e., below 2000 Hz) is very high, and is higher than is physically reasonable for an elastic porous medium, which then suggests that there is an additional loss mechanism working at low frequencies to contribute to

the non-linearity of the sound absorption, e.g., frictional interaction of the particles.

A detailed investigation of aspects (6)–(8) in addition to a summary of design concepts for optimising aerogel granule stacks' wide-band sound absorption, should be the subject of future work. These design concepts can be based on the calculations of the fluid displacement and resulting drag force acting on the aerogel particles, which offer an explanation of the observed level-dependent acoustic absorption behaviour of the aerogel stacks.

Acknowledgements

The authors would like to thank the EPSRC-sponsored Centre for Doctoral Training in Polymers, Soft Matter and Colloids (EP/L016281/1) at The University of Sheffield for their financial support of this work. We would also like to thank our industry partner Armacell and Dr. Mark Swift and Mr. Pavel Holub for their continued support throughout this research study. We extend our thanks to Dr Ian Ross at the University of Sheffield, Sorby Centre, for taking high magnification SEM images.

References

1. J. Yeo, Z. Liu, T.Y. Ng, "Silica Aerogels: A Review of Molecular Dynamics Modelling and Characterization of the Structural Thermal, and Mechanical Properties," In: Andreoni W., Yip S. (eds) Handbook of Materials Modeling. Springer, Cham. pp. 1–22, 2018.
https://doi.org/10.1007/978-3-319-50257-1_83-1
2. J.-F. Allard, N. Atalla, "Propagation of Sound in Porous Media: Modeling Sound Absorbing Materials" , 2nd ed. Wiley, Chichester, pp. 327, 2009.
3. Y. Xue, J.S. Bolton, "Microstructure design of lightweight fibrous material acting as a layered damper for a vibrating stiff panel," *J. Acoust. Soc. Am.*, 143(6), pp. 3254–3265, 2018.
<https://doi.org/10.1121/1.5038255>
4. Y. Xue, J.S. Bolton, T. Herdtle, S. Lee, R.W. Gerdes, "Structural damping by lightweight poro-elastic media" , *J. Sound Vib.*, 459, p. 114866, 2019.
<https://doi.org/10.1016/j.jsv.2019.114866>
5. Y. Xue, "Modeling and design methodologies for sound absorbing porous materials when used as layered vibration dampers," PhD dissertation, Purdue University, 2019.
6. A. Khan, "Vibro-acoustic products from recycled raw materials using a cold raw extrusion process. A continuous cold extrusion process has been developed to tailor a porous structure from polymeric waste, so that the

- final material possesses vibro-acoustic properties," PhD thesis, Chapter 2, University of Bradford, 2010.
7. N.N. Voronina, K.V. Horoshenkov, "A new empirical model for the acoustic properties of loose granular media," *Appl. Acoust.*, 64, pp. 415–432, 2003. [https://doi.org/10.1016/S0003-682X\(02\)00105-6](https://doi.org/10.1016/S0003-682X(02)00105-6)
 8. R. Venegas, O. Umnova, "Acoustical properties of double porosity granular materials," *J. Acoust. Soc. Am.*, 130, pp. 2765–2776, 2011. <https://doi.org/10.1121/1.3644915>
 9. K.V. Horoshenkov, M.J. Swift, "The acoustic properties of granular materials with pore size distribution close to log-normal," *J. Acoust. Soc. Am.*, 110(5), pp. 2371–2378, 2001. <https://doi.org/10.1121/1.1408312>
 10. P. Glé, E. Gourdon, L. Arnaud, K.V. Horoshenkov, A. Khan, "The effect of particle shape and size distribution on the acoustical properties of mixtures of hemp particles," *J. Acoust. Soc. Am.*, 134(6), pp. 4698–4709, 2013. <https://doi.org/10.1121/1.4824931>
 11. M. Vasina, D.C. Hughes, K.V. Horoshenkov, L. Lapčík Jr., "The acoustical properties of consolidated expanded clay granulates," *Appl. Acoust.*, 67, pp. 787–796, 2006. <https://doi.org/10.1016/j.apacoust.2005.08.003>

- 12.R. Bartolini, S. Filippozzi, E. Princi, C. Schenone, S. Vicini "Acoustic and mechanical properties of expanded clay granulates consolidated by epoxy resin," *Appl. Clay Sci.*, 48(3), pp. 460–465, 2010.
<https://doi.org/10.1016/j.clay.2010.02.007>
- 13.Z. Mo, T. Shi, S. Lee, Y. Seo, J.S. Bolton, "A poro-elastic model for activated carbon stacks," *In: Proceedings of the Symposium on the Acoustics of Poro-Elastic Materials (SAPEM) 2021*, online conference, March 2021.
- 14.Z. Mazrouei-Sebdani, H. Begum, S. Schoenwald, K.V. Horoshenkov, W.J. Malfait, "A review on silica aerogel-based materials for acoustic applications," *J. Non-Cryst. Sol.*, 562, p. 120770, 2021.
<https://doi.org/10.1016/j.jnoncrysol.2021.120770>
- 15.A. Ponnappan, A. Choudhary, E. Prasad, "Aerogel Market by Raw Material, Form, and Application: Opportunity Analysis and Industry Forecast, 2020–2027, Allied Market Research," 2020. [Online] Available: www.alliedmarketresearch.com/aerogel-market Accessed: 6 June 2021
- 16.M.M. Koebel, A. Rigacci, P. Achard, "Aerogel-based thermal superinsulation: an overview," *J. Sol-Gel Sci. Technol.*, 63, pp. 315–339, 2012. <https://doi.org/10.1007/s10971-012-2792-9>
- 17.J. Fricke, G. Reichenauer, "Thermal Acoustical and structural properties of silica aerogels," *MRS Proc.*, 73, pp. 73–775, 2011.

<https://doi.org/10.1557/PROC-73-775>

- 18.L. Forest, V. Gibiat, A. Hooley, "Impedance matching and acoustic absorption in granular layers of silica aerogels," *J. Non-Cryst. Sol.*, 285, pp. 230–235, 2001. [https://doi.org/10.1016/S0022-3093\(01\)00458-6](https://doi.org/10.1016/S0022-3093(01)00458-6)
- 19.H. Begum, K.V. Horoshenkov, M. Conte, W.J. Malfait, S. Zhao, M.M. Koebel, P. Bonfiglio, R. Venegas, "The acoustical properties of tetraethyl orthosilicate based granular silica aerogels," *J. Acoust. Soc. Am.*, 149, pp. 4149–4158, 2021. <https://doi.org/10.1121/10.0005200>
- 20.Y. Xue, A. Dasyam, J.S. Bolton, B. Sharma, "Acoustical investigation of aerogel granules modeled as a layer of poro-elastic material," *In: Proceedings of the Symposium on the Acoustics of Poro-Elastic Materials (SAPEM) 2021*, online conference, March 2021.
- 21.K.V. Horoshenkov, K. Attenborough, S.N. Chandler-Wilde, "Pade' approximants for the acoustical properties of rigid frame porous media with pore size distribution," *J. Acoust. Soc. Am.*, 104, pp. 1198–1209, 1998.
<https://doi.org/10.1121/1.424328>
- 22.B.H. Song, J.S. Bolton, "A transfer-matrix approach for estimating the characteristic impedance and wave numbers of limp and rigid porous materials," *J. Acoust. Soc. Am.*, 107, pp. 1131–1152, 2000.
<https://doi.org/10.1121/1.428404>

23. International Organisation for Standardization – Acoustics —
“Determination of sound absorption coefficient and impedance in
impedance tubes — Part 2: Transfer-function method,” ISO10534-2,
International Organisation for Standardization: Geneva, Switzerland,
1998.
24. P. Glé, E. Gourdon, L. Arnaud, “Acoustical properties of materials made
of vegetable particles with severe scales of porosity,” *Appl. Acoust.*, 72,
pp. 249–259, 2011.
<https://doi.org/10.1016/j.apacoust.2010.11.003>
25. [Online] Available:
[https://drive.google.com/drive/folders/1avHWRznOymRB5tA0Jx-
8x1YcCxhD4h-Wc?usp=sharing](https://drive.google.com/drive/folders/1avHWRznOymRB5tA0Jx-8x1YcCxhD4h-Wc?usp=sharing) Accessed: 13 July 2021
26. H. Begum, K.V. Horoshenkov, “Acoustical Properties of Fiberglass
Blankets Impregnated with Silica Aerogel,” *Appl. Sci.*, 11, p. 4593, 2021.
<https://doi.org/10.3390/app11104593>
27. MATERIACUSTICA SRL, “Measurement kit for acoustical complex
properties testing,” [Online] Available:
http://www.materiacustica.it/mat_UKProdotti_MAA.html Accessed: 27
January 2021)

28. D.L. Johnson, J. Koplik, and R. Dashen, "Theory of dynamic permeability and tortuosity in fluid-saturated porous media," *J. Fluid Mech.*, 176, pp. 379–402, 1987. <https://doi.org/10.1017/S0022112087000727>
29. Y. Champoux and J.-F. Allard, "Dynamic tortuosity and bulk modulus in air-saturated porous media," *J. Appl. Phys.*, 70(4), pp. 1975–1979, 1991. <https://doi.org/10.1063/1.349482>
30. K.V. Horoshenkov, A. Hurrell and J.-P. Groby, "A three-parameter analytical model for the acoustical properties of porous media," *J. Acoust. Soc. Am.*, 145(4), pp. 2512–2517, 2019. <https://doi.org/10.1121/1.5098778> and <https://doi.org/10.1121/10.0000560> (Erratum).
31. M.A. Biot, "Theory of propagation of elastic waves in a fluid-saturated porous solid," *J. Acoust. Soc. Am.* **28(2)**, 168–191 (1956), <https://doi.org/10.1121/1.1908239> and <https://doi.org/10.1121/1.1908241>
32. D. Lafarge, P. Lemarinier, J.-F. Allard, and V. Tarnow, "Dynamic compressibility of air in porous structures at audible frequencies," *J. Acoust. Soc. Am.*, 102(4), pp. 1995–2006, 1997. <https://doi.org/10.1121/1.419690>

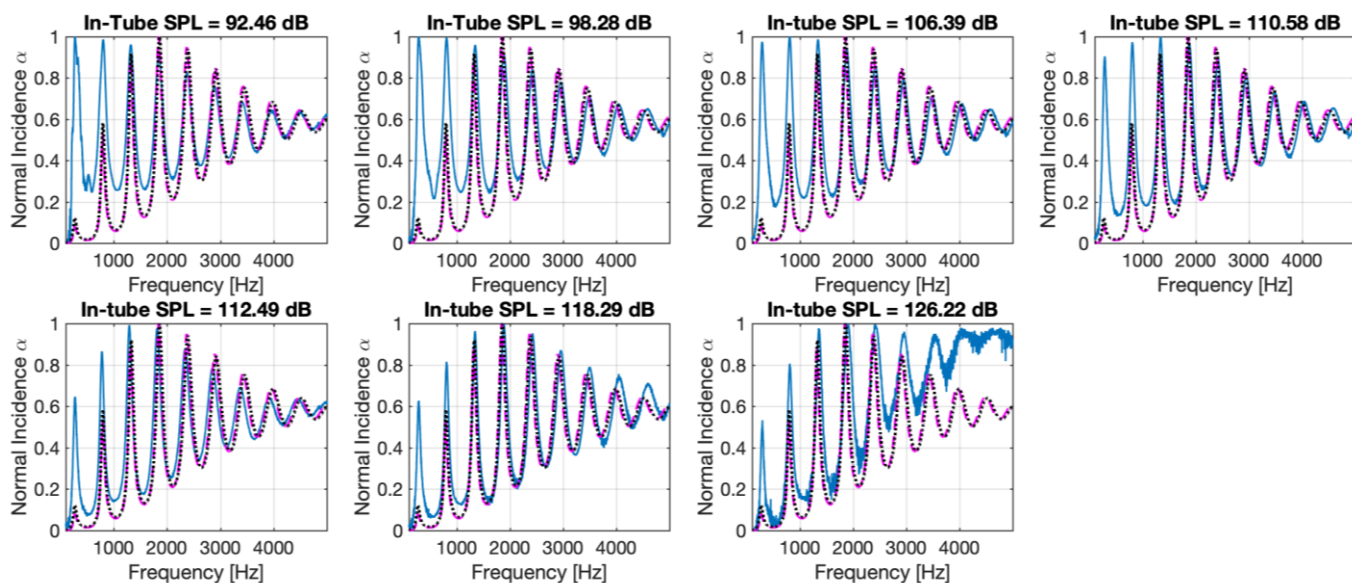
33. D. L. Johnson, J. Koplik, R. Dashen, "Theory of dynamic permeability and tortuosity in fluid-saturated porous media" , *J. Fluid Mechanics*, 176, 379–402, 1987.
34. Y. Xue, J.S. Bolton and Y. Liu, "Modeling and coupling of acoustical layered systems that consist of elements having different transfer matrix dimensions," *J. Appl. Phys.*, 126, p. 165012, 2019.
<https://doi.org/10.1063/1.5108635>
35. J.S. Bolton, N.M. Shiau, and Y.J. Kang, "Sound transmission through multi-panel structures lined with elastic porous materials," *J. Sound Vib.*, 191(3), pp. 317–347, 1996.
<https://doi.org/10.1006/jsvi.1996.0125>
36. L.D. Landau, E.M. Lifshitz, *Fluid Mechanics*, (2nd ed. Elsevier, Oxford), pp. 89-90, 1987.

Appendix A. Demonstration of the necessity to introduce dynamic loss factors in the Biot-poro-elastic theory

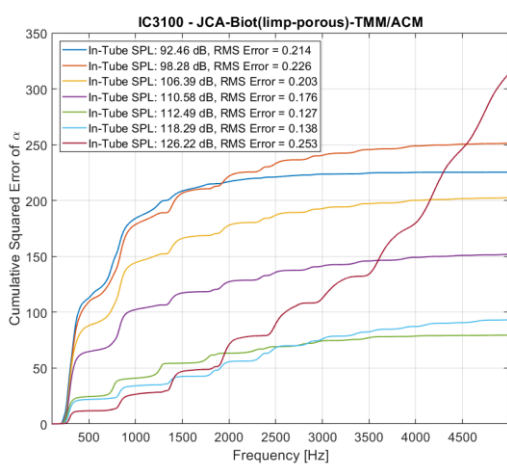
First, the Biot-limp-porous theory [2] was used to predict sound absorption coefficients given the properties listed in Table 3.1 (except for D and η_m , and the same inputs for all of the tube voltages) by following the JCA-Biot (limp-porous)-TMM/ACM calculation routine, and the results are plotted as magenta-

dashed lines in Figures A1 and A2 for the type 1 and type 2 materials, respectively. Secondly, the Biot-type poro-elastic model with a constant $\eta_m=0.2$, was used to predict the sound absorption coefficients given the properties listed in Table 3.1 (except for η_m , same inputs for all of the tube voltages) by following the JCA-Biot(poro-elastic)-TMM/ACM calculation routine, and the results are plotted as black-dotted lines in Figures A1 and A2 for type 1 and type 2 particles, respectively.

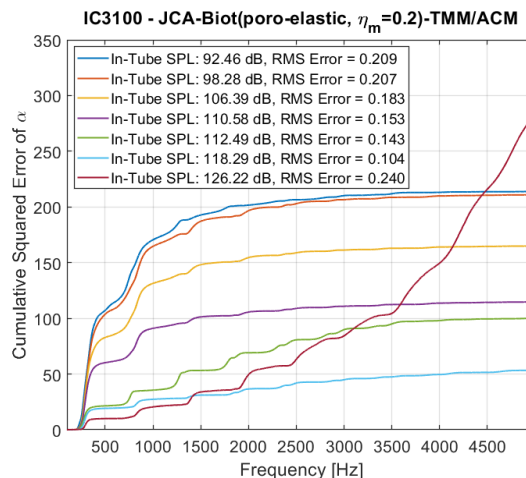
It can be observed that by using either the Biot-limp-porous theory or the Biot-poro-elastic theory with a constant loss factor, we could not realise that predictions that were as accurate as those that were obtained previously with a frequency-dependent loss factor, especially in the frequency region below 2000 Hz. This demonstrated that it is necessary to introduce the dynamic loss factor as a function of frequency in the Biot-type poro-elastic theory to yield a robust prediction of sound absorption coefficients. That conclusion is reinforced by examining the cumulative error plots also presented in Figures A1 and A2. It can be seen that the errors are much larger for these models than was the case for the results plotted in Figures 3.5 and 3.6.



a)



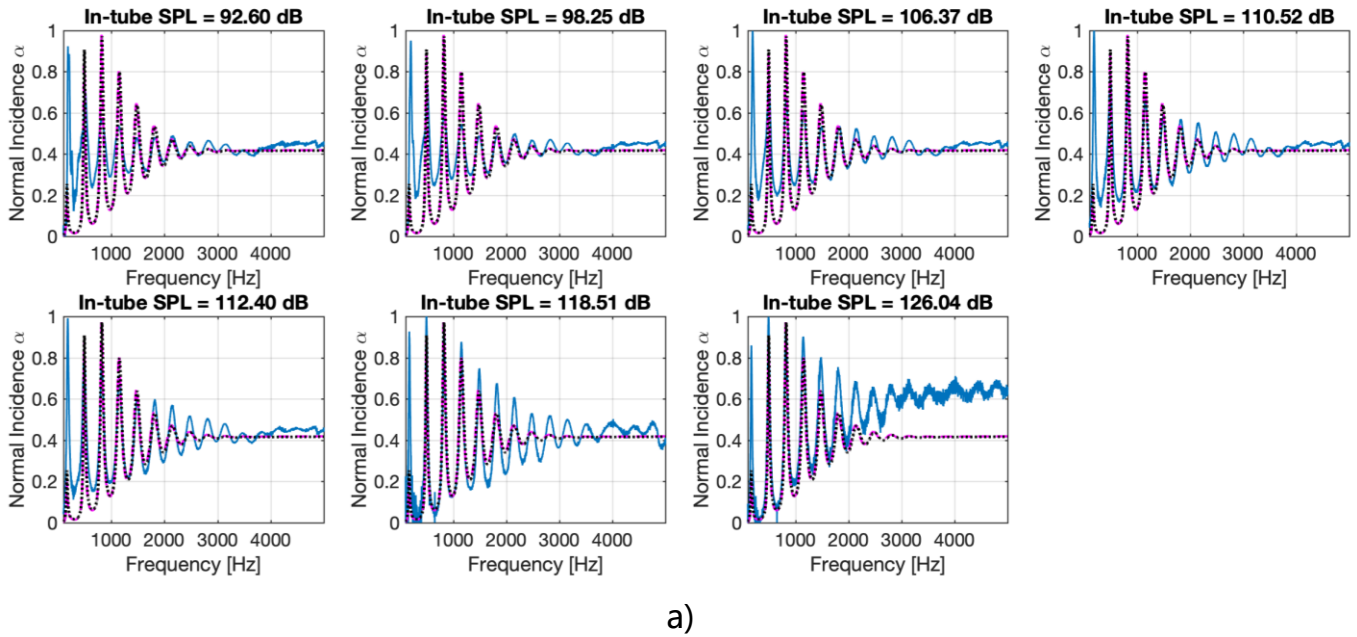
b)



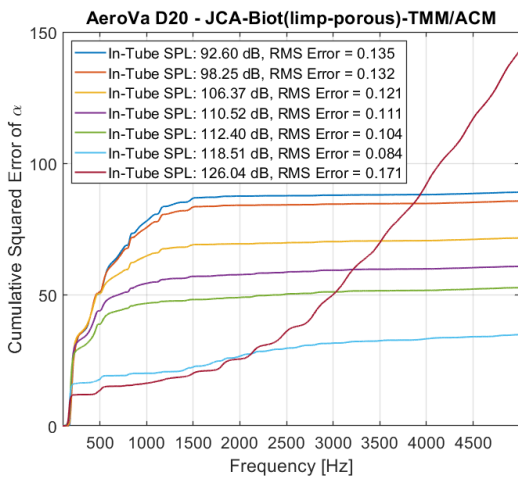
c)

Figure A1 (a) The normal incidence absorption coefficients, α' s, of Enova IC3100 (type 1; Cabot Corporation, Alpharetta, GA) at different incident SPL (i.e., tube voltages) by experimental measurement (blue-solid lines), the JCA-Biot(limp porous)-

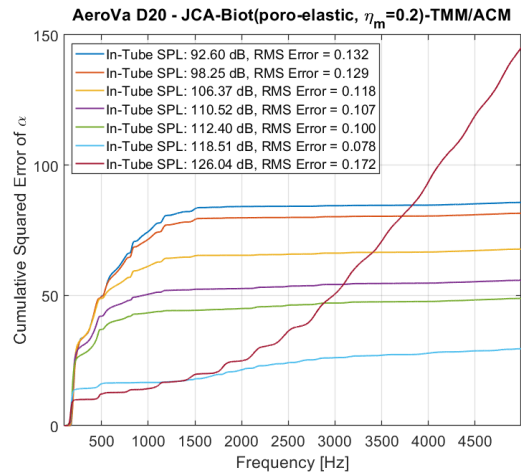
TMM/ACM model prediction (magenta-dashed lines), the JCA-Biot(poro-elastic)-TMM/ACM model prediction (black-dotted lines) with constant $\eta_m=0.2$, (b) cumulative squared error between the JCA-Biot(limp-porous)-TMM/ACM model prediction and experimental measurement, and (c) cumulative squared error between the JCA-Biot(poro-elastic with constant η_m)-TMM/ACM model prediction and experimental measurement are shown.



a)



b)



c)

Figure A2 (a) Normal incidence absorption coefficients, α' s, of JIOS AeroVa D20 (type 2; JIOS Aerogel, Korea) at different incident SPL (i.e., tube voltages) by experimental measurement (blue-solid lines), the JCA-Biot(limp porous)-TMM/ACM model prediction (magenta-dashed lines), the JCA-Biot(poro-elastic)-TMM/ACM

prediction (black-dotted lines) with constant $\eta_m=0.2$, (b) cumulative squared error between the JCA-Biot(limp-porous)-TMM/ACM model prediction and experimental measurement, and (c) cumulative squared error between the JCA-Biot(poro-elastic with constant η_m)-TMM/ACM model prediction and experimental measurement are shown.

Chapter 4:

Acoustical properties of fibreglass blankets impregnated with silica aerogel

This chapter is published as:

H. Begum, K.V. Horoshenkov, "Acoustical Properties of Fiberglass Blankets Impregnated with Silica Aerogel" , *Appl. Sci.*, 11, p. 4593, 2021.

<https://doi.org/10.3390/app11104593>

Authorship statement:

The principal author of the paper is H. Begum. The contribution of H. Begum is the research investigation, experimental data collection and participation in the data interpretation.

4.1 Abstract

It is known that aerogel impregnated fibrous blankets offer high acoustic absorption and thermal insulation performance. These materials are becoming very popular in various industrial and building applications. Although the reasons for high thermal insulation performance of these materials are well understood, it is still largely unclear what controls their acoustic performance.

Additionally, only a small number of publications to date report on the acoustical properties of fibrous blankets impregnated with powder aerogels. There is a lack of studies that attempt to explain the measured absorption properties with a valid mathematical model. This paper contributes to this knowledge gap through a simulation which predicts the complex acoustic reflection coefficient of aerogel blankets with different filling ratios. It is shown that the acoustic performance of a fibrous blanket impregnated with aerogel is generally controlled by the effective pore size and porosity of the composite structure. It is shown that there is a need for refinement of a classical Biot-type model to take into account the sorption and pressure diffusion effects which become important with the increased filling ratio.

Keywords: Acoustics; aerogels; modelling; fibre; porous materials

4.2 Introduction

There is a global need to reduce the use of fossil fuels and release of greenhouse gases. Currently 40% of energy consumption in Europe comes solely from the building sector [1] which is a major source of greenhouse gases. Due to this high level of energy consumption, the European Council has introduced a 27% energy efficiency target for 2030 [2]. This has led to industries sourcing better energy saving products for the market, with thermal insulation being the most effective way to reduce the energy consumption and loss. Achieving such a significant energy efficacy requires the development and upscaling of new commercial products based on aerogels.

One popular emerging thermal insulation product is aerogel blankets. Aerogel blankets consist of a silica aerogel embedded in a reinforcing fibrous matrix which allows the brittle aerogel to become a flexible, durable solid used for buildings [3] and pipelines. The silica aerogel can undergo a surface modification process (typically hydrophobization) to enhance surface life stability [4], thus reducing the aerogel's susceptibility to moisture and rapid spoilage [5]. Silica aerogels themselves have porosity values as high as 98%, densities as low as 0.05-0.5 g/cm³, surface areas in the range of 300-1000 m²/g [6] and thermal conductivity values as low as 0.02 W/mK [7]. Application of aerogels on their own are limited due to their fragility and low mechanical modulus. Using them as composites in the form of aerogel blankets, removes

their fragility as the aerogel grains are now incorporated within the fibrous matrix such as fibreglass or rockwool, giving them impeccable mechanical strength and a breadth of flexibility in terms of product development [8].

Conventional porous materials such as nonwovens and polymer foams [9] can also prevent the reflection of sound incident waves to provide a high sound absorption performance [6,10] that is a highly desired property. Nonwovens in particular are ideal for sound absorption due to their large surface area and high porosity which offers increased frictional losses between sound waves and fibrous matrix leading to their good sound absorption performance [11].

Monolithic silica aerogels alone have unusual viscoelastic properties and have been used in the form of clamped plates to become the main source of intrinsic losses allowing them to exhibit subwavelength resonances for high sound absorption [12,13]. However, these materials are highly fragile. Utilising them as aerogel powder into a fibrous, flexible matrix results in a multi-functional system that can fulfill a range of practical needs in many industry and domestic applications. Their fused nanoparticles in particular result in extremely low elastic stiffness, which provides a relatively low acoustic impedance and exceptionally low flexural wave speed, making it ideal for use as a subwavelength flexural element for controlling airborne sound [14]. Super-insulative acoustic absorbing materials such as aerogel blankets can be tailored and combined with other products to widen their applications and to provide lighter, thinner, and more economical products.

It is known that the acoustic properties of aerogels alone are greatly influenced by the interstitial gas type, pore structure and aerogel density [15,16] and more recently the pioneering efforts to embed granular aerogels into a reinforced fibrous network [3] have shown promising acoustical behaviour. The combination of density and granular size of aerogel [17], and fibre reinforcement and decreased pore size, greatly influences the sound absorption [18]. Motahari et al. [19] investigated the aging time of silica aerogels in cotton nonwoven mats on the sound absorption performance. They found that the

presence of low density (0.088 g/cm^3) silica aerogel at different molar ratios of the precursors MeOH/TEOS used and low aging time, enhanced the sound absorption coefficient in the low frequency range of 250 to 2500 Hz. Furthermore, Eskandari et al. [20] investigated the acoustical behaviour of synthesised silica aerogels mixed into UPVC blankets of different weight ratios. They found that neat UPVC only had a maximum sound absorption of 17% at a frequency of 1800 Hz. However, when silica aerogel was applied at 0.5, 1.5 and 3 weight % the maximum sound absorption of UPVC increased to 24, 28 and 43% respectively, therefore highlighting that acoustical properties were greatly increased upon the addition of silica aerogel. A more extensive review of acoustical properties of aerogels can be found in reference [4].

However, there is a general lack of understanding regarding what leads to the observed acoustical properties of granular aerogels embedded into fibrous mats. Most previous works have not attempted to apply any valid theoretical models to predict key acoustical properties of these systems to explain the measured data. There is limited data on the effect of the filling ratio on the acoustical properties of aerogel impregnated fibrous blankets. Additionally, despite some previous efforts (e.g. [6,9]) there is a limited understanding on the ability of some prediction models to explain the general acoustical behaviour of these materials. There was no discussion on the values of the non-acoustical

parameters that the authors of reference [6,9] had to use in the prediction models they chose in their works to simulate the measured absorption coefficient data.

Our work aims to address this gap via a careful characterisation of the acoustical behaviour of granular silica aerogels impregnated into fibreglass mats. The acoustical properties of five samples of aerogel blankets with varying concentrations of aerogel powder (at micrometric particle sizes) at filling ratio of 0, 25, 50, 75 and 100% were measured and predicted using two mathematical models. This work helps to better understand the relation between their micro-structure and measured acoustical performance.

The structure of this paper is as follows. Section 4.3 highlights the various techniques used to characterise the chemical and physical material properties of aerogel blankets. Section 4.4 looks at the experimental acoustical data derived from the analysis of these materials. Section 4.5 attempts to explain these data with a mathematical model to understand what intrinsic properties of aerogel blankets make them acoustically absorbing and section 4.6 – the conclusions.

4.3 Materials and Methods

4.3.1 Materials preparation

As specified in the patent [21], sodium silicate diluent was prepared using distilled water to achieve 3 to 10 weight % of SiO₂ and stirred with hexamethyldisilazane (HMDS) whilst slowly adding nitric acid (HNO₃) to allow gelation to occur. The silylated hydrogel and co-precursor were gradually immersed in n-hexane for a one-step solvent exchange and sodium ion removal. Water present in the hydrogels is detached due to surface modification of the organic groups (–CH₃)₃ in HMDS. The hydrogel from which water was removed was then dried at ambient pressure and pulverised to form a superhydrophobic synthetic silica aerogel powder [22] with the particle diameter in the range of 1-20 μm impregnated into a fibreglass blanket at different weight % of 25, 50, 75 and 100 powder to blanket at a later manufacturing process. This is a standard process [23]. The fibre diameter in the blanket was 10 mm and its density was approximately 73 kg/m³. It is a standard and commercial E-glass fibre needle mat produced by Lih Feng Jiing Enterprise Co Ltd (Taiwan) [23]. The impregnated fibreglass blankets were then cut to a 10 mm diameter size using a hand-held hole saw which had smooth blade edges to ensure a perfect fit into the impedance tube when tested for acoustical properties.

4.3.2 Materials characterisation

Microstructural observations such as particle distribution of the silica aerogels within fibreglass mats were characterised using scanning electron microscopy (SEM). Images were obtained with a FEI Nova NanoSEM 230 instrument (FEI, Hillsboro, OR, USA) at an accelerating voltage of 10 kV and a working distance of 5 mm. The silica aerogels were fixed on the sample holder using a carbon pad and subsequently coated with 15-20 nm of platinum for SEM analysis.

The acoustical properties of aerogel blankets were measured in a 10 mm impedance tube which was custom made by Materiacustica [24]. This 2-microphone tube setup was developed to test small material specimens in accordance with the standard ISO 10534-2:2001 [25]. This setup enabled us to measure the normalised surface acoustic impedance, complex reflection coefficient and sound absorption coefficient of a hard-backed porous layer in the frequency range of 300-3000 Hz. The spacing between the two microphones was 30 mm which is usual for this frequency range as recommended in the standard [25]. The thickness of the samples used in the acoustic experiments was between 7 and 11 mm which is a typical thickness of a commercial product [23,26]. Figure 4.1 illustrates a typical specimen of fibreglass blanket impregnated with aerogel that was used in the acoustic experiments. Figure 4.2 shows a photograph and jigsaw drawing of the vertically standing impedance tube.



Figure 4.1 10 mm diameter of fiberglass blanket samples cut for fitting into the impedance tube.

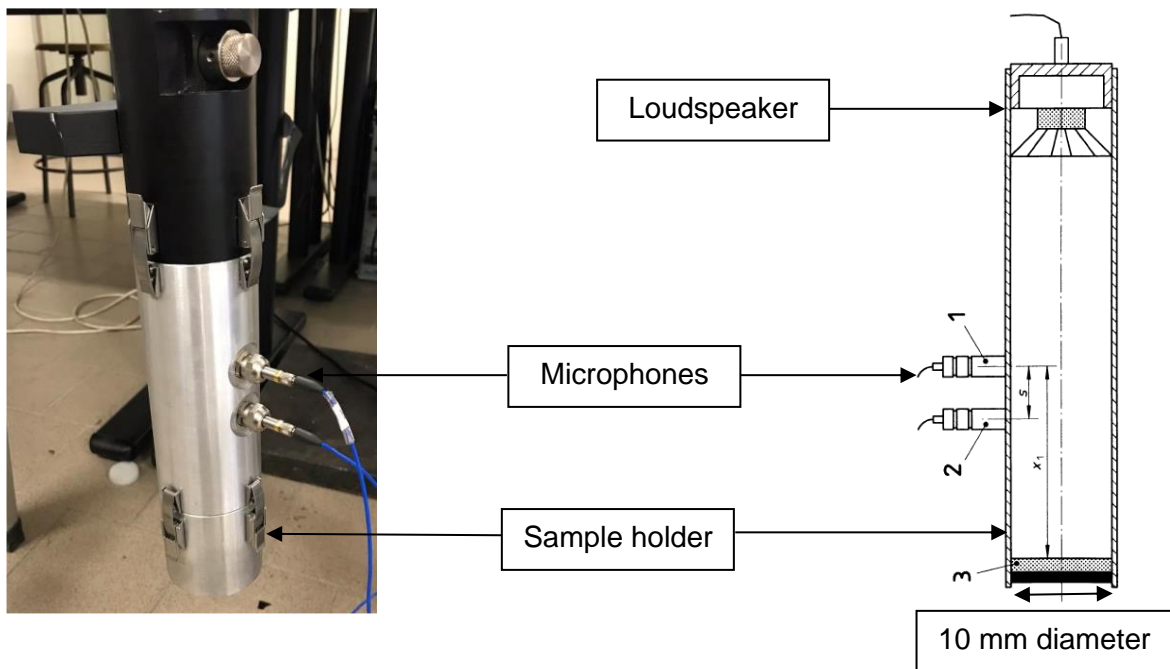


Figure 4.2 2-microphone impedance tube setup to measure the surface impedance of a porous layer [25].

4.4 Modelling of the acoustical properties of fibrous and granular media

Basic modelling of the acoustical properties of this kind of material requires a mathematical model that considers the classical visco-thermal effects in the voids between the fibres and loose granules of powder. However, a fibrous blanket impregnated with aerogel is a more complicated void structure that has at least three scales of porosity. The fibreglass blanket itself consist of 10 μm interlaced fibres that form a porous structure with sub-millimetre size pores of approximately 0.1 mm. The aerogel particles are around 20 μm in size and contain nano-pores of 20 nm in size.

There are several models that exist and that can predict the acoustical properties of classical fibrous media [27]. In this work we attempt to use the model proposed by Horoshenkov et al. [28] which is based on the following three parameters: (i) the median pore size, \bar{s} ; (ii) porosity, ϕ ; and (iii) the standard deviation in pore size, σ_s . This reduced number of parameters allows easier inversion of key morphological characteristics of porous media from acoustical data. This model predicts the dynamic density, $\tilde{\rho}$, and complex compressibility, \tilde{C} , of air in the material pores. These quantities are given by the

analytical equations which are presented in reference [28]. The MATLAB code to predict these quantities can be found in reference [29].

(*Note – the section below is not included in the original published paper)

To fully understand the 3P model [28], the bulk dynamic density can be approximated with the following equation and expression

$$\tilde{\rho}(\omega)/\rho_0 \simeq \frac{\alpha_\infty}{\phi} \left(1 + \epsilon_\rho^{-2} \tilde{F}_\rho(\epsilon_\rho) \right), \quad (1)$$

where

$$\tilde{F}_\rho = \frac{1 + \theta_{\rho,3}\epsilon_\rho + \theta_{\rho,1}\epsilon_\rho}{1 + \theta_{\rho,3}\epsilon_\rho} \quad (2)$$

is the Padé approximant to the viscosity correction function with $\epsilon_\rho = \sqrt{-i\omega\rho_0\alpha_\infty/\phi\sigma}$ and $\theta_{\rho,1} = 1/3$, $\theta_{\rho,2} = e^{-1/2(\sigma_s \log 2)^2} / \sqrt{2}$ and $\theta_{\rho,3} = \theta_{\rho,1}/\theta_{\rho,2}$. The bulk flow resistivity of the porous medium is

$$\sigma = \frac{\eta}{K_0} = \frac{8\eta\alpha_\infty}{\bar{s}^2\phi} e^{6(\sigma_s \log 2)^2} \quad (3)$$

Where η is the dynamic viscosity of air and ρ_0 is the ambient density of air.

The bulk complex compressibility of the fluid in the material pores can be given in the following form

$$\tilde{C}(\omega) = \frac{\phi}{\gamma\rho_0} \left(\gamma - \frac{\gamma - 1}{1 + \epsilon_c^{-2} \tilde{F}_c(\epsilon_c)} \right) \quad (4)$$

where

$$\tilde{F}_c(\epsilon_c) = \frac{1 + \theta_{c,3\epsilon_c} + \theta_{c,1\epsilon_c}}{1 + \theta_{c,3\epsilon_c}} \quad (5)$$

and $\epsilon_c = \sqrt{-i\omega\rho_0\eta\alpha_\infty/\phi\sigma'}$, and $\theta_{c,1} = 1/3$, $\theta_{c,2} = e^{3/2(\sigma_s \log 2)^2}$ and $\theta_{c,3} = \theta_{c,1}/\theta_{c,2}$, γ is the ratio of specific heats, η is the Prandtl number and ρ_0 is the ambient atmospheric pressure. The thermal flow resistivity is defined as the inverse of the thermal permeability

$$\sigma' = \frac{\eta}{K'_0} = \frac{8\eta\alpha_\infty}{\bar{s}^2\phi} e^{-6(\sigma_s \log 2)^2} \quad (6)$$

The normalised surface impedance of a hard-backed layer of porous sample that is typically measured in the impedance tube is

$$Z_s = -jZ_c \cot(k_c d), \quad (7)$$

where $j = \sqrt{-1}$, d is the sample thickness,

$$Z_c = \sqrt{\frac{\tilde{\rho}}{\tilde{C}}} \quad (8)$$

is the characteristic impedance and

$$k_c = \omega \sqrt{\tilde{\rho} \tilde{C}}, \quad (9)$$

is the wavenumber in the porous material. Here ω is the angular frequency of sound. In this work we used the complex reflection coefficient data

$$R = \frac{Z_s - 1}{Z_s + 1}. \quad (10)$$

to fit the model. The work presented in ref. [30] shows that the complex reflection coefficient is a reliable quantity to determine the effective values of the three non-acoustical parameters in the model [28] through the parameter inversion. This is the complex acoustical quantity that is measured directly using the standard impedance tube method [25]. The real and imaginary parts of this quantity are bounded between -1 and +1 which make them attractive to use in the parameter inversion process. The complex reflection coefficient can also be used to predict the acoustic absorption coefficient

$$\alpha = 1 - |R|^2 \quad (11)$$

which is a usual measure of the ability of the porous layer to absorb sound.

4.5 Results & Discussion

4.5.1 Microstructural analysis

Figures 4.3–4.7 present SEM images of the fibreglass blankets with progressive increase in the aerogel powder filing ratio from 0 to 100%. These images can

be used to identify the aerogel particle distribution in fibreglass blankets and structure of the fibre network. The SEM magnification scale in each image changes between 40, 100 and 500 mm to provide a better view inside into the microstructure. We note that SEM image analysis is sensitive to the loading of samples on to the carbon stub, a large amount deposited will affect the coating and this may fracture the image surfaces. Furthermore, there may be sampling bias causing the contrast/brightness settings to be adjusted and this may also affect the results.

Figure 4.3 clearly show that there is little to no aerogel powder present in virgin fibreglass. It also shows that the spacing between individual fibres is in the order of 100s of microns and that these randomly oriented fibres form a complicated network. The addition of a relatively small (25%) amount of aerogel powder does not significantly affect the inter-fibre space (see Figure 4.4). For this case, aerogel particles mainly attach themselves to the fibres (see Figure 4.4(a)) causing an apparent increase in the fibre diameter (see Figure 4.4). In the case of the samples with 50 and 75% concentrations (Figures 4.5 and 4.6, respectively) a similar effect can be visually observed, but the apparent increase in the fibre diameter is more significant whereas the size of the inter-fibrous space is clearly reduced. In the ultimate case, when the aerogel filling ratio in the fibrous sample is 100% (see Figure 4.7), a considerable proportion of the

inter-fibrous space is occupied with aerogel powder so that the effective pore size appears to be significantly reduced visually.

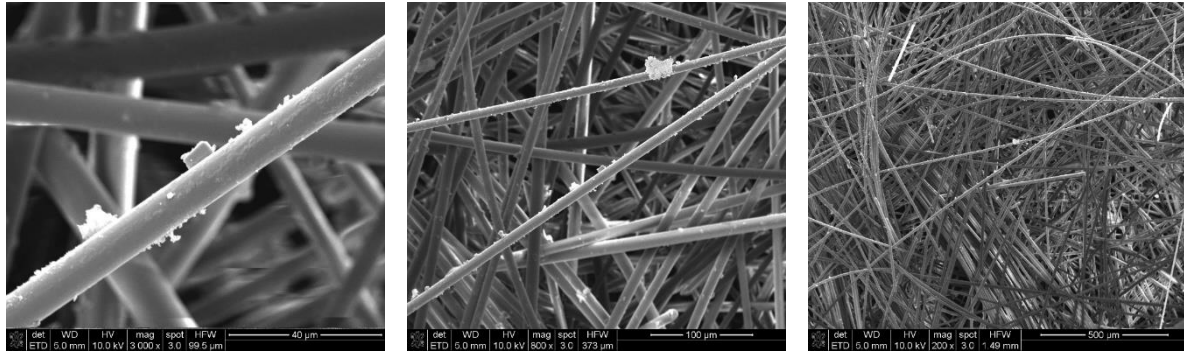


Figure 4.3 SEM images taken at different magnifications (3000x (a), 800x (b) and 200x (c)) showing the fibreglass blanket without any aerogel.

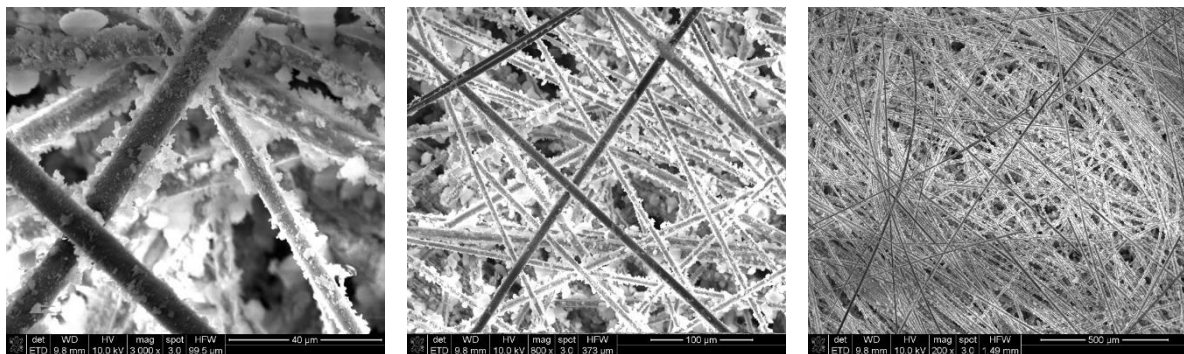


Figure 4.4 SEM images taken at different magnifications (3000x (a), 800x (b) and 200x (c)) showing the fibreglass blanket structure with an aerogel filling ratio of 25%.

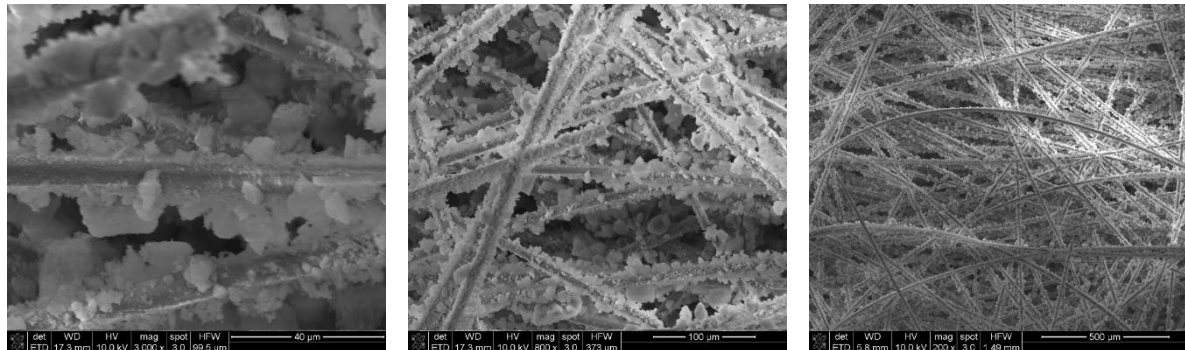


Figure 4.5 SEM images taken at different magnifications (3000x (a), 800x (b) and 200x (c)) showing the fibreglass blanket structure with an aerogel filling ratio of 50%.

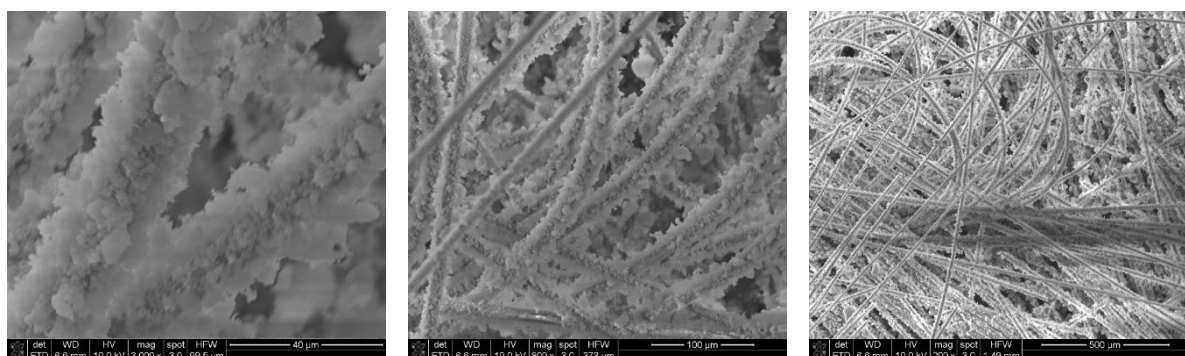


Figure 4.6 SEM images taken at different magnifications (3000x (a), 800x (b) and 200x (c)) showing the fibreglass blanket structure with an aerogel filling ratio of 75%.

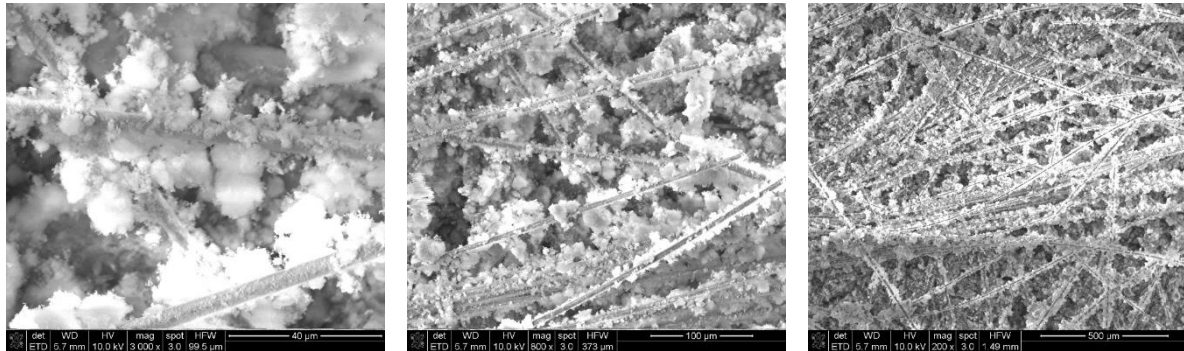


Figure 4.7 SEM images taken at different magnifications (3000x (a), 800x (b) and 200x (c)) showing the fibreglass blanket structure with an aerogel filling ratio of 100%.

4.5.2 Acoustical properties

The acoustical properties were measured at the University of Sheffield in a 10 mm impedance tube [25]. Five specimens were cut from different areas on a sample of each type of fibrous blanket and their properties were measured in the impedance tube. The repeatability of each measurement was found within $\pm 2.9\%$ for the absorption coefficient and $\pm 5.8\%$ for the reflection coefficient. Figure 4.8 shows a comparison between the measured absorption coefficients for the five samples. Figure 4.9 presents a comparison between measured and predicted real and imaginary parts of the complex reflection coefficients for these five materials.

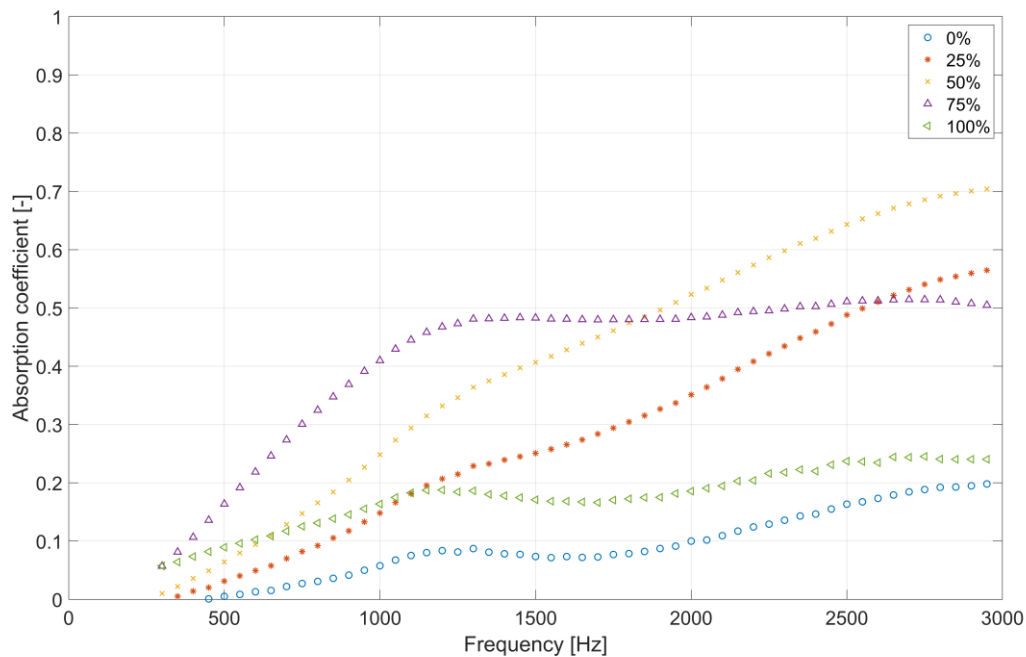
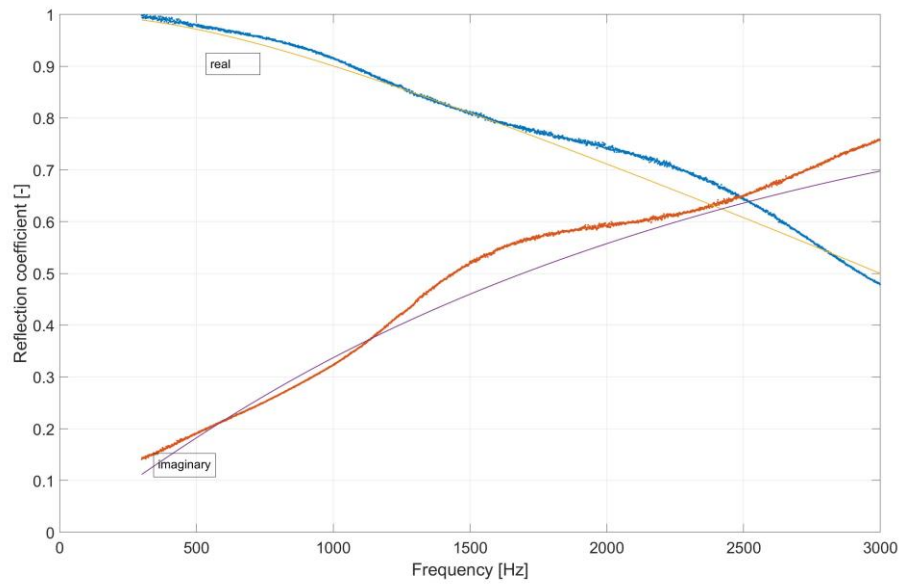


Figure 4.8 An example of the measured sound absorption coefficient of a 8-9 mm thick hard-backed layer of the five fibrous blankets with a progressive increase in the aerogel filling ratio.



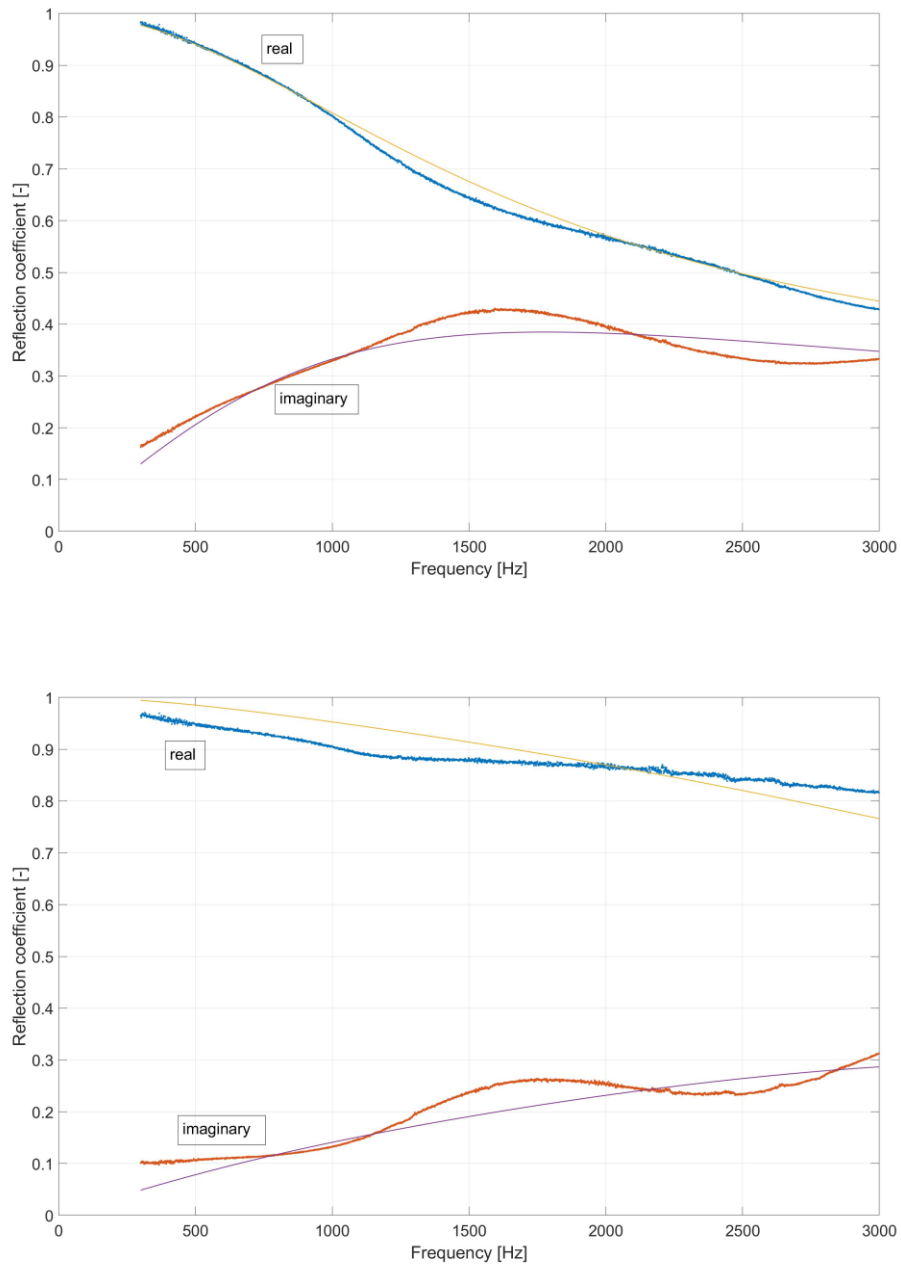


Figure 4.9 Examples of the measured (marker) and predicted (solid lines) complex reflection coefficient data for fibreglass blanket without any

aerogel (top), 50% aerogel impregnated aerogel (middle) and 100% aerogel impregnated blanket (bottom).

The results presented in Figure 4.8 suggest that there is a progressive increase in the absorption coefficient as the aerogel impregnation increases from 0 to 50%. When the aerogel filling ratio reaches 75% this increase becomes less pronounced. Increasing the filling ratio beyond 75% reduces the absorption coefficient significantly. This reduction makes sense because it is likely associated with a densely packed inter-fibrous space which becomes almost full of aerogel (see Figures 4.6 and 4.7), causing a considerable reduction in the pore size (see Table 4.1) in a relatively thin material layer. For the filling ratios of 75% and above the characteristic impedance (see Figure 4.9) and attenuation of sound in a layer with such small pores becomes very high, limiting the value of the absorption coefficient [27]. The absorption coefficient of this relatively thin fibrous blanket with 50-75% filling ratios is still relatively high (30-70%) particularly above 1000 Hz (see references [4,13]). This level of absorption has a practical value in applications related to engineering noise control.

Table 4.1 Values of the non-acoustical parameters inverted from fitting the model [28] to the measured complex reflection coefficient data for the five types of fibreglass blankets.

Filling ratio, %	Layer thickness, d, mm	Pore size, $\bar{s}^{(i)}$, μm	Porosity, $\phi^{(i)}$	Standard deviation in pore size, $\sigma_s^{(i)}$	Calculate d Porosity, ϕ	RMS error, %
0	8.12 ± 0.77	99.4 ± 4.15	0.994 ± 0.0098	0	0.965 ± 0.0041	1.4
25	9.33 ± 1.60	48.0 ± 20.2	0.938 ± 0.018	0.160 ± 0.213	0.960 ± 0.0044	1.7
50	9.26 ± 0.47	32.8 ± 2.00	0.929 ± 0.011	0	0.952 ± 0.0026	1.8
75	10.35 ± 0.85	20.5 ± 1.35	0.959 ± 0.032	0	0.951 ± 0.0036	3.6
100	9.34 ± 0.84	83.0 ± 2.04	0.505 ± 0.091	0.55 ± 0.015	0.94 ± 0.0067	2.5

An obvious question here is *What happens to the fibreglass pore properties when the percentage of aerogel powder impregnating the blanket increases?*

In order to answer this question, we attempted to fit the mathematical model [28] to the complex acoustic reflection coefficient data measured in the impedance tube. We used the optimisation procedure described in reference [30] to invert the three parameters of the best fit. This procedure has been used by many researchers (see [27] for a review of parameter inversion methods). Figure 4.9 show three examples of this fit for fibreglass blankets with aerogel filling ratios of 0, 50 and 100%.

Table 4.1 present a summary of the mean values of the three non-acoustical parameters in the adopted theoretical model [28] which were inverted from its fit to the measured data for the five filling ratios. This table also provides the porosity values calculated from the material density data, mean layer thickness measured directly and root mean square error (RMS) calculated between the predicted and measured reflection coefficient spectra. The superscript ⁽ⁱ⁾, which appears with a non-acoustic parameter in this table, means that the values of this parameter were inverted rather than measured directly.

The results shown in Figure 4.9 and parameter values listed in Table 4.1 suggest that the model generally provides a very close fit to the data (an RMS error, $\sqrt{\bar{x}^2}$ better than 2.5%) particularly when the filling ratio is equal to or below 50%. The agreement between the predicted and measured reflection coefficient

spectra reduces slightly with the increased filling ratio. The inverted value of the median pore size (Table 4.1) decreases progressively from 99.4 μm to 20.5 μm as the filling ratio increases from 0 to 75%. This makes physical sense as the SEM images in Figures 4.3-4.7 illustrate this. This range of pore sizes is also consistent with that measured non-acoustically for similar materials [6]. When the filling ratio increases, the inter-fibre pores are progressively replaced with much smaller inter-grain pores. The transport (inner) pores in the grains of aerogel do not seem to contribute significantly to the measured acoustical properties. This is reflected in a consistently underpredicted porosity value, $\phi^{(i)}$. The progressive change in the inverted porosity value make sense for the filling ratios between 0 and 50%, dropping from 99.4% to 92.9%, respectively. These values match the measured porosity values within 3%. When the filling ratio increases to 100% the inverted porosity of $\phi^{(i)} = 50.5\%$ is significantly below the measured porosity of $\phi = 93.6\%$. Additionally, the median pore size inverted for this type of blanket is not realistic. This suggests that the physical behaviour of the blanket layer with 100% filling ratio is no longer captured accurately by the model. As the proportion of aerogel powder in the material approaches 100%, the sorption and thermal diffusion effects are likely to become much more important [31]. These effects are not captured by the adopted model [28], which only accounts for the classical visco-thermal and inertia effects.

4.6 Conclusions

This work is a systematic study of the acoustical properties of fibrous blankets that are impregnated with an aerogel powder. The level of impregnation (filling ratio) has been progressively changed from 0 to 100% with respect to the material weight. The complex acoustic reflection coefficient of these materials was measured in the frequency range of 300-3000 Hz using a standard impedance tube setup [25]. These data were used to invert the three parameters of the theoretical model [28] via the best fit method [30]. It is found that the adopted model can predict the reflection coefficient spectrum relatively accurately with the RMS error being below 4%. The absorption coefficient of these relatively thin (8-9 mm thick) fibrous blankets with 50-75% filling ratios is relatively high (30-50%) particularly above 1000 Hz. This level of absorption has a practical value in applications related to engineering noise control.

The results of the parameter inversion obtained with the adopted model suggest that the impregnation of fibrous blanket with an aerogel powder results in a progressive reduction in the effective pore size. For the filling ratios in the range of 0-50% there is also a small but progressive reduction in the inverted porosity, which is within 3% of that measured directly. The absorption coefficient increases progressively with the increased filling ratio, reaching the maximum when the filling ratio is between 50 and 75%. This decrease in the effective pore size results in an increased acoustic attenuation and better

coupling, which are important to maximise the acoustic absorption for such a thin, porous layer. Increasing the filling ratio beyond 75% results in a significant drop in the absorption. This drop is associated with a considerable drop in the porosity value ($\phi = 0.505$) and substantial increase in the pore size ($\bar{s} = 83 \mu\text{m}$) inverted for the filling ratio of 100%. The discrepancy between the model and data for this filling ratio increases. As the proportion of aerogel powder in the material approaches the 100%, the open porosity does not drop significantly, i.e., the proportion of the open interconnected pores remain relatively constant. However, the sorption and thermal diffusion effects in the inner pores in the aerogel grains are likely to become much more important [31]. These pores have nanometre scales [6], which is much smaller than the values of \bar{s} inverted with the model [28] (see Table 4.1). The effects that occur in nanometre pores cannot be captured by the adopted model [28] which only accounts for the classical visco-thermal and inertia effects in pores which are much larger than the mean free path (68 nm in air at ambient pressure and temperature).

This work suggests that in order to predict the acoustic behaviour of a fibrous blanket with high aerogel filling ratios there is a clear need to refine the model [28] to include the sorption and pressure diffusion effects. The adopted model does require unrealistic values of the median pore size and porosity to achieve a good fit. This model can be refined by including in it the work by Venegas and Umnova [31]. In this way the dynamic compressibilities of the air filling the

inter-fibre pores and in the pores in the aerogel grains can be combined to account for all the physical effects which contribute to the observed acoustical behaviour.

Acknowledgements

The authors would like to thank the EPSRC-sponsored Centre for Doctoral Training in Polymers, Soft Matter and Colloids (EP/L016281/1) at The University of Sheffield for their financial support of this work. We would also like to thank our industry partner Armacell and Dr. Mark Swift and Mr. Pavel Holub for their continued support throughout this research study. We extend our thanks to Dr Shanyu Zhao at the Swiss Federal Laboratories for Materials Science and Technology for allowing us to use their electron microscopy centre for high magnification SEM image analysis.

References

1. "DIRECTIVE 2012/27/EU OF THE EUROPEAN PARLIAMENT AND OF THE COUNCIL of 25 October 2012 on energy efficiency, amending Directives 2009/125/EC and 2010/30/EU and repealing Directives 2004/8/EC and 2006/32/EC", *OJEU*, 55, 315/97, 2012.

2. "DIRECTIVE (EU) 2018/2002 OF THE EUROPEAN PARLIAMENT AND OF THE COUNCIL of 11 December 2018 amending Directive 2012/27/EU on energy efficiency", *OJEU*, 328/20, 2018. [Online] Available: https://eur-lex.europa.eu/legal-content/EN/TXT/?uri=uriserv%3AOJ.L_.2018.328.01.0210.01.ENG
Accessed: 17 May 2021
3. S.B. Riffat, G. Qiu, "A review of state-of-the-art aerogel applications in buildings", *Int. J. Low-Carbon Technol.*, vol. 8, pp. 1–6, 2013.
<https://doi.org/10.1093/ijlct/cts001>
4. Z. Mazrouei-Sebdani, H. Begum, S. Schoenwald, K.V. Horoshenkov, W.J. Malfait, "A review on silica aerogel-based materials for acoustic applications", *J. Non Cryst. Solids*, 562, p. 120770, 2021.
<https://doi.org/10.1016/j.jnoncrysol.2021.120770>
5. K. Duer, S. Svendsen, "Monolithic silica aerogel in superinsulating glazings", *Solar Energy*, 63, pp. 259–67, 1998.
[https://doi.org/10.1016/S0038-092X\(98\)00063-2](https://doi.org/10.1016/S0038-092X(98)00063-2)
6. Z. Talebi, P. Soltani, N. Habibi, F. Latif, "Silica aerogel/polyester blankets for efficient sound absorption in buildings", *Constr. Build. Mater.*, 220, pp. 76–89, 2019.
<https://doi.org/10.1016/j.conbuildmat.2019.06.031>
7. M.M. Koebel, A. Rigacci, P. Achard, "Aerogel-based thermal

superinsulation: an overview", *J. Sol-Gel Sci. Technol.*, 63, pp. 315–339, 2012.

<https://doi.org/10.1007/s10971-012-2792-9>

8. K. Nocentini, P. Achard, P. Biwole, M. Stipetic, "Hygro-thermal properties of silica aerogel blankets dried using microwave heating for building thermal insulation", *Energy Build.*, 158, pp. 14–22, 2018.

<https://doi.org/10.1016/j.enbuild.2017.10.024>

9. S. Rwawiire, B. Tomkova, J. Militky, L. Hes, B.M. Kale, "Acoustic and thermal properties of a cellulose nonwoven natural fabric (barkcloth)", *Appl. Acoust.*, 116, pp. 177–183, 2017.

<https://doi.org/10.1016/j.apacoust.2016.09.027>

10. M. Ramamoorthy, A.A. Pisal, R.S. Rengasamy, A.V. Rao, "In-situ synthesis of silica aerogel in polyethylene terephthalate fibre nonwovens and their composite properties on acoustical absorption behavior", *J. Porous Mater.*, 25, pp. 179–187, 2018.

<https://doi.org/10.1007/s10934-017-0431-0>

11. M. Tascan, E.A. Vaughn, K.A. Stevens, P.J. Brown, "Effects of total surface area and fabric density on the acoustical behavior of traditional thermal-bonded highloft nonwoven fabrics", *J. Text. I.*, 102, p. 746, 2011.

<https://doi.org/10.1080/00405000.2010.515731>

12. A.A. Fernandez-Marin, N. Jimenez, J.-P. Groby, J. Sanchez-Dehesa, V.

Romero-Garcia, "Aerogel-based metasurfaces for perfect acoustic energy absorption", *Appl. Phys. Lett.*, 115, p. 061901, 2019.

<https://doi.org/10.1063/1.5109084>

13.A. Geslain, J.-P. Groby, V. Romero-Garcia, F. Cervera, J. Sanchez-Dehesa, "Acoustic characterization of silica aerogel clamped plates for perfect absorption", *J. Non Cryst. Solids*, 499, pp. 283–288, 2018.

<https://doi.org/10.1121/1.5014784>

14.M.D. Guild, V.M. Garcia-Chocano, J. Sanchez-Dehesa, "Aerogel as a soft acoustic metamaterial for airborne sound", *Phys. Rev. Appl.*, 5, p. 034012, 2016.

<https://doi.org/10.1103/PhysRevApplied.5.034012>

15.J. Gross, J. Fricke, "Sound propagation in SiO₂ aerogels", *J. Acoust. Soc. Am.*, 91, pp. 2004–2006, 1992.

<https://doi.org/10.1121/1.403684>

16.L. Forest, V. Gibiat, T. Woignier, "Biot' s theory of acoustic propagation in porous media applied to aerogels and alcogels", *J. Non Cryst. Solids*, 225, pp. 287–292, 1998.

[https://doi.org/10.1016/S0022-3093\(98\)00325-1](https://doi.org/10.1016/S0022-3093(98)00325-1)

17.V. Gibiat, O. Lefeuvre, T. Woignier, J. Pelous, J. Phalippou "Acoustic properties and potential applications of silica aerogels" *J. Non Cryst. Solids*, 186, pp. 244–55, 1995.

[https://doi.org/10.1016/0022-3093\(95\)00049-6](https://doi.org/10.1016/0022-3093(95)00049-6)

- 18.L. Forest, V. Gibiat, A. Hooley, "Impedance matching and acoustic absorption in granular layers of silica aerogels" *J. Non Cryst. Solids*, 285, pp. 230–5, 2001.

[https://doi.org/10.1016/S0022-3093\(01\)00458-6](https://doi.org/10.1016/S0022-3093(01)00458-6)

- 19.S. Motahari, H. Javadi, A. Motahari, "Silica-aerogel cotton composites as sound absorber", *J. Mater. Civ. Eng.*, 27, pp. 1–6, 2014.

[https://doi.org/10.1061/\(ASCE\)MT.1943-5533.0001208](https://doi.org/10.1061/(ASCE)MT.1943-5533.0001208)

- 20.N. Eskandari, S. Motahari, S. Atoufi, G.H. Motlagh, M. Najafi, "Thermal, mechanical, and acoustic properties of silica aerogel/UPVC composites", *J. Appl. Polym. Sci.*, 134, pp. 1–8, 2017.

<https://doi.org/10.1002/app.44685>

- 21.Y.C. Joung, M.J. Roe, Y.J. Yoo, J.C. Park, H.J. Choi, M.W. Kim, "Method of preparing silica aerogel powder", U.S. Patent No. US 2012/0225003 A1, 6 September 2012.

- 22.T. Sobha Rani, M.C.S. Subha, G. Venkata Reddy, Y.-H. Kim, Y.-S. Ahn, "Synthesis of Water-Glass-Based Silica Aerogel Powder via with and Without Squeezing of Hydrogels", *J. Appl. Polym. Sci.*, 115, pp. 1675–1679, 2009.

<https://doi.org/10.1002/app.31191>

- 23.[Online] Available: <https://www.lih-fe.com/en/product/Fiberglass->

[Needle-Mat-E-650C/fiberglass_needled_mat-001.html](#) Accessed: 14 April 2021

24. MATERIACUSTICA SRL, "Measurement kit for acoustical complex properties testing," [Online] Available: http://www.materiacustica.it/mat_UKProdotti_MAA.html Accessed: 27 January 2021).

25. International Organisation for Standardization – Acoustics — "Determination of sound absorption coefficient and impedance in impedance tubes — Part 2: Transfer-function method," ISO10534-2, International Organisation for Standardization: Geneva, Switzerland, 1998.

26. [Online] Available: https://local.armacell.com/fileadmin/cms/downloads/others/armagel/marketing-brochure/ArmaGelHT_Marketing_Brochure_English.pdf, Accessed: 14 April 2021

27. K.V. Horoshenkov, "A review of acoustical methods for porous material characterisation", *Int. J. Acoust. Vib.*, 22, pp. 92–103, 2017.
<https://doi.org/10.20855/ijav.2017.22.1455>

28. K.V. Horoshenkov, A. Hurrell, J.-P. Groby, "A three-parameter analytical model for the acoustical properties of porous media", *J. Acoust. Soc. Am.*, 145, pp. 2512–2517, 2019.

<https://doi.org/10.1121/1.5098778> and

<https://doi.org/10.1121/10.0000560> (Erratum).

29. [Online] Available:

<https://drive.google.com/drive/folders/1D9CNQjOIKHnA-zfx1TLD3e768aZ0qdJH?usp=sharing> Accessed: 16 April 2021

30.A. Hurrell, K.V. Horoshenkov, "On the relationship of the observed acoustical and related non-acoustical behaviours of nanofibers membranes using Biot and Darcy-type models", *Appl. Acoust.*, 179, p. 108075, 2021.

<https://doi.org/10.1016/j.apacoust.2021.108075>

31.R. Venegas, O. Umnova, "Influence of sorption on sound propagation in granular activated carbon", *J. Acoust. Soc. Am.*, 140, pp. 755–766, 2016.

<https://doi.org/10.1121/1.4959006>

Chapter 5:

The acoustical properties of tetraethyl orthosilicate based granular silica aerogels

This chapter is published as:

H. Begum, K.V. Horoshenkov, M. Conte, W.J. Malfait, S. Zhao, M.M. Koebel, P. Bonfiglio, R. Venegas, "The acoustical properties of tetraethyl orthosilicate based granular silica aerogels" , *J. Acoust. Soc. Am.*, 149(6), pp. 4149–4158, 2021. <https://doi.org/10.1121/10.0005200>

Authorship statement:

The principal author of the paper is H. Begum. The contribution of H. Begum is the research investigation, experimental data collection and participation in the data interpretation.

5.1 Abstract

Available data suggests that granulated aerogels can be of interest in terms of their sound absorption performance in the audio frequency range. However, there is still no thorough understanding of the complex physical phenomena which are responsible for their observed acoustical properties. This work is an

attempt to address this gap through advanced material characterisation methods and mathematical modelling. Aerogel samples are produced through a two-step, acid-base sol-gel process, with sol silica concentration and density being the main variables. Their pore structure is carefully characterised by nitrogen sorption analysis and scanning electron microscopy. The acoustical properties of hard-backed granular silica aerogels are measured in an impedance tube and the results predicted accurately with the adopted theoretical model. Although silica aerogels have over 90% of open interconnected pores, this was neither reflected in the measured acoustical properties nor the parameter values predicted with the model. Novel results show that only a proportion of the micro and mesopores in the direct vicinity of the grain surface influenced the acoustical properties of aerogels. Further work in the hierarchical pore structure of aerogels is required to better understand the roles of different pore scales on the measured acoustical properties of granulated aerogel.

Keywords: Acoustics; aerogels; absorption; impedance; porous materials

5.2 Introduction

Aerogels have gathered increasing interest from industry in recent years. Their highly porous nature allows sound waves to penetrate far enough into the structure and multiple interactions to take place, making them efficient acoustic absorbers [1]. As a result, they are now used in a broad range of commercial products with potential applications as catalyst supports [2], CO₂ adsorbents [3], black material absorbers for solar harvesting [4], and drug delivery systems [5] in the form of bulk materials. These materials behave as membranes [6] and effective thermal and acoustic insulation materials for industrial installations, pipelines and buildings [2,7]. The latter is directly relevant to this work

Silica aerogels are predominantly mesoporous (2-50 nm pore size) materials in which the liquid part of the gel has been replaced by air, with unique properties such as high porosity (80–99.8%), low density (0.003–0.5 g cm⁻³), large specific surface area (500–1000 m² g⁻¹) [8] and outstanding thermal insulation performance [2,9]. Typical thermal conductivity values are around 0.015 W m⁻¹ K⁻¹, approximately half of that of standing air (0.026 W m⁻¹ K⁻¹) and much better than that of conventional insulation materials (0.03–0.040 W m⁻¹ K⁻¹) [10]. Silica aerogel is available commercially in the form of particles (granulate and powder) and aerogel-fibre blankets. Particulate/granulated aerogels are applied in renders, concrete, cavities, or translucent elements, whereas aerogel blankets can be applied for pipe or building insulation [11]. Production

methods include supercritical drying (SCD, mostly for blankets) and ambient pressure drying (APD, mostly for granulates and powder).

The thermal insulation properties and the physics of heat transport of aerogels are well studied [12]. However, the acoustical properties are not so well understood. Earlier research on sound propagation in aerogels largely focused on sound velocity as a function of aerogel density [13,14] which was measured mainly in the ultrasonic frequency range above 20 kHz. Although basic models were proposed to predict the sound speed in aerogel, no attempt was made to account for the frequency-dependent sorption-influenced diffusion in micro- and mesopores. Some later publications in reference [15] and [16] extended measurements to the audible frequency range below 20 kHz. For example, the work by Buratti et al. [15] used a standard impedance tube setup to measure the acoustic absorption coefficient and transmission loss of layers of aerogel granules in the frequency range of 100–6400 Hz. However, no theory was proposed to explain the presented data and no attempt was made to relate these data to the physical mechanisms that are responsible for sound attenuation. In fact, a majority of published acoustic studies on aerogels carried out in the audible frequency range were focused on measuring the ability of an aerogel layer to absorb sound or resist sound transmission [16–19]. Other studies measured the sound speed in and reflection coefficient from a layer of aerogel (e.g., reference [20]). More recent work by Takeshita et al. [21] estimated the specific pore surface area, peak pore size and porosity in chitosan

aerogels with three different densities. They measured the absorption coefficient of layers of these samples in the frequency range of 500–6500 Hz illustrating its resonance behaviour and some dependence on aerogel microstructure. However, as in the case of the other cited studies, no attempt was made to propose a theory to explain the measured absorption data [18,19].

To the best of our knowledge, there is still a lack of understanding of the key relations between the aerogel microstructure and a range of physical mechanisms responsible for the frequency-dependent acoustical properties of aerogel granules. Therefore, the purpose of this work is to attempt to explain the acoustic properties of some specific aerogels, with microstructure parameters measured non-acoustically by using a valid theoretical model that accounts for the complexity of acoustic phenomena in multiscale materials. These and other typical aerogel granule mixes are characterised by a pore size distribution which spans across a vast range of scales. We focus on a specific grain size of silica aerogels but introduce some variation in porosity and density that was achieved by changing the sol silica content.

A main novelty of this paper is the use of a well understood model [22] which can predict the acoustical properties of rigid frame porous media with a vast range of pore scales (i.e., from macropores to micropores) which are carefully characterised. In this paper we use the International Union of Pure and Applied Chemistry (IUPAC) [23] recommendation to define pores smaller than 2 nm as

micropores, pores in the ranges of 2–50 nm as *mesopores* and pores larger than 50 nm as *macropores* (inner-particle transport pores). This paper attempts to understand how the presence of these pores contribute to the measured acoustical properties of aerogel in its granular form. Advanced material characterisation methods and mathematical modelling are used to explain the measured acoustical properties of aerogels in terms of three characteristic sizes and associated scale porosities. This work paves the way to understanding key physical mechanisms which contribute to the routinely measured acoustical properties of aerogels.

The paper is organised in the following manner. Section 5.3 describes the methods to synthesise aerogels and to characterise their microstructure acoustically and non-acoustically. Section 5.4 presents the model [22] which was used to predict the measured acoustical data. Section 5.5 and 5.6 present the results and discussion. The conclusions of this work are presented in Section 5.7.

5.3 Materials and Methods

5.3.1 Aerogel synthesis

Polyethoxydisiloxane (PEDS) [24] a pre-polymerised silica precursor made from tetraethyl orthosilicate (TEOS), water and sulfuric acid, was used for the silica

aerogel synthesis. As shown in Table I, TEOS was mixed with half of the final amount of ethanol (95% EtOH, denatured with 5 vol. % isopropyl alcohol) and water, and stirred at 35–40 °C and 250 rpm for 5 minutes. In another vessel, the second half of ethanol and water was mixed with 0.41 g of sulfuric acid and this solution was slowly added to the first vessel, while stirring over 30 minutes at room temperature.

Table 5.1 Materials and quantities used to prepare polyethoxydisiloxane (PEDS) [24].

Material	Quantity [g]
TEOS	491.2
Ethanol	88
Water	32
Ethanol	88
Water	32
Sulfuric acid	0.41

Silica aerogels were prepared with variable PEDS content in the sol to produce aerogels with different densities (Table 5.2 i.e., TEOS concentration of 30%, 60%,

90%). These materials were named PEDS E30, PEDS E60, PEDS E90, respectively. We describe the synthesis of the PEDS E30 aerogel as an example. To prepare 30 cm³ of gel, corresponding to a packed volume of 50 cm³ granular aerogel sample, 9 mL PEDS was diluted with 21 mL EtOH and 1 mL distilled water under constant stirring for 5 minutes at room temperature. 0.36 mL of 5.5M ammonium hydroxide solution (NH₄OH in water) was then added, and gelation occurred in 3-5 minutes. The ammonia activated sol was poured into square polystyrene moulds with dimensions 5×5×2 cm³. The gel was covered with an additional 0.4 mL of ethanol to prevent solvent evaporation due to exposure to air, which would result in cracking of the gel. All sample boxes were closed with lids and aged for 24 hours at 65 °C depending upon the wt. % of SiO₂. The same procedure was carried out for the rest of the samples, adjusting the quantities according to Table 5.2.

Table 5.2 The preparation of three standard equivalents at weight percentages of silica (expressed as SiO₂) for samples with TEOS concentration of 30, 60 and 90% [25].

Sample name	SiO₂ wt %	PEDS [mL]	EtOH [mL]	Water [mL]	5.5M NH₄OH [mL]
PEDS E30	6	9	21	1	0.36
PEDS E60	12	18	12	1	0.36
PEDS E90	18	27	3	1	0.36

The gels were washed with ethanol twice overnight at 65 °C. To maintain a hydrophobic product and to enable ambient pressure drying, a hydrophobization treatment was carried out to replace the silanol and ethoxy surface groups with hydrophobic trimethylsilyl groups. The aged gels were hydrophobized in a mixture of hexamethyldisiloxane (HMDSO), concentrated hydrochloric acid (12M) and ethanol at 65 °C for 24 hours (Table 5.3).

Table 5.3 Materials and quantities used to age aerogels.

Material	Quantity [mL]
HMDSO	60
HCl (12M)	0.34
95% EtOH	2.205

The hydrophobized gels were dried by APD in a ventilated oven for 3 hours at 150 °C. In parallel, monolithic silica aerogel samples were prepared by supercritical CO₂ drying, but the focus of this paper is on the APD granulate. The structure of pure monolithic silica aerogel as a photographic image, drawing and TEM image to show its pearl-like necklace shape before it shatters into its granular form is shown in Figure 5.1.

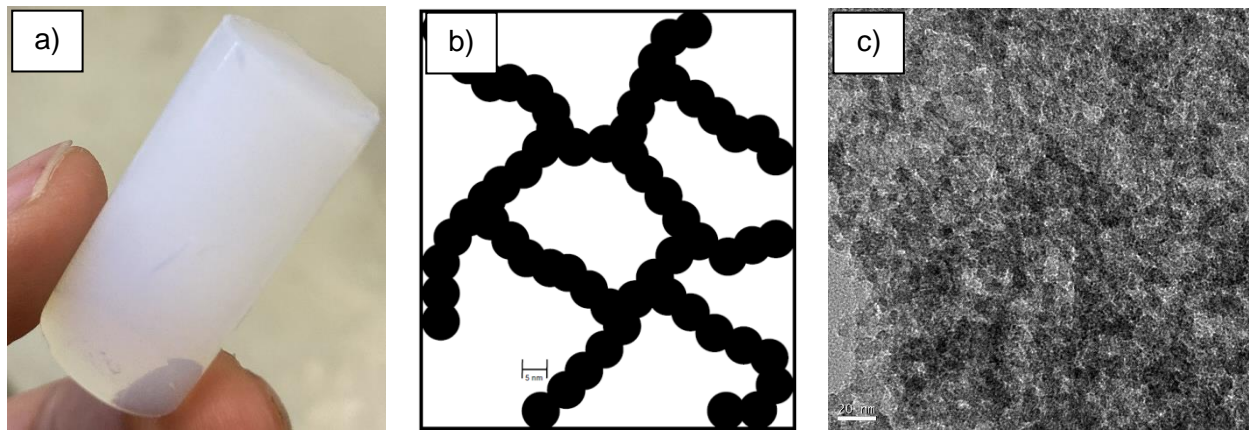


Figure 5.1 Structure of monolithic silica aerogel as a) a photographic image, b) drawing and c) TEM image.

5.3.2 Characterisation

The apparent bulk or envelope density was measured from the mass and volume by the powder displacement method (Micrometrics GeoPyc 1360). The specific surface area, S_{BET} was calculated from nitrogen sorption isotherms (Micrometrics 3flex) using Brunauer–Emmet–Teller (BET) analysis [26]. The porosity (ϕ) was calculated according to eq. (1) (e.g., reference [27]) from the bulk (ρ_b) and skeletal (ρ_s) density, where the skeletal density of 2.0 g cm^{-3} was adopted [28] (a typical value for silica aerogel)

$$\phi = 1 - \frac{\rho_b}{\rho_s}. \quad (1)$$

The effective pore size and average pore diameter from adsorption (ads) and desorption (des) data were calculated using the Barrett–Joyner–Halenda (BJH) method [29]. The BJH method yields the derivative of pore volume (dV) plotted versus pore width (d_n), i.e., differential distribution plots [30]. It is important to note, however, that the BJH method is affected by the mechanical deformation of the aerogel when it undergoes a second drying from purging with liquid nitrogen [31], so results should be taken as referential. In addition, nitrogen sorption analysis does not sample pores larger than ~50 nm.

Therefore, the specific pore volume (V_p) and average pore size of the mesopores (D_p) were also evaluated from the density and surface area assuming that the pores are cylindrical:

$$V_p = \frac{1}{\rho_b} - \frac{1}{\rho_s} \quad (2)$$

$$D_p = \frac{4V_p}{S_{BET}} \quad (3)$$

Scanning electron microscopy (SEM) images were obtained using a FEI Nova NanoSEM 230 instrument (FEI, Hillsboro, OR) at an accelerating voltage of 10 kV and a working distance of 4.1 mm. Aerogel samples were fixed on to carbon taped stubs and subsequently coated with 15–20 nm platinum for SEM analysis. A Java-based image processing program, ImageJ, was used to manually measure the size of 50 individual pores obtained on a high magnification SEM

image. The data were collated to determine their normal approximate of the pore size distribution, see supplementary material at reference [32].

The acoustical properties of aerogel samples were measured in a bespoke, 10 mm bore impedance tube [33] to test aerogels made in relatively small batches. This 2-microphone tube setup was developed to test 40 mm³ material specimens in accordance with the standard ISO 10534-2: 2001 [34]. This setup enabled us to measure the surface acoustic impedance, reflection, and absorption coefficient in the frequency range of 300–3000 Hz. The impedance tube was installed in an upright position to allow the acoustic properties of unconsolidated material to be measured accurately. The spacing between the two microphones was 30 mm which is usual for this frequency range as recommended in the standard [34]. A specimen from each granulate sample was deposited through a funnel into a 10 mm diameter, 50 mm deep sample holder (see Figure 2). The thickness of each specimen in the impedance tube was kept close to 50 mm to ensure reliability. This choice of the sample thickness is typical for commercially available acoustic absorbers such as foams and fibreglass. The choice of the sample thickness is not critical for this work because it is accounted for accurately by the adopted model [22] (also see Section 5.4). The packed-bed (bulk) density of the material sample was measured and recorded to ensure that the specimen density was controlled within 1%.

This impedance tube setup was calibrated in accordance with the standard method detailed in reference [34] and validated against data obtained with larger tube setups for a 50 mm layer of identical glass beads with 1 mm radius. This is a well characterised material [35] with solid glass particles whose size is similar to that found in our aerogels so that it was used for a comparison with the results presented in Section 5.5. Three measurements of each of the three different concentrations of PEDS samples was taken to ensure repeatability which was 1–2%.

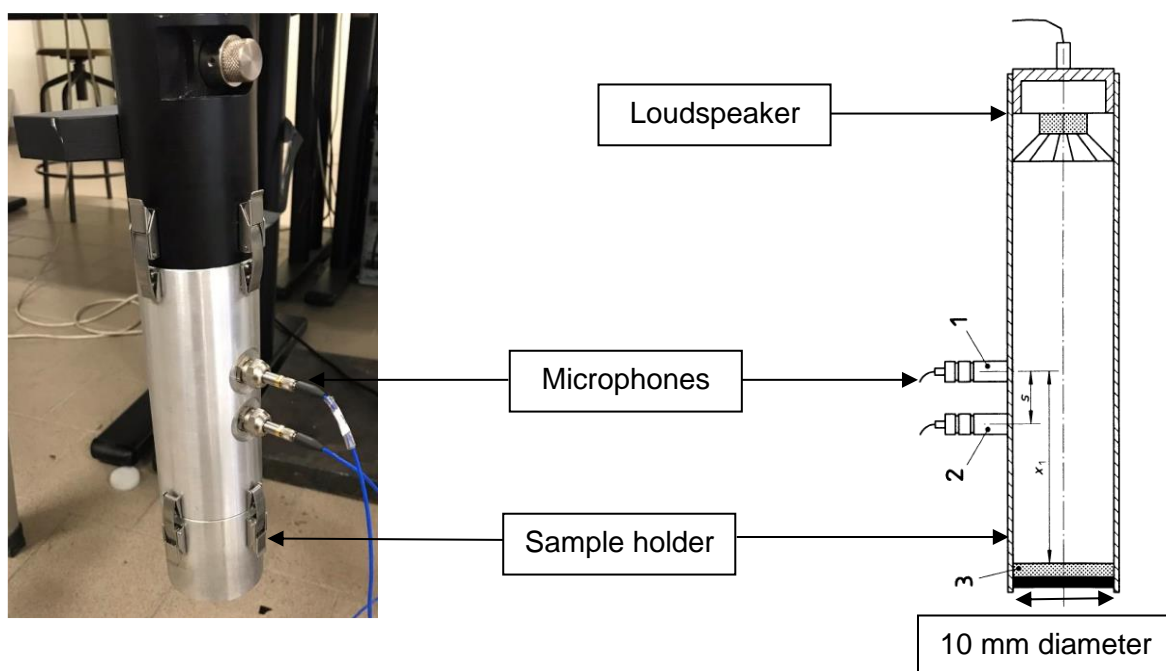


Figure 5.2 Vertically standing 10 mm impedance tube (adapted from reference [34]).

5.4 Modelling of the acoustical properties of aerogels

Granular aerogels consist of highly porous particles with a large internal pore surface area. Modelling of their acoustical properties requires accounting for its multiscale nature and physical processes that occur at different scales. In this work, the model proposed by Venegas et al. [22] is applied. This upscaled analytical model has been developed for an array of spherical porous grains in which two inner-particle scales of porosity are considered. The two different types of inner particle pores are modelled as an array of monodisperse cylindrical inner-particle (transport) pores with size greater or comparable with the mean free path and a network of mesopores modelled as an effective medium where diffusion determines the mass transfer. The model also accounts for the viscosity and heat transfer effects in the voids formed between the particles, rarefied gas flow and heat transfer in the inner-particle transport pores, interscale (voids to/from inner-particle pores) pressure diffusion, interscale (transport- to/from mesopores) mass diffusion, and sorption in the micro- and mesopores. Due to the characteristic sizes of the synthesised granular aerogel samples, it will be shown that the latter has a negligible influence on the acoustic properties of the said samples. The model is based on 6 parameters which are [22]: (i) the effective particle radius (r_p); (ii) the voids porosity (ϕ_p), i.e., porosity related to the proportion of the air space between the aerogel particles; (iii) the inner-particle macropore radius (r_t); (iv) their associated porosity (ϕ_t); (v) the effective diffusion coefficient (D_e) determining

the mass transport in the mesopores [35]; and (vi) the effective linearised sorption equilibrium constant (H_e), which can be interpreted as an apparent porosity of the smallest pores (ϕ_n) [22,36].

(*Note – the section below is not included in the original published paper)

To understand this in detail the MATLAB functions in ref. [37] model [22] is explained clearly below. For the dynamic compressibility of the effective fluid saturating a multiscale sorptive granular material the effective dynamic compressibility is

$$C(\omega) = C_p(\omega) + (1 - \phi_p)C_{mn}F_{pmn}(\omega), \quad (4)$$

where

$$F_{pmn}(\omega) = 1 - \frac{j\omega B(\omega)}{(1 - \phi_p)\mathcal{B}_{app}(\omega)}. \quad (5)$$

The effective dynamic compressibility and thermal permeability of the inter-granular voids is

$$C_p(\omega) = \frac{\phi_p}{P_0} \left(1 - j\omega\rho_0 C_p \frac{\gamma - 1}{\gamma} \frac{\Theta_\rho(\omega)}{\phi_p \kappa} \right), \quad (6)$$

$$\Theta_\rho(\omega) = -j(1 - \beta^3)\delta_t^2 \left(1 - \frac{\beta}{1 - \beta^3} \frac{3}{z_t^2} \left(1 - \beta z_t \frac{1 + z_t \tanh(z_t(\beta - 1))}{z_t + \tanh(z_t(\beta - 1))} \right) \right), \quad (7)$$

where

$$\beta = \sqrt[3]{1 - \phi_p}, \quad (8)$$

$$z_t = j^{1/2} \frac{r_p}{\beta \delta_t}, \quad (9)$$

$$\delta_t = \sqrt{\frac{\kappa}{\rho_0 C_p \omega}}. \quad (10)$$

The effective dynamic compressibility of the micro-nano-porous domain (i.e., the grains) is

$$C_{mn}(\omega) = C_m(\omega) + (1 - \phi_m) C_n F_{mn}(\omega), \quad (11)$$

where

$$F_{mn}(\omega) = 1 - \frac{j\omega G(\omega)}{(1 - \phi_m) \mathcal{D}_{app}}. \quad (12)$$

The effective dynamic compressibility and thermal permeability of the inner grain micropores is

$$C_m(\omega) = \frac{\phi_m}{P_0} \left(1 - j\omega \rho_0 C_p \frac{\gamma - 1}{\gamma} \frac{\Theta_m(\omega)}{\phi_m \kappa} \right), \quad (13)$$

$$\Theta_m(\omega) = -j\phi_m \delta_t^2 \left(1 - \frac{2}{X_t} \frac{J_1(X_t)}{J_0(X_t) - k_t X_t J_1(X_t)} \right), \quad (14)$$

where

$$X_t = j^{3/2} \frac{r_m}{\delta_t}, \quad (15)$$

$$k_t = 2 \frac{\gamma \text{Kn}}{(\gamma + 1) \text{Pr}}, \quad (16)$$

$$\text{Kn} = \frac{\ell}{r_m}, \quad (17)$$

$$\text{Pr} = \frac{C_p \eta}{\kappa}. \quad (18)$$

The effective compressibility of the inner-grain nano-porous domain is

$$C_n = \frac{H_e}{P_0}. \quad (19)$$

The inter-scale (inner-grain micropores to/from the nano-porous domain) mass diffusion function is

$$G(\omega) = -j(1 - \phi_m) \delta_d^2 \left(1 - \frac{2\phi_m}{1 - \phi_m} \frac{R_1(\xi_d)}{R_0(\xi_d)} \right), \quad (20)$$

$$R_i(\xi_d) = \left(\frac{1}{\xi_d} \right)^i \left(K_i(\xi_d) + (-1)^i \frac{K_1(\xi_d/\sqrt{\phi_m})}{I_1(\xi_d/\sqrt{\phi_m})} I_i(\xi_d) \right), \quad i = 0, 1, \quad (21)$$

$$\xi_b = j^{3/2} \frac{r_p}{\delta_b}, \quad (22)$$

$$\delta_b = \sqrt{\frac{\mathcal{B}_{app}}{\omega}}, \quad (23)$$

$$\mathcal{B}_{app}(\omega) = \frac{\mathcal{K}_m(\omega)}{\eta C_{nm}(\omega)}. \quad (24)$$

The viscous permeability of the inner grain micropores is

$$\mathcal{K}_m(\omega) = -j\phi_m\delta_v^2 \left(1 - \frac{2}{X_v} \frac{J_1(X_v)}{J_0(X_v) - k_v X_v J_1(X_v)} \right), \quad (19)$$

where

$$X_v = j^{3/2} \frac{r_m}{\delta_v}, \quad (20)$$

$$k_v = \text{Kn} = \frac{\ell}{r_m}, \quad (21)$$

$$\delta_v = \sqrt{\frac{\eta}{\rho_0 \omega}}. \quad (22)$$

The full analytical model for the dynamic viscous permeability of a multiscale sorptive granular material is

$$\mathcal{K}(\omega) = \mathcal{K}_p(\omega) = -j(1 - \beta^3)\delta_v^2 \left(1 - \frac{\beta^3}{1 - \beta^3} \frac{\zeta \frac{1 - \beta^3}{\beta^3} + 1}{\zeta - 1} \right), \quad (23)$$

$$\zeta = \frac{3}{z^2} \frac{A_p z + B_p \tanh(z(\beta - 1))}{a_p z + b_p \tanh(z(\beta - 1))} \quad (24)$$

where

$$A_p = (3 + (\beta z)^2) \left(1 + \frac{z^2}{6} \right) - 3\beta \left(1 + \frac{z^2}{2} \right), \quad (25)$$

$$a_p = \frac{1}{3} (3 + (\beta z)^2) - 3\beta - \frac{2}{\beta} \left(1 + \frac{z^2}{6} \right) + \frac{4}{\cosh(z(\beta - 1))}, \quad (26)$$

$$B_p = (3 + (\beta z)^2) \left(1 + \frac{z^2}{2} \right) - 3\beta z^2 \left(1 + \frac{z^2}{6} \right), \quad (27)$$

$$b_p = 3 + \beta(\beta - 1)z^2 - \frac{2}{\beta} \left(1 + \frac{z^2}{2}\right), \quad (28)$$

where

$$\beta = \sqrt[3]{1 - \phi_p}, \quad (29)$$

$$z = j^{1/2} \frac{p}{\beta \delta_v}, \quad (30)$$

These, together with other fundamental physical properties of the saturating fluid, are the input parameters to predict the dynamic density (ρ) and the effective compressibility (C) of the effective fluid in the aerogel pores (see Tables I and II in ref. [22]) which are then used to calculate the complex acoustic characteristic impedance

$$Z_c = \sqrt{\frac{\bar{\rho}}{C}}, \quad (31)$$

and wavenumber

$$k_c = \omega \sqrt{\rho C}, \quad (32)$$

which is the function of frequency, ω . Since the effective particle radius is usually millimetric and therefore much larger than the inner-particle submicron pores, the dynamic density, which accounts for viscosity effects in the pores, is well approximated with that of the voids (ρ_p), i.e.,

$$\rho = \frac{\eta}{j\omega k_p} = \rho_p, \quad (33)$$

where k_p is the dynamic viscous permeability of the interparticle space which is primarily controlled by the particle radius (r_p). Its expression for an array of spherical particles has been introduced in ref. [38] and can also be found in Table II of reference [22].

The effective compressibility of the fluid in the aerogel pores captures a number of effects. These effects include heat transfer in the interparticle voids, rarefied gas flow and heat transfer in the inner-particle transport macropores, interscale pressure and mass diffusion processes affected by sorption. Following the original definitions [22] the effective compressibility is in eq. 4. where C_p is the effective compressibility of the fluid that saturates the interparticle voids. The other terms in eq. (4) are in eq. (11) which is the compressibility of the effective fluid in the macro- and mesopores in the aerogel particles, C_m (in eq. (13)) is the effective compressibility of the fluid that saturates the macropores and C_n (in eq. (19)) is the compressibility of the fluid that saturates the mesopores. The function F_{pmn} and F_{mn} (in eq. (5) and (12)) describe the pressure and mass diffusion processes, respectively. These quantities are complex, frequency-dependent and controlled by the fundamental properties of the saturating fluid and parameters r_p , ϕ_p , r_t , ϕ_t , D_e and H_e . Their analytical expressions can also be found in Table I of reference [22].

Eqs. (31) and (32) can be used to predict the surface impedance of a hard-backed layer of aerogel which is typically measured using the standard

impedance tube method as described in Section 5.3. The surface impedance of a hard-backed layer of aerogel of thickness d is

$$Z_s = -jZ_c \cot(k_c d), \quad (34)$$

where $j = \sqrt{-1}$. The normalised surface impedance

$$z = \frac{Z_s}{\rho_0 c_0}, \quad (35)$$

can then be used to predict the frequency dependent, normal incidence pressure reflection coefficient

$$R = \frac{z - 1}{z + 1}, \quad (36)$$

where ρ_0 and c_0 are the ambient density of air and sound speed in air, respectively. The acoustic absorption coefficient of this layer is

$$\alpha = 1 - |R|^2. \quad (37)$$

The quantities predicted with eqs. (34)-(36) are complex and frequency-dependent quantities and their behaviour is rarely explained theoretically in the published literature of aerogels. The absorption coefficient predicted with eq. (37) is a real, frequency-dependent quantity that is often quoted in research on acoustical properties of aerogels (e.g., references [15,16]), but rarely predicted.

5.5 Results

5.5.1 Density, nitrogen sorption analysis and microstructure

TEM analysis confirms the pearl-like necklace type structure typical for silica aerogels (Figure 5.1). During APD, the gel bodies fractured into mm-sized granules, which were sieved to select particle sizes between 2 and 3 mm for further analysis (Figure 5.3). Figure 5.4 shows that these particles are not spherical as assumed in the model presented in Section 5.4, but angular, with sharp edges and some resembling platelets. Much smaller fractions are also present in these images suggesting that this material is fragile and can crumble. The presence of smaller particle fractions is likely to affect the measured acoustical properties as it will be illustrated in Section 5.5.2. The analysis of these images suggests that the size of the particles in the mix PEDS E90 is relatively smaller than that in the other two mixes.

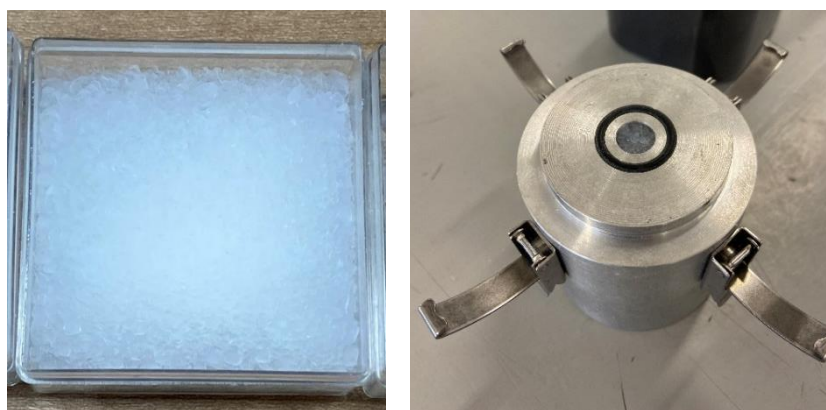


Figure 5.3 Photographs of the 50 mm x 50 mm container with granular silica aerogel 2-3 mm sieved mix (left) and 40 mm³ of it in the 10 mm diameter, 50 mm deep impedance tube sample holder (right).

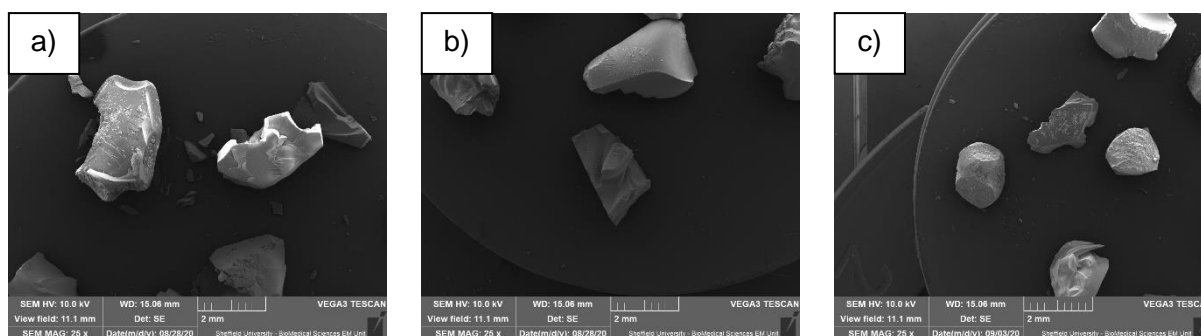


Figure 5.4 SEM images of micrometric grains of the 2-3 mm fraction of a) PEDS E30, b) PEDS E60, c) PEDS E90.

The pore size and microstructure were analysed for three different aerogels prepared with three different PEDS concentration of TEOS vol. % 30, 60 and 90%. Note that the accurate determination of aerogel pore size distributions is not a trivial task. SEM image analysis is particularly sensitive to meso- and macropores, but not to micropores. In addition, manual peak-picking is subject to sampling bias, the imaged fracture surfaces may not be representative of the bulk, and the coating and contrast/brightness settings may affect the results. In contrast, nitrogen sorption analysis does probe the bulk of the material but is not sensitive to macroporosity (> 50 nm). In addition, sample deformation

during nitrogen sorption can affect the pore size. Finally, simple approximations of average pore size rely on simplistic approximations of meso- and micropore pore geometry, e.g., cylindrical (see eq. (3)), and it does not fully capture the complexity of the real aerogel pore structure.

Using SEM images and ImageJ software the average pore size of the normal distributions derived by manually estimating pore diameters of PEDS E30 is 45 nm, PEDS E60 is 33 nm and PEDS E90 is 27 nm (Figure. 5.5). Pore size distribution data calculated by individually measuring the diameter of the pore from SEM using ImageJ are provided as supplementary data [32].

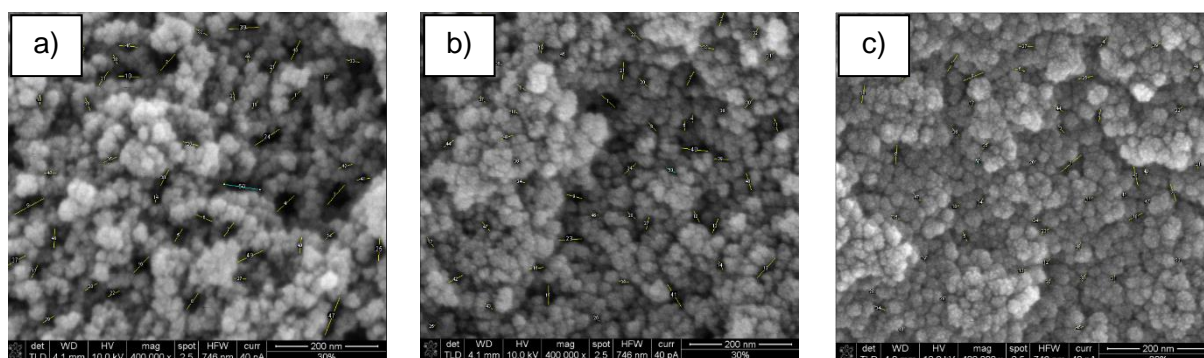


Figure 5.5 Analysis of the size of 50 individual pores using ImageJ software applied to SEM images of a) PEDS E30, b) PEDS E60, c) PEDS E90.

All aerogels, prepared with variable PEDS concentration and hence variable final bulk densities, display type IV nitrogen isotherms [29] typically observed for silica aerogel (Figure 5.6). The distributions of pore widths obtained from these

histograms obtained with the BJH method can be found in the supplementary data [32]. The smallest maximum frequency counts obtained for the BJH pore width (desorption) for PEDS E30, PEDS E60 and PEDS E90 specimens was 3.67, 6.94 and 5.78 nm, respectively. These were estimated from the desorption data [32]. The largest maximum frequency counts obtained for the BJH pore width (adsorption) for PEDS E30, PEDS E60 and PEDS E90 specimens' aerogels was 11.27, 28.87 and 15.34 nm, respectively. These were estimated from the adsorption isotherms [32]. It is seen that during desorption there is a smaller distribution of pore sizes than during adsorption. This may be due to ink-bottle pores (see Figure 7 in ref. [39]), or interconnected pores of complex geometry, where the condensation pressure within the cavity is smaller than the evaporation pressure as the presence of condensed liquid in the constriction helps to nucleate the liquid phase [40]. As consistent with the hysteresis loop observed in Figures 5.6 (a-c). In this case when the pressure of capillary evaporation is reached in the small pore opening, the whole pore is emptied through a desorption percolation [41] process leading to an artificially narrow pore size distribution.

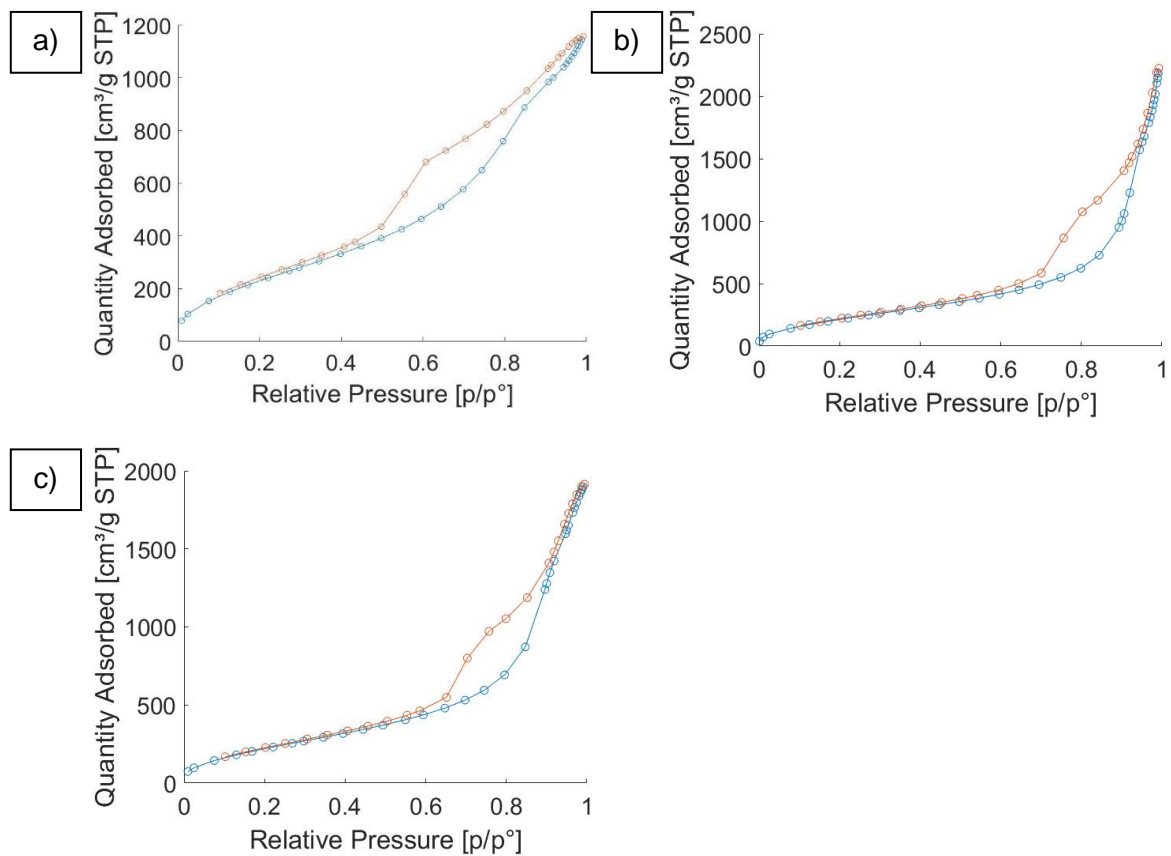


Figure 5.6 BET isotherm linear plots of a) PEDS E30, b) PEDS E60, c) PEDS E90.

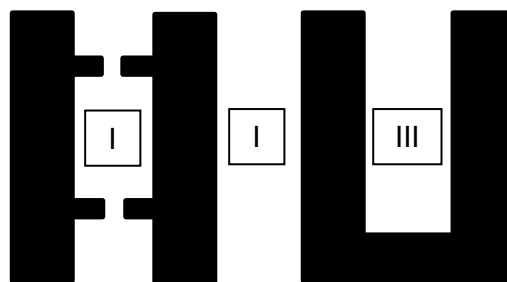


Figure 5.7 Schematic for 3 generic types of pores, i) ink bottle, ii) straight with both ends open and iii) straight with only one end open.

Table 5.4 lists key parameters for these three aerogels. Both the SEM data and the calculated pore sizes (eq. (3)) display the expected monotonic decrease in average pore width with increasing PEDS concentration and density. In contrast, the BJH average pore widths are highest at intermediate densities, presumably because of the limitations with sample deformation and macroporosity during nitrogen sorption analysis (see Section 5.3.2).

Table 5.4 Properties of density, pore structures, surface area, adsorption (ads) and desorption (des) coefficients of silica aerogels for PEDS E30, PEDS E60, and PEDS E90.

Properties	PEDS E30	PEDS E60	PEDS E90
ρ_b [g cm ⁻³]	0.130	0.163	0.227
ρ_s [g cm ⁻³]	2	2	2
ϕ , porosity %	93.5	91.9	88.7
S_{BET} [m ² g ⁻¹]	946	885	917
BJH ads	3.67	6.94	5.78
BJH des	11.27	28.87	15.34
d_n , nm			
SEM	45.3	33.1	27.4
$4V_{pore}/S_{BET}$	30.5	25.6	17.1

5.5.2 Acoustical properties

Figure 5.8 illustrates the absorption coefficient spectra for the 50 mm layer of glass beads and three layers of granular aerogels developed in this work. This example illustrates well the effect of the micropores, which is a clear shift in the frequency of the first destructive interference maximum in the material layer towards the lower frequency range. This shift is associated with a relative decrease in the sound speed in aerogel which is caused by an increase in dynamic compressibility (or reduced dynamic bulk modulus) of the air in the material pores. This is mainly a result of the pressure diffusion effect in the inner-particle pores. This effect is more pronounced for aerogel PEDS E90 with a smaller pore width (see Table 5.4). Above the interference maximum, the absorption coefficient depends less on the compressibility and more on viscous permeability of aerogel. In this frequency range the higher absorption coefficient is for the mix PEDS E90 because it is composed of slightly smaller particles (see Figure 5.4) so that its permeability is smaller than that of the other two aerogel mixes.

In order to explain the acoustical absorption behaviour shown in Figure 5.8 the complex reflection coefficient data for the three aerogels and theoretical model described in Section 5.4 were used to invert the parameters of the model: r_p , ϕ_p , r_{t1} , ϕ_{t1} , D_e and H_e . The differential evolution algorithm [42] was used in the fitting

process. It enabled us to determine the best set of the non-acoustical parameters to find the minimum of the following objective function:

$$G(x) = \sum_{m=1}^M |R^{(t)}(x, \omega_m) - R^{(e)}(\omega_m)|^2, \quad (38)$$

where M is the number of frequency points (ω_m) in the measured reflection coefficient spectrum $R^{(e)}(\omega_m)$ and $x = [r_p, \phi_p, r_t, \phi_t, D_e, H_e]$ is the design variable vector. In eq. (38), $R^{(t)}(x, \omega_m)$ is the reflection coefficient predicted with eq. (11) for the given values of frequency and non-acoustical parameters in the design vector. This minimisation procedure was carried out in the frequency range of 300–3000 Hz for $M = 448$ frequency points. The fundamental properties of air were taken as their ambient values at 20 °C.

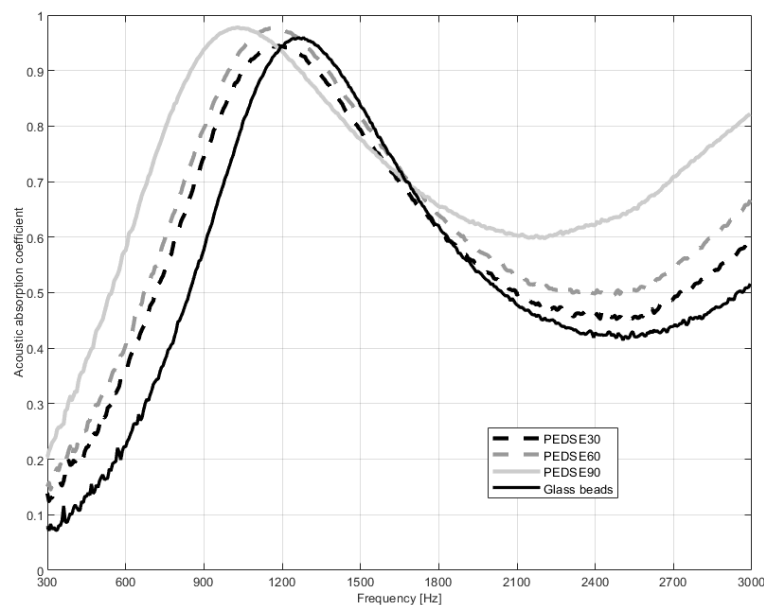


Figure 5.8 The measured absorption coefficient spectra for a nominal 50 mm hard-backed layer of the four materials studied in this work.

The inversion algorithm was initially tested on a layer of loosely packed non-porous glass beads with nominal particle diameter of 2 mm and a thickness 50 mm, respectively. This is a well characterised material (e.g., reference [35]). Note that since the beads are non-porous the model used corresponds to that of a packing of solid particles [38,43], i.e., $\rho = \rho_p$ and $C = C_p$. Figure 5.9 presents the measured and predicted spectra of the complex reflection coefficient for a 50 mm layer of glass beads. The mean error between the model and data is less than 5.5%, which suggests a close fit. This fit was achieved with the following values of the non-acoustical parameters: $r_p = 0.95$ mm, $\phi_p = 0.4$ and $d = 53.4$ mm. Using the measured acoustical data, the value of the inverted void porosity is close to that expected [43–45] from a loose packing of identical beads ($0.32 \leq \phi_p \leq 0.45$). The particle radius is also in the order of its nominal value provided by the glass bead manufacturer. The value of the layer thickness d used in this model was slightly larger than the nominal value and corresponds to approximately a single extra layer of particles. This trend was also observed in reference [44] for a packing of non-porous lead shots. The slight disagreement between the data and the predictions could be due to the fact that the used

model does not account for the exact particle arrangement but models the dynamic density and effective compressibility by making use of a self-consistent approach in which the packing condition is accounted for in a generic way, as discussed in detail in reference [38] and [43]. It is clear, however, that the physics is well captured by the model.

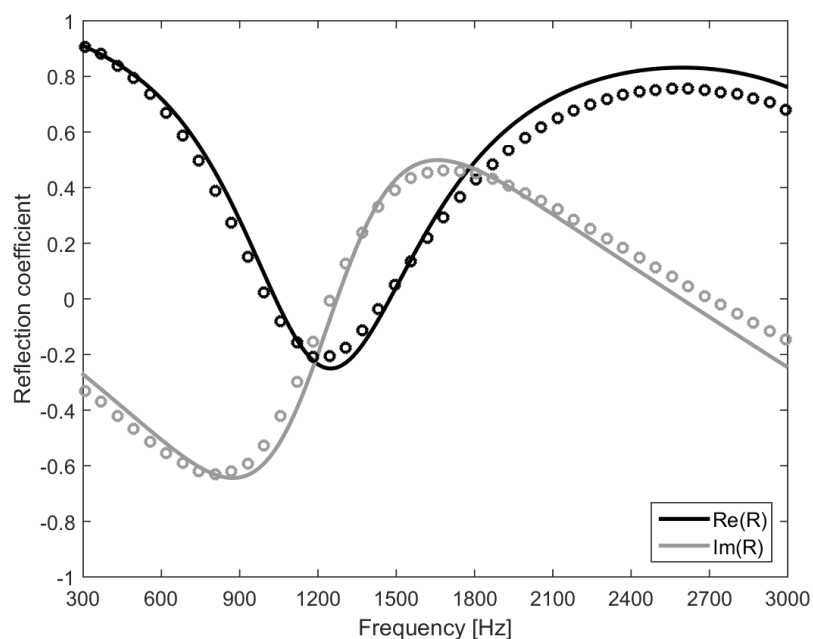


Figure 5.9 Model validation. The measured (circles) and predicted (lines) reflection coefficient for a hard-backed layer of loosely packed glass beads.

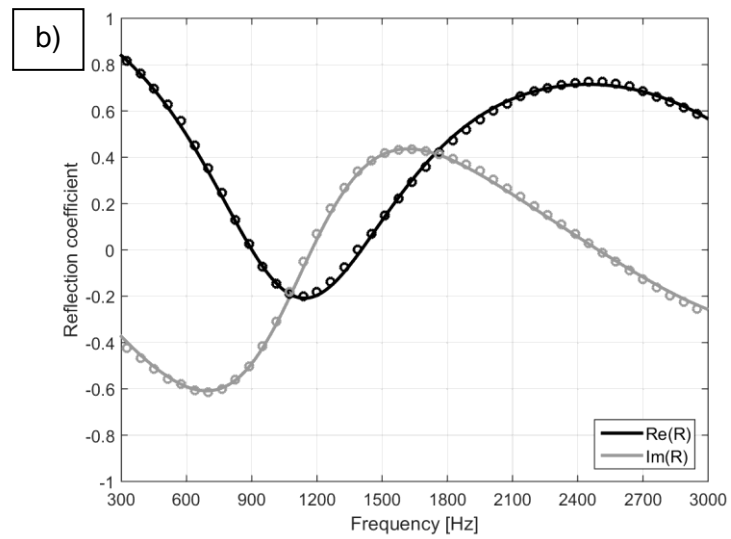
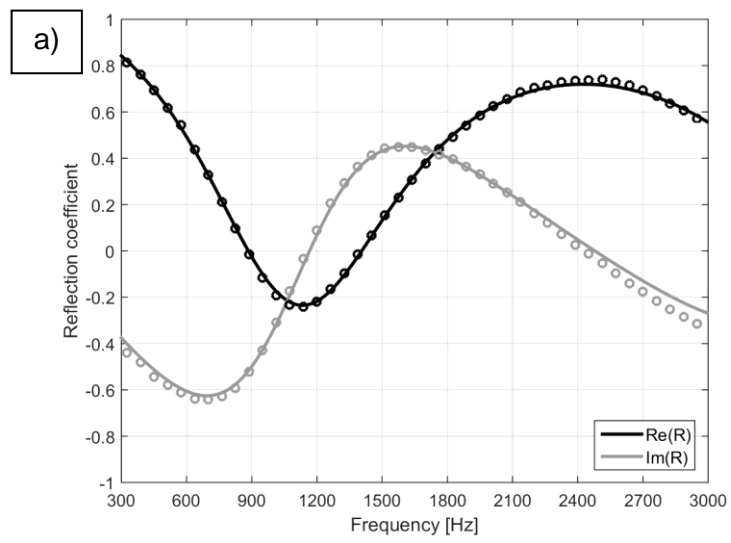
With the model validated against the glass beads data, the parameter inversion algorithm was applied to the reflection coefficient data measured with the impedance tube to determine the non-acoustical parameters characteristic to

the aerogel' s granular mixes produced in this work. The results of this inversion are summarised in Table 5.5.

Table 5.5 The results of the inversion of the three materials studied in this work.

Material	r_p [mm]	ϕ_p	r_t [μm]	ϕ_t	D_e [$\mu\text{m}^2 \text{s}^{-1}$]	H_e	d [mm]
PEDS E30	0.85	0.45	1.50	0.059	0.99	0.18	52.9
PEDS E60	0.80	0.45	1.19	0.074	0.80	0.17	52.4
PEDS E90	0.70	0.36	1.50	0.079	0.60	0.16	52.9

Figures 5.10 show examples of the agreement between the measured and predicted acoustical surface impedance spectra. The relative mean error between these data and predictions was generally less than 3.1% suggesting that the model captures the acoustical behaviour of aerogels accurately. Here, the error is lower compared to that found for glass beads due to the higher number of fit parameters used to predict the acoustical properties of the aerogel mixes.



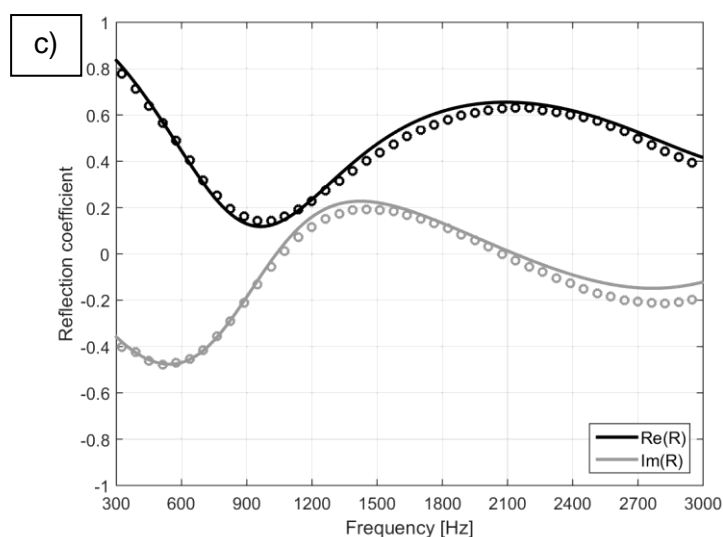


Figure 5.10 Examples of the measured and predicted reflection coefficient for hard-backed layers of aerogel granulate. a) PEDS E30, b) PEDS E60, c) PEDS E90.

5.6 Discussion

The values of the inverted parameters for aerogel pore microstructure (Tables 5.4 and 5.5) make physical sense. For example, the particle radius (r_p) is smaller than the nominal value, which can be explained by the non-spherical shape of the particles and the expected presence of small particles, such as those shown in Figures 5.4, that may sit in between the larger particles. The values of the void porosity (ϕ_p) are in the range 0.35 - 0.45, which are expected values for packings of non-spherical grains (see refs [44 and 45]). The radius of the macropores is in the order of 1 μm , which is a typical value for this type of transport pores (see

ref. [42,46, 47]) for the case of activated carbons). The existence of the small but non-negligible transport porosity (ϕ_t) ensures that the fluid saturating molecules are transported to the smaller inner-grain pores and influences the effects of pressure and mass diffusion in the material [22,36,43]. The acoustic measurements also show that the overall porosity of aerogels is not as high as the one measured non-acoustically. This can be seen by looking at the low-frequency limit of the imaginary part of the surface impedance. Figure 5.11 shows that the porosity inverted from acoustical data is around 0.60–0.65 for the three aerogels samples.

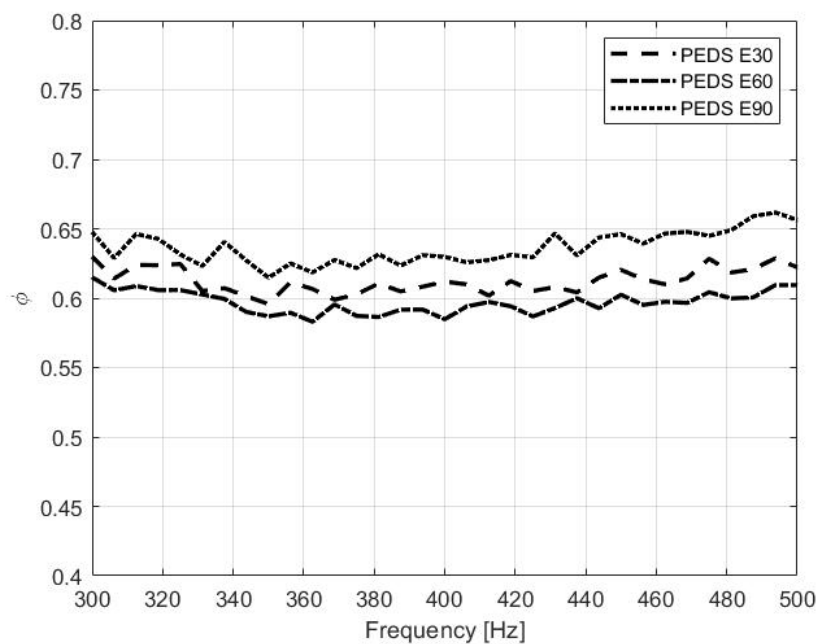


Figure 5.11 Acoustically determined porosity for PEDS E30, PEDS E60 and PEDS E90.

The mesopore radius, measured from the SEM images, for the samples PEDS E30, PEDS E60, and PEDS E90 are 22.7, 16.8, and 13.7 nm, respectively. For mesopores of this size, the theory developed in reference [22] and [36] predicts that the effects of sorption on the acoustical properties of the material are negligible and that the effective linearised sorption equilibrium constant reduces to the apparent porosity of the smallest pores in the grains, i.e., $H_e = \phi_n$. Moreover, at normal conditions, the transport mechanism that dominates the behaviour in the nanopores is Knudsen diffusion [46]. Therefore, the effective diffusion coefficient is determined by the Knudsen diffusion coefficient, i.e., $D_e = D_k$, which for an array of cylindrical nanopores can be assessed as reference [46],

$$D_e = \frac{2\phi_n r_n v}{3}, \quad (39)$$

where v is the thermal velocity. Making use of the D_e data in Table 5.5 and eq. (14) yields the nanopore radius of 17.7, 15.4, and 12.3 nm for the samples PEDS E30, PEDS E60, and PEDS E90, respectively. These nanopore radius values are close to those measured from the SEM images (see Table 5.4). The overall porosity estimated from

$$\phi = \phi_p + (1 - \phi_p)(\phi_t + (1 - \phi_t)\phi_n), \quad (40)$$

and porosity data given in Table 5.5 is 0.577, 0.576 and 0.503 for the samples PEDS E30, PEDS E60, and PEDS E90, respectively. These are 30–40% lower than those measured directly (see Table 5.4). Silica aerogels usually have close to

100% open porosity measured with He pycnometry so that the inner-particle pores should remain open for the incident sound wave. However, this is not reflected in the porosity values inverted using the measured acoustical data and proposed sound propagation model. One can argue that only a proportion of the micro- and mesopore pore length which is in the direct vicinity of the transport pores or grain surface may influence the acoustical properties of the produced aerogels. This remains an open question.

In summary, the produced aerogels can be considered as triple porosity nonsorptive materials in which the sound dissipation is determined by viscosity and heat transfer effects in the voids formed between the particles, rarefied gas flow and heat transfer in the inner-particle transport pores, inter-scale (voids to/from inner-particle pores) pressure diffusion and inter-scale (transport-to/from mesopores) mass diffusion.

5.7 Conclusions

In this work, three granular aerogel formulations were produced, and their microstructural and acoustical properties were measured using a range of characterisation methods. The acoustical properties were predicted using the model by Venegas et al. [22,36], an inversion method based on experimental data and function minimisation (eq. 13). It is a main novelty of this work because there is a general lack of understanding of how to predict and interpret the

measured acoustical behaviour of granular aerogels. The theoretical model adopted in this work considers three scales of heterogeneities where different physical phenomena affect sound propagation. Such a model explains that the dissipation of sound in the studied granular aerogels is due to viscous and thermal effects in the voids, rarefied gas flow and heat transfer in the inner-particle transport macropores, inter-scale (voids to/from inner-grain pores) pressure diffusion and inter-scale (transport- to/from meso pores) mass diffusion, with the latter two largely influencing the acoustic absorption behaviour at the lower frequencies of sound. These are controlled by the presence of transport and mesopores in the material grains. It is shown that the absorption coefficient of these materials increases significantly due to the presence of pores whose scale is comparable with the mean free path. This is explained by an increase in the complex compressibility (reduced bulk modulus) of air in the inner-particle pores due to the said diffusion effects.

Chemical modification allowed us to produce aerogels with inner-particle microstructure that was well characterized using SEM and BJH methods. This work showed that the wt. % of silica has an effect on the pore structure. There was some decrease in the width of mesopores and increase in the proportion of the so-called transport pores on the particle surface leading to the mesopores in PEDS E90 aerogel. The overall porosity inverted from the experimental acoustical data was found to be 30–40% lower than the values measured directly *via* the material density estimate. The fact the aerogels

usually consist of fully interconnected pores is not reflected in the pore parameter values inverted using the experimental acoustical data and adopted sound propagation model. It is likely that only a proportion of the mesopore length in the direct vicinity of the transport pores or grain surface may influence the acoustical properties of the produced aerogels. This remains an open question and naturally suggests that more research is needed to understand better the relative roles of macro-, meso- and micropores on the acoustical properties of aerogels. In particular, it is of research interest to understand the effective path length along the meso- and macropores which contributes to the measured acoustical properties of aerogels.

Acknowledgements

The authors would like to thank the EPSRC-sponsored Centre for Doctoral Training in Polymers, Soft Matter and Colloids (EP/L016281/1) at The University of Sheffield for their financial support of this work. We would also like to thank our industry partner Armacell and Dr. Mark Swift and Mr. Pavel Holub for their continued support throughout this research study. Dr. Rodolfo Venegas acknowledges partial support from Corporación de Fomento de la Producción CORFO Chile (Production Development Corporation) through grant 16ENI2-66903 Innovating2030.

References

1. M.A. Kuczumski, J.C. Johnston, "Acoustic absorption in porous materials," NASA/TM—2011-216995, 2011. [Online] Available: www.sti.nasa.gov Accessed: 27 April 2021
2. G. Reichenauer, A.M. Aegerter, N. Leventis, M.M. Koebel, (Eds.), "Aerogels Handbook," Springer, New York, Chapter 1–History of aerogels, p. 8, 2011.
<https://doi.org/10.1007/978-1-4419-7589-8>
3. S. Cui, W. Cheng, X. Shen, M. Fan, A. Russell, Z. Wu, X. Yi., "Mesoporous amine-modified SiO₂ aerogel: a potential CO₂ sorbent," *Energy Environ. Sci.*, 4, p. 2070, 2011.
<https://doi.org/10.1039/C0EE00442A>
4. W. Sun, A. Du, Y. Feng, J. Shen, S. Huang, J. Tang, B. Zhou, "Super black material from low-density carbon aerogels with subwavelength structures," *ACS Nano.*, 10, p. 9123, 2016.
<https://doi.org/10.1021/acsnano.6b02039>
5. Z. Ulker, C. Erkey, "An emerging platform for drug delivery: Aerogel based systems," *J. Controlled Release*, 177, pp. 51–63, 2014.
<https://doi.org/10.1016/j.jconrel.2013.12.033>
6. A.A. Fernandez-Marin, N. Jimenez, J.-P. Groby, J. Sanchez-Dehesa, V. Romero-Garcia, "Aerogel-based metasurfaces for perfect acoustic energy absorption," *Appl. Phys. Lett.*, 115, p. 061901, 2019.

<https://doi.org/10.1063/1.5109084>

7. R.G. Martinez, E. Goiti, G. Reichenauer, S. Zhao, M.M. Koebel, A. Barrio, "Thermal assessment of ambient pressure dried silica aerogel composite boards at laboratory and field scale," *Energy Build.*, 128, pp. 111–118, 2016.

<https://doi.org/10.1016/j.enbuild.2016.06.071>

8. N. Husing, U. Schubert, "Aerogels – airy materials: chemistry, structure and properties," *Angew Chem., Inc. Ed.*, 37, pp. 22–45, 1998.

[https://doi.org/10.1002/\(SICI\)1521-3773\(19980202\)37:1/2<22::AID-ANIE22>3.0.CO;2-I](https://doi.org/10.1002/(SICI)1521-3773(19980202)37:1/2<22::AID-ANIE22>3.0.CO;2-I)

9. C. Li, X. Cheng, Z. Li, Y. Pan, Y. Huang, L. Gong, "Mechanical, thermal and flammability properties of glass fiber film/silica aerogel composites," *J. Non-Cryst. Sol.*, 457, pp. 52–59, 2017.

<https://doi.org/10.1016/j.jnoncrysol.2016.11.017>

10. M.M. Koebel, A. Rigacci, P. Achard, "Aerogel-based thermal superinsulation: an overview," *J. Sol-Gel Sci. Tech.*, 63, pp. 315–339, 2012.

<https://doi.org/10.1007/s10971-012-2792-9>

11. M. Ganobjak, S. Brunner, J. Wernery, "Aerogel materials for heritage buildings: Materials, properties and case studies," *J. Cult. Herit.*, 42, pp. 81–98, 2020.

<https://doi.org/10.1016/j.culher.2019.09.007>

12. Y.L. He, T. Xie, "Advances of thermal conductivity models of nanoscale silica aerogel insulation material," *Appl. Therm. Eng.*, 81, pp. 28–50, 2015.
<https://doi.org/10.1016/j.applthermaleng.2015.02.013>
13. J. Gross, J. Fricke, L. Hrubesh, "Sound propagation in SiO₂ aerogels," *J. Acoust. Soc. Am.*, 91(4), pp. 2004–2006, 1992.
<https://doi.org/10.1121/1.403684>
14. L. Forest, V. Gibiat, T. Woignier, "Biot's theory of acoustic propagation in porous media applied to aerogels and alcogels," *J. Non-Cryst. Sol.*, 225, pp. 287–292, 1998.
[https://doi.org/10.1016/S0022-3093\(98\)00325-1](https://doi.org/10.1016/S0022-3093(98)00325-1)
15. V. Gibiat, O. Lefeuvre, T. Woignier, J. Pelous, J. Phalippou, "Acoustic properties and potential applications of silica aerogels," *J. Non-Cryst. Sol.*, 186, pp. 244–255, 1995.
[https://doi.org/10.1016/0022-3093\(95\)00049-6](https://doi.org/10.1016/0022-3093(95)00049-6)
16. C. Buratti, F. Merli, E. Moretti, "Aerogel-based materials for building applications: Influence of granule size on thermal and acoustic performance," *Energy Build.*, 152, pp. 472–482, 2017.
<https://doi.org/10.1016/j.enbuild.2017.07.071>
17. F. Merli, A.M. Anderson, M.K. Carroll, C. Buratti, "Acoustic measurements on monolithic aerogel samples and application of the selected solutions to standard window systems," *Appl. Acoust.*, 142, pp. 123–131, 2018.

<https://doi.org/10.1016/j.apacoust.2018.08.008>

18.S. Malakooti, H. G. Churu, A. Lee, T. Xu, H. Luo, N. Xiang, C. Sotiriou-Leventis, N. Leventis, H. Lu, "Sound insulation properties in low-density, mechanically strong and ductile nanoporous polyurea aerogels," *J. Non-Cryst. Sol.*, 476, 36–45, 2017.

<https://doi.org/10.1016/j.jnoncrysol.2017.09.005>

19.S. Malakooti, H.G. Churu, A. Lee, S. Rostami, S.J. May, S. Ghidei, F. Wang, Q. Lu, H. Luo, N. Xiang, C. Sotiriou-Leventis, N. Leventis, H. Lu, "Sound Transmission Loss Enhancement in an Inorganic-Organic Laminated Wall Panel Using Multifunctional Low-Density Nanoporous Polyurea Aerogels: Experiment and Modeling," *Adv. Eng. Mater.*, 20(6), p. 1700937, 2018.

<https://doi.org/10.1002/adem.201700937>

20.L. Forest, V. Gibiat, A. Hooley, "Impedance matching and acoustic absorption in granular layers of silica aerogels," *J. Non-Cryst. Sol.*, 285, pp. 230–235, 2001.

[https://doi.org/10.1016/S0022-3093\(01\)00458-6](https://doi.org/10.1016/S0022-3093(01)00458-6)

21.S. Takeshita, S. Akasaka, S. Yoda, "Structural and acoustic properties of transparent chitosan aerogel," *Mater. Lett.*, 254, pp. 258–261, 2019.

<https://doi.org/10.1016/j.matlet.2019.07.064>

22.R. Venegas, C. Boutin, O. Umnova, "Acoustics of multiscale sorptive porous materials," *Phys. Fluids*, 29(8), p. 082006, 2017.

<https://doi.org/10.1063/1.4999053>

- 23.K.S. W. Sing, D.H. Everett, R.A.W. Haul, L. Moscon, R.A. Pierotti, J. Rouguerol, T. Siemieniowska, "Reporting physisorption data for gas/solid systems with special reference to the determination of surface area and porosity," *Pure Appl. Chem.*, 57(4), pp. 603–619, 1985.
<https://doi.org/10.1351/pac198557040603>
- 24.G.M. Pajonk, E. Elaloui, P. Achard, B. Chevalier, J.-C. Chevalier, M. Durant, "Physical properties of silica gels and aerogels prepared with new polymeric precursors," *J. of Non-Cryst. Sol.*, 186, pp. 1–8, 1995.
[https://doi.org/10.1016/0022-3093\(95\)00210-3](https://doi.org/10.1016/0022-3093(95)00210-3)
- 25.S. Iswar, W.J. Malfait, S. Balog, F. Winnefeld, M. Lattuada, M.M. Koebel, "Effect of aging on silica aerogel properties," *Micropor. Mesopor. Mat.*, 241, pp. 293–302, 2017.
<https://doi.org/10.1016/j.micromeso.2016.11.037>
- 26.S. Brunauer, P.H. Emmett, E. Teller, "Adsorption of gases in multimolecular layers," *J. Am. Chem. Soc.*, 60, pp. 309–319, 1938.
<https://doi.org/10.1021/ja01269a023>
- 27.H.-Y. Nah, V.G. Parale, K.-Y. Lee, H. Choi, T. Kim, C.-H. Lim, J.-Y. Seo, Y.S. Ku, J.-W. Park, H.-H. Park, "Silylation of sodium silicate-based silica aerogel using trimethylethoxysilane as alternative surface modification agent," *J. Sol-Gel Sci. & Tech.*, 87, pp. 319–330, 2018.
<https://doi.org/10.1007/s10971-018-4729-4>

- 28.A. Ayral, J. Phalippou, T. Woignier, "Skeletal density of silica aerogels determined by helium pycnometry," *J. Mater. Sci.*, 27, pp. 1166–1170, 1992.
<https://doi.org/10.1007/BF01142014>
- 29.E.P. Barrett, L.G. Joyner, P.P. Halenda, "The Determination of Pore Volume and Area Distributions in Porous Substances. I. Computations from Nitrogen Isotherms," *J. Am. Chem. Soc.*, 73, pp. 373–380, 1951.
<https://doi.org/10.1021/ja01145a126>
- 30.H. Tian, L. Pan, X. Xiao, R. W. T. Wilkins, Z. Meng, B. Huang, "A preliminary study on the pore characterization of Lower Silurian black shales in the Chuandong Thrust Fold Belt, southwestern China using low pressure N₂ adsorption and FE-SEM methods," *Mar. Petrol. Geol.*, 48, pp. 8–19, 2013.
<https://doi.org/10.1016/j.marpetgeo.2013.07.008>
- 31.G. Reichenauer, M.A. Aegerter, N. Leventis, M.M. Koebel, (Eds.), "Aerogels Handbook," Springer, New York, Chapter 21–Structural characterization of aerogels, pp. 480–482, 2011.
<https://doi.org/10.1007/978-1-4419-7589-8>
- 32.[Online] Available: https://drive.google.com/drive/folders/1-_bwUVuf1uKdQdSON2hUsIWxs1ZBsOnd?usp=sharing Accessed: 11 May 2021
- 33.[Online] Available: MATERIACUSTICA SRL, "Measurement kit for acoustical complex properties testing,"

http://www.materiacustica.it/mat_UKProdotti_MAA.html Accessed: 27 January 2021

34. International Organisation for Standardization – Acoustics — “Determination of sound absorption coefficient and impedance in impedance tubes — Part 2: Transfer-function method,” ISO10534-2, International Organisation for Standardization: Geneva, Switzerland, 1998.
35. K.V. Horoshenkov, A. Hurrell, J.-P. Groby, “A three-parameter analytical model for the acoustical properties of porous media,” *J. Acoust. Soc. Am.*, 145(4), pp. 2512–2517, 2019.
<https://doi.org/10.1121/1.5098778> and
<https://doi.org/10.1121/10.0000560> (Erratum).
36. R. Venegas, C. Boutin, “Acoustics of sorptive porous materials,” *Wave Motion*, 68, pp. 162–181, 2017.
<https://doi.org/10.1016/j.wavemoti.2016.09.010>
37. K. Price, R. Storn, and J. Lampinen, “Differential evolution: A practical approach to global optimization,” Berlin: Springer-Verlag, 2005.
38. C. Boutin, C. Geindreau, “Estimates and bounds of dynamic permeability of granular media,” *J. Acoust. Soc. Am.*, 124, pp. 3576–3593, 2008.
<https://doi.org/10.1121/1.2999050>

- 39.A.P. Malanoski, F. V. Swol, "Lattice density functional theory investigation of pore shape effects. II. Adsorption in collections of non-interconnected pores," *Phys. Rev. E*, 66, p. 041603, 2002.
<https://doi.org/10.1103/PhysRevE.66.041603>
- 40.B. Coasne, A. Galarneau, R.J.M. Pellenq, F. Di Renzo, "Adsorption, intrusion and freezing in porous silica: the view from the nanoscale," *Chem. Soc. Rev.*, 42, pp. 4141–4171, 2013.
<https://doi.org/10.1039/C2CS35384A>
- 41.N.A. Seaton, "Determination of the connectivity of porous solids from nitrogen sorption measurements," *Chem. Eng. Sci.*, 46, pp. 61895–1909, 1991.
[https://doi.org/10.1016/0009-2509\(91\)80151-N](https://doi.org/10.1016/0009-2509(91)80151-N)
- 42.K. Price, R. Storn, J. Lampinen, "Differential Evolution: A Practical Approach to Global Optimization," Springer-Verlag, Berlin, 2005.
- 43.R. Venegas, O. Umnova, "Acoustical properties of double porosity granular materials," *J. Acoust. Soc. Am.*, 130(5), pp. 2765–2776, 2011.
<https://doi.org/10.1121/1.3644915>
- 44.W. Man, A. Donev, F. Stillinger, M. Sullivan, W. Russel, D. Heeger, S. Inati, S. Torquato, P. M. Chaikin, "Experiments on random packings of ellipsoids," *Phys. Rev. Lett.*, 94, p. 198001, 2005.
<https://doi.org/10.1103/PhysRevLett.94.198001>

45.A. Wouterse, S. R. Williams, A. P. Philipse, "Effect of particle shape on the density and microstructure of random packings," *J. Phys. Condens. Matter.*, 19, p. 406215, 2007.

<https://doi.org/10.1088/0953-8984/19/40/406215>

46.D.D. Do, "Adsorption Analysis: Equilibria and Kinetics," Imperial College Press, London, pp. 1–892, 1998.

47.R. Venegas, O. Umnova, "Influence of sorption on sound propagation in granular activated carbon," *J. Acoust. Soc. Am.*, 140(2), pp. 755–766, 2016.

<https://doi.org/10.1121/1.4959006>

Chapter 6: Conclusions & Future work

6.1 Conclusions

The main aim of this PhD project was to systematically characterise the microstructural and acoustical properties of commercially available silica aerogel in its pure powder and composite form. The acoustical properties of these materials were experimentally measured for their normalised surface acoustic impedance, complex reflection coefficient and sound absorption coefficient. This was then validated using several numerical and analytical models. To fully understand the complex physical phenomena, silica aerogels were then synthesised at Empa, Swiss Federal Laboratories for Materials Science and Technology. A two-step, acid-base sol-gel process was used to produce millimetric grain-sized aerogels of different sol silica concentration and density. This was to understand how changing the pore structure would affect the acoustical behaviour in the so-called transport pores.

An extensive review was initially carried out to identify the existing data that were available to predict the acoustical properties of silica aerogels used for vibro-acoustic applications, such as sound insulation in pipes and buildings. The review identified the need for more advanced, analytical models that

understood the acoustical properties of silica aerogels in its pure and composite form.

Powder and fiberglass blankets impregnated with silica aerogel powder were provided by our industry partner, Armacell. Industries prefer to use aerogels of this form as in their neat (monolithic) form they are known to be brittle and have poor mechanical strength due to their complex dependence on bulk or envelope density.

Chapter 3 presents evidence of the non-linear behaviour of the acoustical properties of such aerogel (micron sized particles) powders. The sound energy dissipation of powder silica aerogels was correlated with the understanding of the particle elastic frame using two Biot-type poro-elastic models. It was found that the non-linear behaviour of such small-sized powder materials was dependent on the amplitude of the incident sound pressure level used. The aerogel's mass density varied under different in-tube sound pressure levels and loading conditions. It was found that the model required different groups of dynamic loss factors dependent on both the frequency and sound pressure level. It was also found that a much higher than physically reasonable loss factor value was required to fit the measured data. Therefore, a loss mechanism different to classical friction damping is likely to exist contributing to the observed non-linearity of the sound absorption spectra.

Chapter 4 demonstrated that the sound absorption coefficient of powder silica aerogels embedded into fiberglass mats depends strongly on the filling ratios. The data presented in this chapter suggested that there was a progressive increase in sound absorption as the aerogel impregnation increased from 0 to 50%. When this reached 75% it became less pronounced. A mathematical model was then applied to the complex reflection coefficient data measured in the impedance tube. It was found that the model could not fully capture the physical behaviour of the blanket layer at 75 and 100%. The model parameters inverted, made sense for filling ratios between 0 and 50%, where the measured porosity values were within 3%. When the filling ratio reached 100%, the inverted porosity was 50.5% - significantly lower to that measured at 93.6%. The model needs to account for sorption and thermal diffusion effects, it was only able to account for the classical visco-thermal and inertia effects in the pores.

Chapter 5 demonstrated that there three scales of heterogeneities in the case of granular aerogels in which different physical phenomena affect sound propagation. This work describes, through a careful experiment and mathematical simulation, the acoustical properties of silica aerogel with millimetric grain size synthesised using a two-step, acid-base sol-gel process. In this process, sol silica concentration and density were the main variables. The pore structure of this material was carefully characterised and the acoustical properties were measured and predicted accurately with an advanced

theoretical model. This work used a model which considered three scales of heterogeneities, where different physical phenomena affected sound propagation. The dissipation of sound in the studied granular aerogels was due to the visco-thermal and inertia effects, rarefied gas flow and heat transfer in the inner-particle transport macropores, inter-scale (voids to/from inner-grain pores) pressure diffusion, and inter-scale (transport- to/from meso pores) mass diffusion. The absorption coefficient of these materials increased significantly due to the presence of pores whose scale is comparable with the mean free path. This was explained by an increase in the complex compressibility (reduced bulk modulus) of air in the inner-particle pores due to the said diffusion effects. The wt. % of silica used has an effect on the pore structure. The overall porosity data inverted from the model was 30-40% lower than those measured directly from the aerogel granular materials. The pore parameters inverted using the model did not fully reflect the understanding that aerogels consist of interconnected pores. Only a proportion of the mesopore length in the direct vicinity of the transport pores or grain surface influence the acoustical properties.

It was found that sorption is not very important because the nanopores are too large, in the order of 20-40 nm, for the pores of aerogels. The sorption effects are not very important. The model that included sorption was included, but the effect of sorption is negligible because of the large size of the pores. This effect is only strong in the pores that are much smaller than the ones that were found

acoustically and in the SEM images. Sorption is therefore not very important in the aerogels that were tested. The model used cannot be applied directly to fibre impregnated aerogels because powders have a very small particle radius of 20 μm , the model used only assumes 3 inner scales, of nm, μm and mm. For a powder, only μm and nm is used. In fibre impregnated blankets, the fibre structure must also be considered, and a model for this is unavailable in the model used. The physics of a triple and double porosity material are similar. $C_n = H_e/P_0$, this accounts for sorption. The model in chapter 5 however is not directly applicable to blanket coated aerogels in chapter 4. more research is required to fully understand the roles of the macro-, meso- and micropores on the acoustical properties of aerogels

6.2 Future work

There remain many more areas to understand and refine the existing mathematical models used for modelling the acoustical properties of silica aerogels in vibro-acoustic applications. More work is required to systematically change the microstructure of silica aerogels and enhance its end use in acoustic applications – whether that is in powder or composite form. We need to fully capture the physics of hierarchical pore structures and grain sizes of silica aerogels from micron size to sub-millimetre to millimetric size.

If given more time it would be interesting to use a broader range of grain sizes in the experimental analysis of sound absorption of silica aerogels. This would indicate better how the physical structures, layer thickness, and volume compaction affect the particle elastic frame. This would also provide better insight into the sound absorption properties at the quarter wavelength.

As silica aerogels are increasingly becoming popular in their use as composites impregnated into non-wovens such as fiberglass mats, it would be interesting to determine *“what is the optimal filling ratio of these materials for maximum acoustic performance and minimal material used?”* . It is important to understand this, so we can refine current mathematical models and validate the in-situ performance at the industrial scale.

Furthermore, had there been more time, there is great benefit in being able to chemically change the pore structure to enhance the acoustical properties. Not only are silica aerogels attractive for acoustic applications, their counterparts like: xerogels, cryogels, organic-inorganic aerogels, and hybrid-polymeric aerogels have an abundance of understanding to be achieved, particularly in other noise control applications.

At the University of Sheffield, we wanted to exaggerate the macro-, meso- and micro- structures of silica aerogels whilst maintaining similar density values; measure its acoustical properties and validate/refine existing mathematical models. We were interested in understanding how the hierarchical nature of

the nanopores of silica aerogels strongly affect the value of the effective bulk modulus at normal conditions and thus modifies their acoustical properties. There is very little literature available in the knowledge of using sound absorption properties of porous materials in different fluid filled mediums and using this data to characterise pore structures. If acoustical properties are proven to be sensitive enough to the composition of adsorbed gas/fluid mixtures, this could form a basis for the acoustic method of monitoring the composition of these mixtures inside the pores of a material.

Had there been more time it would also have been noteworthy to better understand, the viscoelastic properties of granular and powder aerogels using experimental methods such as dynamic mechanical analysis (DMA). Accurate simulation of the vibro-acoustic performance of these powders and fibreglass mats impregnated with these powders are of importance for many noise control applications. Unfortunately, classical DMA uses block structures, so it was difficult to determine the viscous and elastic properties of the aerogel grains due to their fragility. Therefore, more work is required to develop alternative experimental methods of capturing mechanical properties of powder/granular materials.

